PERFORMANCE EVALUATION OF MATRIX CONVERTER FED INDUCTION MOTOR DRIVE

A DISSERTATION

Submitted in partial fulfillment of the requirements for the award of the degree of

MASTER OF TECHNOLOGY

in

ELECTRICAL ENGINEERING

(With Specialization in Power Apparatus and Electric Drives)

By

N.V.D.V PRASAD MADASU

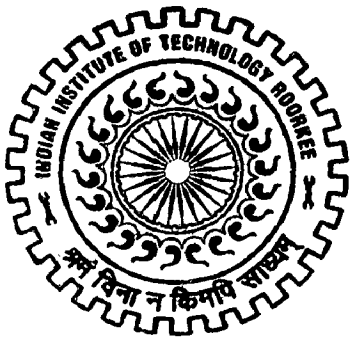

DEPARTMENT OF ELECTRICAL ENGINEERING
INDIAN INSTITUTE OF TECHNOLOGY ROORKEE
ROORKEE - 247 667 (INDIA)

JUNE, 2008

I.D. No.-M.T. 454/2008-38/SPD/PA

CANDIDATE'S DECLARATION

I hereby declare that the work which is being presented in this dissertation entitled, "**Performance Evaluation Of Matrix Converter Fed Induction Motor Drive**" submitted in the partial fulfillment of the requirements for the award of the degree "**Master of Technology**" with specialization in **Power Apparatus And Electric Drives**, to the **Department of Electrical Engineering, IIT Roorkee, Roorkee,** is an authentic record of my own work carried out during the period from August 2007 to June 2008 under the supervision of **Dr. Pramod Agarwal**, Professor, Department of Electrical Engineering, IIT Roorkee, Roorkee and **Dr. S. P. Dubey**, Assistant Professor, Department of Electrical Engineering, IIT Roorkee, Roorkee.

The matters embodied in this report have not been submitted by me for the award of any other degree or diploma.

Date: June 2008

Place: Roorkee

(N.V.D.V.PRASAD MADASU)

CERTIFICATE

This is to certify that above statement made by candidate is correct to the best of my knowledge.

Dr. S. P. Dubey,
Assistant Professor,
Department of Electrical Engineering,
IIT Roorkee

Dr. Pramod Agarwal,
Professor,
Department of Electrical Engineering,
IIT Roorkee.

ACKNOWLEDGEMENT

I would like to give my sincere gratitude to **Dr. Pramod Agarwal**, Professor, Department of Electrical Engineering, **Indian Institute of Technology, Roorkee**, and Dr. S. P. Dubey, Assistant Professor, Department of Electrical Engineering, **Indian Institute of Technology, Roorkee**, for pointed me to the topic **Performance Evaluation Of Matrix Converter Fed Induction Motor Drive,** as well as providing me all the necessary guidance and the inspirational support throughout the Dissertation.

My heartfelt gratitude and indebt ness goes to all the staff of **Power apparatus & Electric drives** group who, with their encouraging and caring words, constructive criticism and suggestions have contributed directly or indirectly in a significant way towards completion of this Dissertation.

I convey my deep sense of gratitude to the Head of Electrical Engineering Department, who directly or indirectly helped me during the work.

I am indebted to all my classmates from Power apparatus & Electric drives group for taking interest in discussing my problems and encouraging me.

N. V. D. V. PRASAD MADASU
M.Tech (Power apparatus & Electric drives)

Abstract

In recent the progress of power device technology and development of large power integrated circuits have sparked renewed interest in direct ac-ac conversion. Although cycloconverters are well established as a means of direct ac-ac conversion, naturally commutated cycloconverters has serious problems as regard to output frequency range, input power factor and distortion of input and output waveform. Many of these problems can be overcome by a forced commutated cycloconverter comprising bilateral power switches, but more number of pulses is needed to achieve waveform quality with unrestricted output frequency resulting in more cost.

Matrix converter is a three-pulse forced commutated cycloconverter. Matrix converter is an array of controlled semiconductor switches that connects directly the three-phase source to any of the three-phase load without using any DC link or large energy storage elements, and therefore it is called "all-silicon solution". This converter has several attractive features such as: sinusoidal input and output currents, operation with unity power factor for any load, regeneration capability.

There are various control strategies used for Matrix converter, some modulation strategies for the matrix converter are reviewed. Simulation models of these control strategies are developed in MATLAB Simulink. This thesis concerns the matrix converter as an alternative power converter for induction motor drives and presents performance evaluation of Matrix Converter fed Induction Motor drive using Field-Oriented Control (FOC) and Direct Torque control (DTC) schemes. It is concluded that the matrix converter will be a powerful alternative to the existing drives in the future.

CONTENTS

LIST OF FIGURES

LIST OF TABLES

Chapter 1

Introduction

This chapter gives a brief overview on the static AC/AC power frequency conversion structures and introduces the matrix converter, which is the topic of this thesis. The matrix converter is a flexible power converter whose employment has been proposed in many different applications. The focus of this thesis will be upon the application of the matrix converter to induction motor drives or AC drives.

Firstly proposed in 1976, the interest in matrix converter has a steady growth, pushed by the progress of the power electronics device technology and the prospect of realizing a very compact and reliable all-silicon AC/AC converter. The historical path of the matrix converter technology is shortly covered, pointing out what the main issues are. Finally, structure of the thesis is explained.

1.1 Static AC/AC Power Frequency Converter

Many parts of industrial application request AC/AC power conversion. An AC/AC converter takes power from one ac system and delivers it to another with waveforms of different amplitude and frequency. This can be obtained with different systems, employing rotating electrical machinery, nonlinear magnetic devices or static circuits containing controllable power electronic switches. Restricting the analysis of AC/AC power frequency conversion to static circuits, there are two types:

a) Indirect AC/AC converter
b) Direct AC/AC converter

Indirect schemes consist of two or more stages of conversion and an intermediate DC-link stage is always present. A typical example of two stage indirect AC/DC/AC power frequency conversion is the diode-

bridge rectifier-inverter structure, in which an AC power is firstly converted to a DC power (diode rectifier), and then converted back to an AC power at variable frequency (inverter). In direct conversion schemes a single stage carries out the AC/AC power frequency conversion.

1.1.1 Indirect AC/AC power Frequency Converter

In Fig. 1.1 two indirect schemes are shown. The scheme showed in Fig.1.1 (a) represents the well-known Diode-Bridge Voltage Source Inverter (DB-VSI) topology that is today the preferred solution in AC drive technology, especially in the low- and medium-power range. The diode-bridge converts the electrical power from AC to DC, realizing along with the DC-link filter the rectification stage, while the voltage source inverter converts DC back to AC with variable amplitude and frequency voltages, carrying out what is usually named inversion stage.

This is a very popular and consolidated conversion scheme. It is a reliable solution with low production costs, simple to implement and with high performance modulation strategies available (Pulse Width Modulation, Space Vector Modulation, etc.). But it has also some drawbacks. The input AC currents drawn by the diode-bridge rectifier contain a large amount of harmonics that produces distortion of the input line voltages, having a negative impact on the performance of sensitive loads and equipments connected to the same supply. These current harmonics cause additional harmonic losses on the utility system and may excite electrical resonance, leading to large overvoltages.

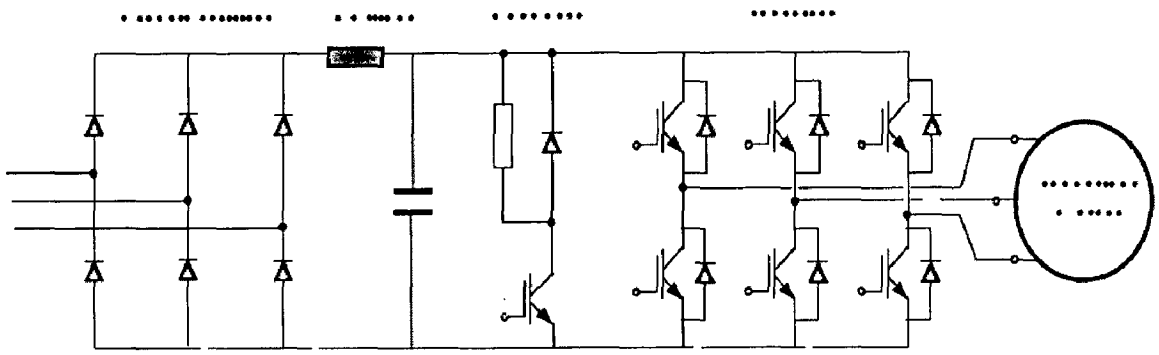

(a)

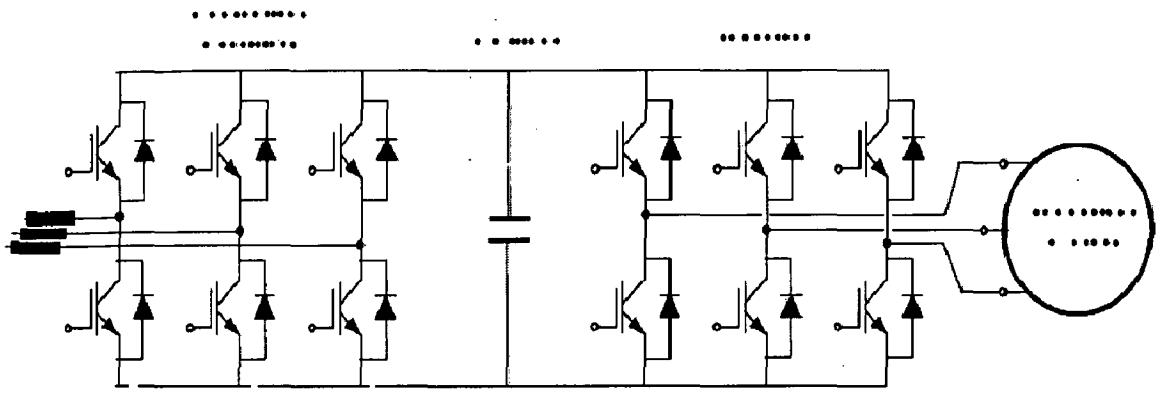

(b)

Fig.1.1. AC/AC indirect power frequency converter, with intermediate DC-link a) Diode rectifier-PWM VSI converter. b) PWM rectifier-PWM VSI converter.

As the current direction in a diode rectifier cannot reverse, some mechanism must be implemented to handle an eventual energy flow reversal, as during an electromagnetic braking of the motor, in order to avoid that the DC-bus voltage can reach destructive levels. In the DB-VSI conversion scheme such mechanisms are always dissipative ones and hence they can be effectively employed only when the energy to dissipate is low.

The DC-link capacitor represents another weak point of the indirect conversion scheme, particularly for those using electrolytic capacitors. These capacitors have high energy storage capability but also a high temperature sensitivity which reduces their lifetime, as shown in Fig.1.2, determining higher maintenance costs of the conversion system. It should be noted that the electrolytic capacitor have by far the shortest lifetime of any element, active or passive, used in power electronic converters.

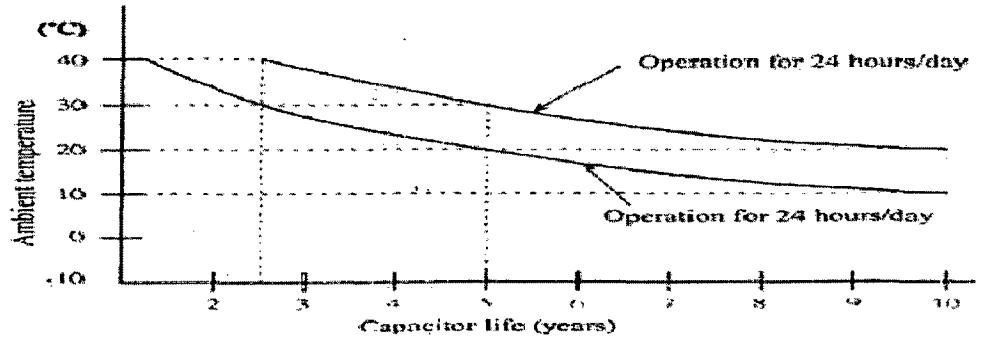

Fig.1.2. Capacitor life-time expectation depending on the ambient temperature in a low-power industrial diode-bridge VSI

The topology of the indirect conversion scheme (b), shown in Fig.1.1, differs from (a) for the rectification stage, where the diode-bridge rectifier is replaced by PWM-controlled- rectifier. This solution makes possible for the conversion system a bidirectional power flow from the main to the motor, which might become attractive for those medium and high power range applications in which regenerative operations and speed reversals are involved in steady state operating conditions, as in hoisting applications like elevators and cranes. Moreover, a PWM controlled rectifier allows for a strong reduction of the input currents harmonic distortion content, due to the high switching frequency of the rectifier, and a consequent reduction of the filtering components required.

But there are also some disadvantages. The cost is higher, due to a higher number of power semiconductor devices, the combined control of the PWM-controlled rectifier and inverter is quite complicated. In addition, the reliability problem related to the reduced lifetime of the DC link capacitor holds. For these reasons, the indirect conversion scheme (b) of Fig. 1.1. is still scarcely employed.

1.1.2 Direct AC/AC power Frequency Converter

Direct static AC/AC power frequency converters basically consist of an array of static power switches connected directly between the input and output terminals. The basic operating principle is to piece together an output voltage waveform with the desired fundamental component from selected segments of the input voltage waveforms. The most-known example of this type of power frequency converter probably is the classical cycloconverter, proposed in the early 1930s. There are two types of cycloconverters:

a) Naturally commutated cycloconverter (NCC)
b) Forced commutated cycloconverter (FCC).

In NCC the switches are naturally turned-off by the voltages of the AC supply. Also for these reasons thyristors are commonly used as switches. As a consequence of such operating mode, in NCC the maximum output frequency is limited to a value that is only a fraction, one third or

one-half, of the source frequency. This upper output frequency limit is a serious constraint in AC motor drive applications, which can be overcome only when the AC power supply for the cycloconverter is generated by an engine-driven high frequency generator.

In FCC the turn-off of the switches is independent of the source and load voltages allowing by proper switching techniques the output frequency to be higher than the input frequency. For FCC thyristors are not the best-suited switches as they do not have self-turn off-capability; auxiliary commutating circuits and components should be added.

A cycloconverter can be viewed as made up of a number of phase-controlled converter circuits connected to an AC supply system. Each converter circuit is controlled so that a different-frequency output voltage waveform is generated from segments of the same polyphase input voltages. In Fig. 1.3 a three-phase to three-phase cycloconverter consisting of three-phase, half wave, phase-controlled converters is shown.

In NCC the control of the output voltage and frequency is carried out by a proper modulation of the thyristors firing angle α. For given input supply voltages and number of input phases, the thyristors' firing angle α represents the unique control variable of converters output. In Fig. 1.4 it is shown the voltage and current waveforms for one of the positive group converter of the phase-controlled cycloconverter in Fig. 1.3. as result of a proper modulation of the thyristors firing angle. For a naturally commutated cycloconverter the theoretical maximum input/output voltage transfer ratio r_{max} is given by

$$\frac{V_{omax}}{V_{imax}} = r_{max} = \frac{m}{\pi}\sin\left(\frac{\pi}{m}\right)$$

where m is the number of the input phases. In the case of three input phases $r_{max} = 0.827$.

Since based on a phase-controlled operating mode, the cycloconverter draws from and feed to the AC supply non-sinusoidal currents. Moreover, due to the direct connection between the input and

output phases, when a reactive load has to be fed by the AC supply through a cycloconverter, a reactive power transfer must take place through the cycloconverter itself. As a consequence, power factor, fundamental input displacement angle and harmonic distortion have to be considered as functional characteristics of the converter; this holds for all the direct power frequency converters.

In NCC the input current always lags the supply voltage, because phase delay is always present, irrespective of the nature of the load. This

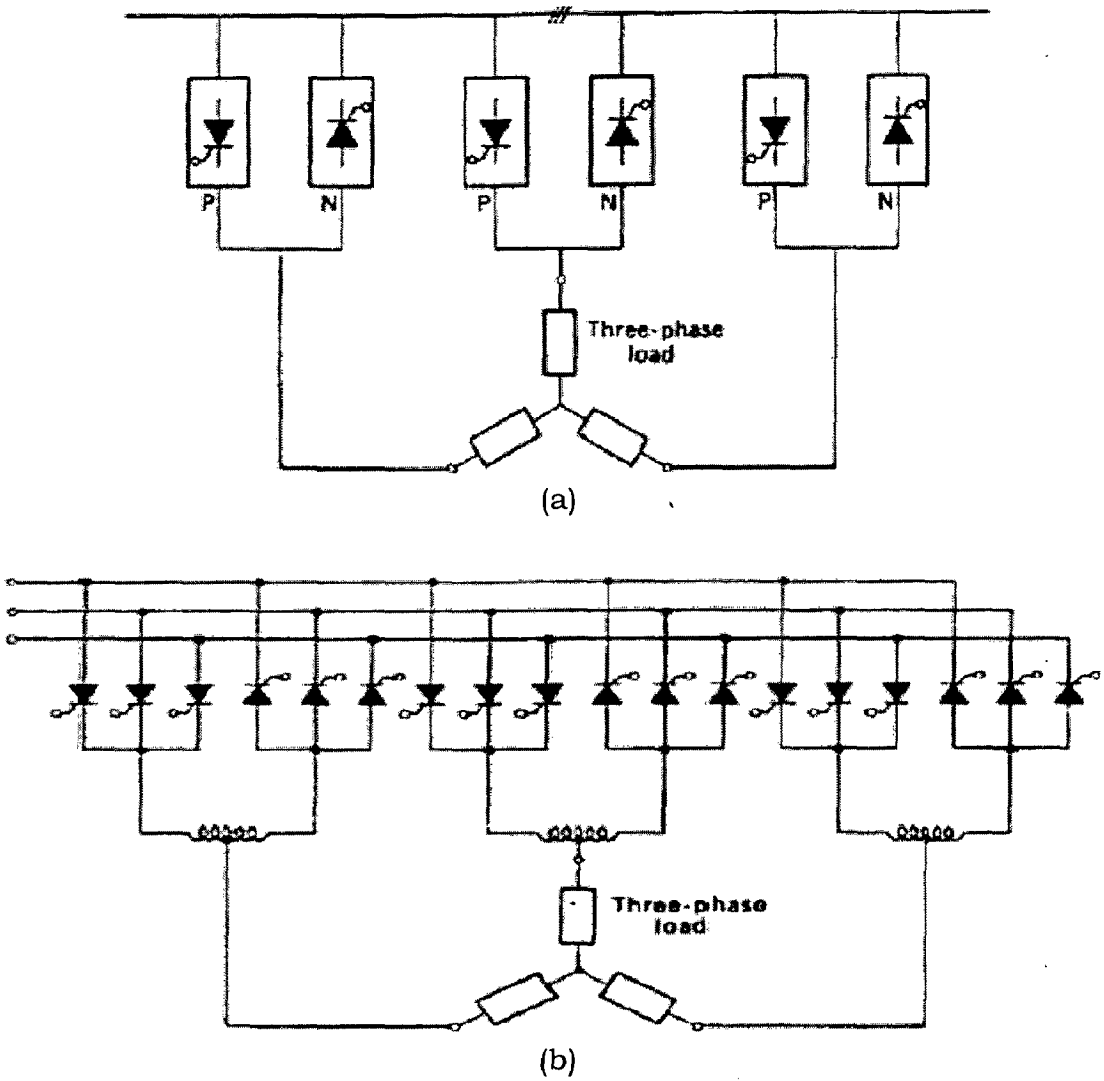

Fig.1.3. Three-phase to three-phase half wave cycloconverter
(a) Schematic diagram (b) basic circuit

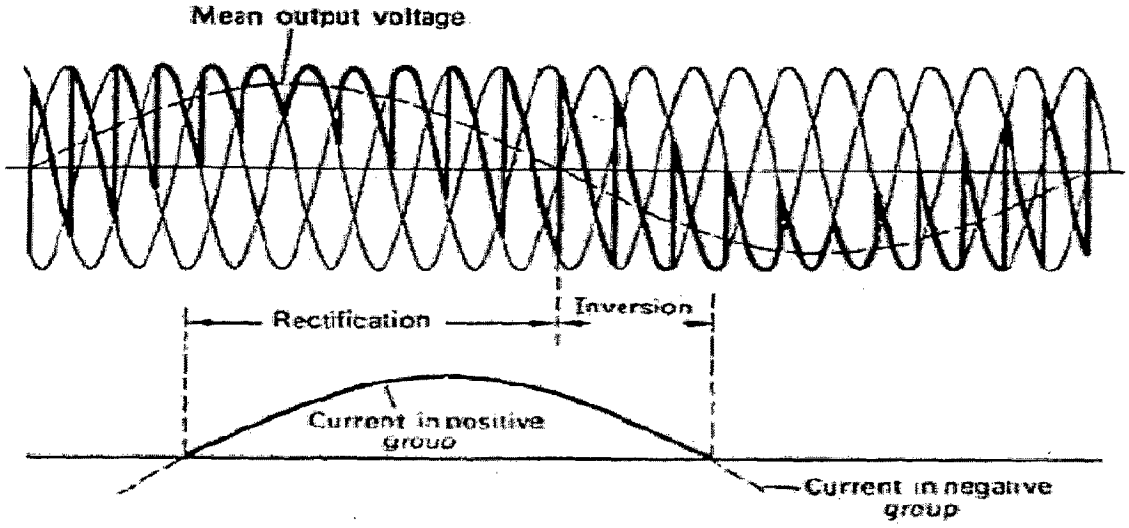

Fig. 1.4. Voltage and current waveforms for the positive group of a Phase-controlled cycloconverter when feeding an inductive load at 0.6 power factor.

means that the fundamental input displacement factor can be never at unity, as it is shown in Fig. 1.5. The harmonic distortion factor of input currents is also significant.

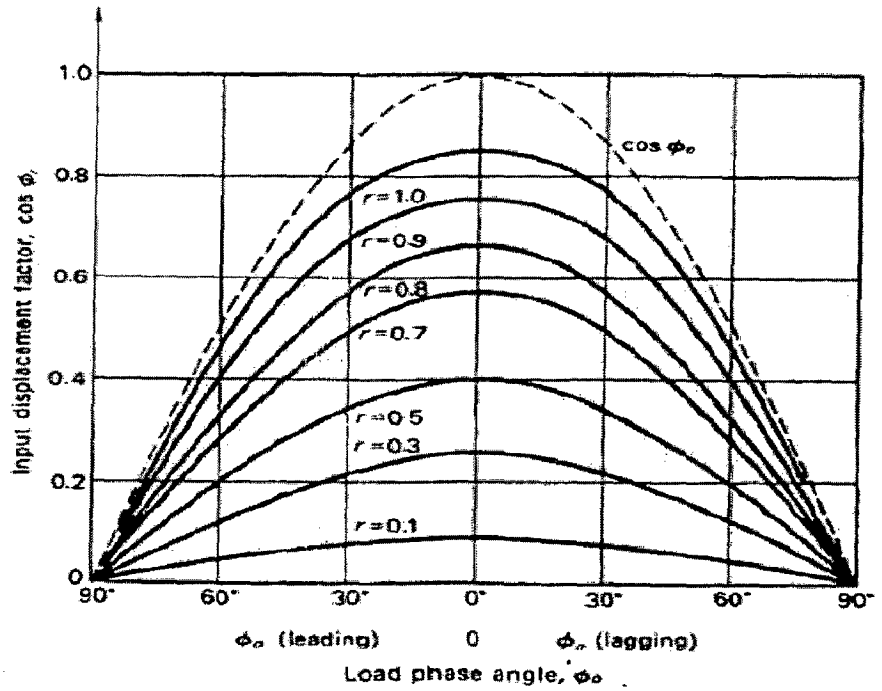

Fig 1.5: Variation of the input displacement factor for a phase controlled cycloconverter

Making a comparison with indirect DC-link converter, the naturally commutated cycloconverter has the advantages of having lower

commutation and conduction losses, allowing for a more compact power circuit design, and of having inherent bidirectional power flow capability. But it has also some relevant disadvantages, as the low output frequency upper limit, the lower input/output voltage transfer ratio, the large number of thyristors which requires complex control circuitry, and last, but not least, the poor input power factor. Because of these features, the major applications of naturally commutated cycloconverters have been restricted to low-speed, high power reversible AC drives.

Many of the above NCC limitations can be overcome with forced-commutated cycloconverter. By introducing semiconductor devices with self-turn-off capability it becomes possible to implement more sophisticated control algorithms that using high switching frequency allow the output frequency to be higher than the input frequency, the input power factor and the input/output voltage transfer ratio to be improved.

1.2 Matrix Converter

The matrix converter is nothing but a three-phase to three-phase forced commutated cycloconverter. It consists of nine bidirectional switches that connect each output phase to each input phase without using DC link elements, as it is shown in Fig.1.6.

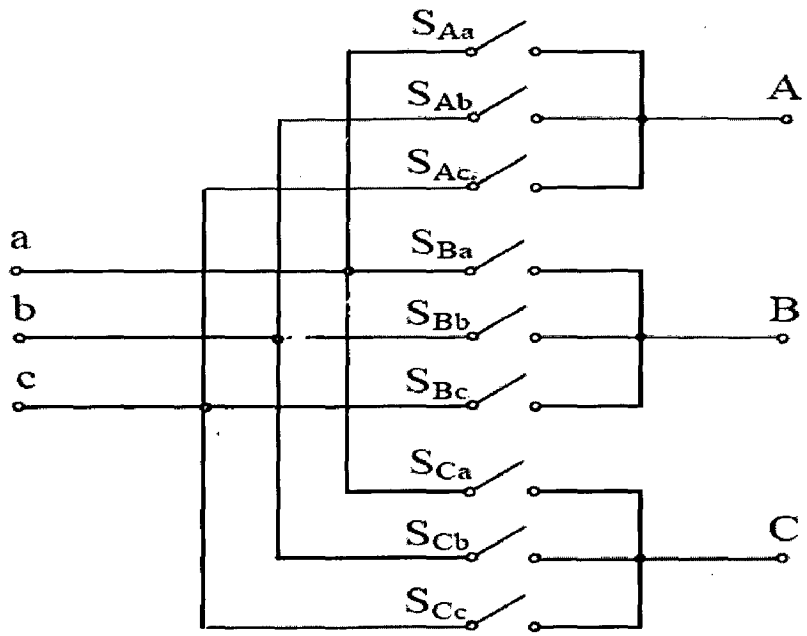

Fig. 1.6. Schematic circuit of a three-phase to three-phase matrix converter [5].

1.3 Literature Survey

Development of matrix converter:

The matrix converter topology was originally presented in 1976 by Gyugyi-Pelly [1] but it was in 1980 that the basic configuration and control of three-phase matrix converter were introduced by Venturini in [2]. In this method, the voltage transfer ratio was limited to 0.5. Later, the voltage transfer ratio was extended to 0.866 by taking advantage of a third harmonic injection method known as the Optimum Alesina–Venturini method [3].

The literature review on Matrix converter is classified into the following categories:

a. Modulation techniques of matrix converter
b. Commutation techniques of matrix converter
c. Protection circuit for matrix converter
d. Modeling, simulation and construction of matrix converter
e. Applications of matrix converter
f. New topologies based on matrix converter

Modulation techniques of matrix converter:

Alesina and Venturini proposed a modulation technique in [2],[3] which is called direct transfer function approach, the output voltages are obtained by the multiplication of the modulation matrix with the input voltages.

A conceptually different control technique based on the 'fictitious dc link' idea was introduced by Rodriguez in 1983 [4][5]. In 1985-86, P. D. Ziogas along with S.I. Khan and M. H. Rashid published [6] and [7] which expanded on the "fictitious dc link" idea of Rodriguez and provided a rigorous mathematical explanation.

In 1989, L. Huber along with D. Borojevic and N. Burany published a set of papers [8]-[12]. In these papers analysis, design and implementation of the space vector modulated (SVM) 3-φ to 3-φ matrix converter with input power factor correction, simultaneous output voltage and input current space vector modulation, is systematically reviewed.

In 1997, Jun Oyama, Xiaorong Xia, Tsuyoshi Higuchi, Koji Kuroki and Eiji Yamada proposed a paper on "Variable Voltage Variable Frequency (VVVF) online control of matrix converter" [13]. This control method can online control input current waveform and output voltage waveform to sinusoidal even if there is fluctuation, asymmetry and harmonics in the supply voltage.

In 2002, Frede Blaabjerg, Domenico Casadei, Christian Klumpner and Marco Matteini proposed a paper [14] in which the input current performance of matrix converters is analyzed, especially with reference to the operating conditions determined by unbalanced supply voltages. The space-vector modulation (SVM) technique is utilized to calculate the duty cycles of the active voltage vectors that must be applied, in each switching cycle period, in order to satisfy the input and output requirements.

In 2002, P. Mutschler and M. Marcks proposed "Direct control" modulation method [15]. In this a direct current control method of matrix converter is developed.

In 2002, Domenico Casadei, Giovanni Serra, Angelo Tani, and Luca Zarri proposed a paper [16] in which a novel representation of the switch state of a three-phase to three-phase matrix converter is presented. This approach, based on space-vector notation, simplifies the study of the modulation strategies, leading to a complete general solution of the problem and providing a very useful unitary point of view.

In 2004, Lars Helle, Kim B. Larsen, Allan Holm Jorgensen, Stig Munk-Nielsen, and Frede Blaabjerg, proposed a paper [17] which presents a method for evaluating different modulation schemes employed with three-phase to three-phase matrix converters.

In 2006, Christian Klumpner, Frede Blaabjerg, Ion Boldea, Peter Nielsen proposed a paper [18] on new modulation method which uses stator flux vector reference in the inversion stage and selects a single active voltage vector and an associated zero vector in order to minimize the stator flux error.

In 2007, Matti Jussila, and Heikki Tuusa proposed a paper [19] which concerns the effect of symmetric supply voltage harmonics in a space-vector modulated three-phase indirect matrix converter (IMC).

Commutation techniques of matrix converter:

A critical issue in control of this converter is current commutation as no freewheel path is available for the load current.

In 1989, Burany proposed a paper [20] which is a radical solution for the commutation process and concerns 4QSWs where separated internal conduction paths exist in the two possible directions of the load current.

During 1998-2004, Patrick W. Wheeler, Jon C. Clare, Lee Empringham, Michael Bland and Maurice Apap proposed a set of papers [21][22][23] which deals with the problem of snubberless commutation in matrix converters. A novel method employs current detection within intelligent gate drive circuits for each bidirectional cell which communicate with the gate drives of other cells.

During 1998-2003, M. Ziegler and W. Hofmann proposed a set of papers [24]-[27] which deals with a two steps and one-step commutation strategy for Matrix Converters.

In 2001, Lixiang Wei and Thomas A. Lipo proposed a paper [28] which discloses a novel matrix topology with advantages over the usual matrix converter topology in which all the switches at line side turn on and turn off at zero current; the converter does not have any commutation problems as required by the conventional matrix converter.

In 2006, A. Dasgupta, S. Mukherjee, M. Sengupta, P. Syam and A. K. Chattopadhyay presented a paper [29] in which FPGA implementation of a semi-soft four- step commutation technique based on output current direction in matrix converter is presented. The same program can be used implementing a three-step commutation process.

Protection circuit for matrix converter:

During 1997-1999,P.Nielsen, F. Blaabjerg, J. K. Pedersen, in their papers [30] [31] presents the design of snubber/clamp circuit protection for a matrix converter for induction motor and it also proposes two new component minimized protection circuits which have half the number of diodes.

During 2002-2004, Christian Klumpner and Frede Blaabjerg presents a set of papers [32] [33] in which a new solution to provide limited ride-through operation is presented with a matrix converter using a scalar controlled induction motor for a duration of hundreds of millisecond and a new method to provide short-term braking capability during a power outage for matrix converters.

In 2002, Eduardo P. Wiechmann, Rolando P. Burgos and José Rodriguez proposed a paper [34] which presents a ride-through strategy for MC adjustable-speed drives.

In 2002, Han Ju Cha and Prasad N. Enjeti proposed a paper [35] in which a new ride-through approach for matrix converter fed adjustable speed drives (ASDs) is discussed and the topology of conventional matrix converter is modified with the addition of three IGBTs and a dc-link capacitor.

In 2005, B. W. Augdahl, H. L. Hess, B. K. Johnson and D.C. Katsis proposed a paper [36] in which a new output protection strategy is presented. This added output protection will be capable of protecting a matrix converter and load when used in battlefield applications.

Modeling, simulation & construction of Matrix Converter:

In 2005, J. Rodriguez, E. Silva, F. Blaabjerg, P. wheeler, J. Clare and J. Pontt presented a paper [37] in which a complete simulation scheme, using Matlab–Simulink, is discussed.

In 2005, Christian Dufour, Lixiang Wei. Thomas A. Lipo proposed a paper [38] which describes real time simulator of matrix converter system with source, input filter and load.

During 2004-2006, M. Imayavaramban, A.V. Krishna Chaithanya and B.G. Fernandes presented a set of papers [39] [40] which presents the work carried out in developing a mathematical model for a Matrix converter. The power circuit of the matrix converter is realized by using mathematical expressions.

Applications of matrix converter:

In 1994, Sedat Stinter and Jon C Clare proposed a paper [41] which describes the design and construction of a matrix converter rated at 4OOV. 10A. A novel gate drive arrangement which has transformer isolation and does not require the use of isolated power supplies is used.

In 2001, Domenico Casadei, Giovanni Serra, and Angelo Tani proposed a paper [42] in which a new control method for matrix converters is proposed which allows, under the constraint of unity input power factor, the generation of the voltage vectors required to implement the direct torque control (DTC) of induction machines.

In 2002, Christian Klumpner, Peter Nielsen, Ion Boldea and Frede Blaabjerg proposed a paper [43] which presents the first integrated regenerative frequency converter motor for industry applications, based on a matrix converter topology.

In 2005, Thomas F. Podlesak, Dimosthenis C. Katsis, Patrick. Wheeler, Jon C. Clare, Lee Empringham and Michael Bland proposed a

paper [44] which describes the design; construction, and testing of a 150-kVA closed-loop vector-controlled matrix converter induction motor drive.

In 2005, Hassan Nikkhajoei and M. Reza Iravani proposed a paper [45] which investigates the use of an AC–AC matrix converter, as an alternative to AC–DC–AC converter system, to interface a high-speed micro-turbine generator (MTG) to a utility grid as a distributed generation unit.

In 2005, S. M. Barakati, M. Kazerani and X. Chen proposed a paper [46] in which a wind energy conversion scheme based on the matrix converter topology is proposed.

In 2005, Yang Mei, Kai Sun, Daning Zhou, Lipei Huang and Kouki Matsuse proposed a paper [47] in which an auxiliary drive system for diesel using matrix converter is proposed and the working principles are discussed.

In 2006, Yang Mei, Kai Sun, Daning Zhou, Lipei Huang and Xuansan Cai proposed a paper [48] in which a novel power device application and high performance control for a matrix converter fed induction motor drive system, as well as the behavior the MC drive under abnormal input voltage conditions have been investigated.

In 2006, Kyo-Beum Lee and Frede Blaabjerg proposed a set of papers [49] [50] [51] in which a simple direct torque control (DTC) method for sensor less matrix converter drives and a new sensor less vector control system for high performance induction motor drives fed by a matrix converter with nonlinearity compensation and disturbance observer are proposed.

New topologies based on matrix converter:

In 2000, Siyoung Kim, Seung-Ki Sul and Thomas A. Lipo proposed a paper [52] in which a new type of ac/ac converter is proposed. The proposed converter is capable of direct ac/ac power conversion and, except for a few small snubber elements; it does not require the use of any input inductors or a dc-link capacitor. In contrast to the matrix converter,

which requires bidirectional switches, the proposed converter consists of only unidirectional switches such as insulated gate bipolar transistors.

In 2002, Christian Klumpner and Frede Blaabjerg proposed a paper [53] in which a new Direct Power Electronic Conversion Topology suited for multi-drive application is proposed, having an input port for a three-phase power supply and several output ports to connect three-phase loads, which are independently controlled.

1.4 Author's Contribution

In this thesis different modulation techniques of Matrix Converter (MC) are presented along with their simulations. Compensation techniques for unbalanced and distorted voltages are presented. In this thesis performance evaluation of MC fed Induction motor drive is done using both Direct Torque Control and Field Oriented Control and their results are compared. In this thesis parameter sensitivity of DTC and FOC using MC are presented.

1.5 Dissertation Outline

The contents of this dissertation are organized in six chapters in the following manner.

Chapter 1 introduces AC/AC converters and Matrix Converter as an advanced direct AC/AC converter. Then, a review of the previous work in the area of Matrix Converter is addressed.

Chapter 2 gives a general description of the fundamentals of matrix converters. The topology is presented and the possible configurations which allow implementing a bi-directional switch are discussed. A qualitative analysis of the matrix converter performance is carried out; advantages and disadvantages are emphasized. The chapter also presents an overview of the complete matrix converter drive, paying attention to some implementation aspects which are still somehow outstanding matters like the input filter and the protection strategy of the converter.

Chapter 3 focuses on the modulation and control of the three-phase matrix converter. A brief review of the different control strategies proposed in literature is given. Then, three modulation strategies based on the Space Vector modulation (SVM) technique are considered.

Chapter 4 presents a control algorithm which allows the use of matrix converter in Direct Torque Control (DTC) and Field Oriented Control (FOC) for induction motor.

Chapter 5 presents the simulation results for 3-phase to 3-phase Matrix Converter using Venturini modulation method and SVM technique for different output frequencies with R-L load. Simulation results for Matrix Converter in Direct Torque Control (DTC) and Field Oriented Control (FOC) for induction motor and their comparison are presented.

Chapter 6 presents conclusions drawn from the work done are presented. Future scope for improvements in the field to improve the performance and to handle the problems associated are briefly studied and presented to carry out in upcoming projects.

Chapter 2

Fundamentals of Matrix Converter

This chapter aims to give a general description of the basic features of a three phase to three phase matrix converter in terms of performance and of technological and implementation issues.

2.1 Introduction

The transformation and control of energy is one of the most important processes in electrical engineering. In recent years this work has been done with the use of power semiconductors and energy storage elements such as inductances and capacitors. Several converter families have been developed: rectifiers, inverters, choppers, cycloconverters, etc. Each of these families has its own advantage and limitations. The main advantage of all static converters over other energy processors is the high efficiency that can be achieved. One of the most interesting families of converters is that of the so called matrix converter.

Characteristics:

1) Simple and compact power circuit due to absence of large energy storage elements.
2) Generation of output voltage with arbitrary amplitude and frequency.
3) Sinusoidal input and output currents.
4) Operation at unity input power factor.
5) Bidirectional power flow.
6) 4-quadrant operation.
7) High reliability.
8) Harmonic reduction

Limitations:

1) Lack of bidirectional switches.
2) Lower voltage transfer ratio.
3) Sensitive to power disturbances as they will transmit directly to output side of the converter.
4) No freewheeling paths, it is difficult to reliably commutate current from one switch to another.
5) Input power factor cannot be lower than output power factor.

2.2 Topology

In general matrix converter is a single stage converter with m x n bidirectional power switches, designed to connect m-phase voltage sources to n-phase load. The matrix converter of 3 x 3 switches, shown in Fig 2.1 connects a three phase source to three phase load.

In the basic topology of the Matrix Converter shown in Fig 2.1, V_{si} i={A,B,C}, are the source voltages, i_{si}, i={A, B,C}, are the source currents, V_{jn} , j={a, b, c}, are the load voltages with respect to neutral n, and i_j , j={a, b, c}, are the load currents. Additionally, other auxiliary variables have been defined to be used as a basis of the modulation and control strategies: V_i i={A, B,C}, are the matrix converter input voltages i_i ; i={A, B,C}, are the converter input currents.

Each switch S_{ij}, i = {A, B, C}, j ={a, b, c}, can connect or disconnect phase i of the input stage to phase j of the load and, with a proper combination of the conduction states of these switches, arbitrary output voltages V_{jN} can be synthesized. Each switch is characterized by a switching function, defined as follows:

S_{ij} (t) = 0 if switch S_{ij} is open

S_{ij} (t) = 1 if switch S_{ij} is closed (2.1)

Switching state rules:

1) Do not connect two different input lines to same output line. This

results in short circuit as the matrix converter is fed by voltage source.

2) Do not disconnect the output line. This results in open circuit and causes overvoltage as the load is inductive load.

These conditions can be stated in more compact form as follows:

$$\sum_{i=A,B,C} S_{ij}(t) = 1; j = \{a, b, c\} \tag{2.2}$$

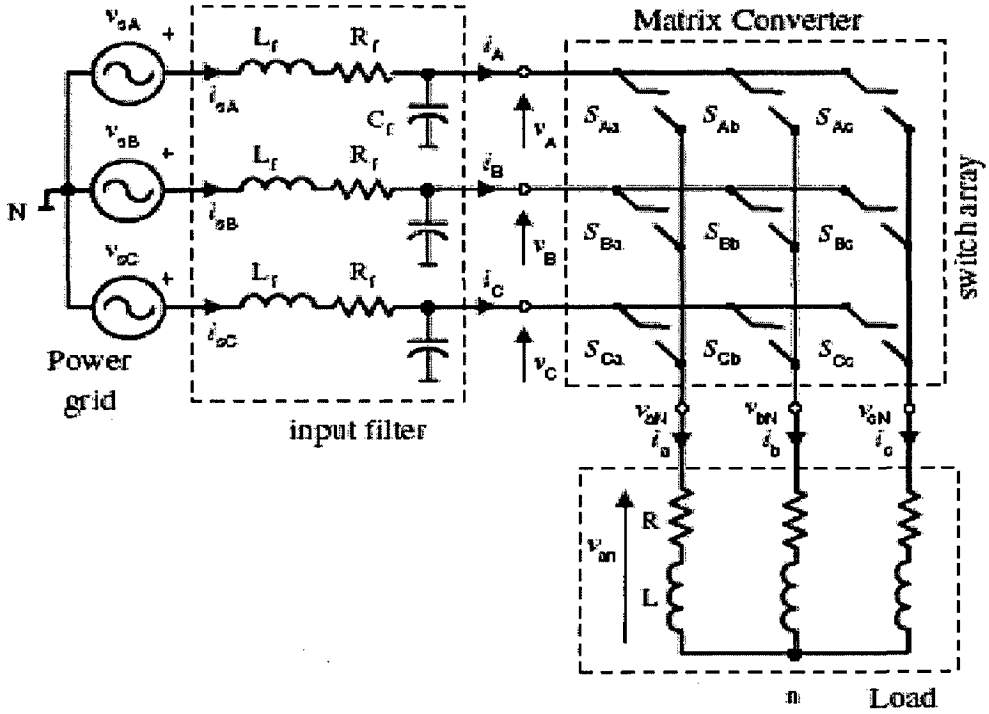

Fig 2.1: Basic power circuit of matrix converter [5]

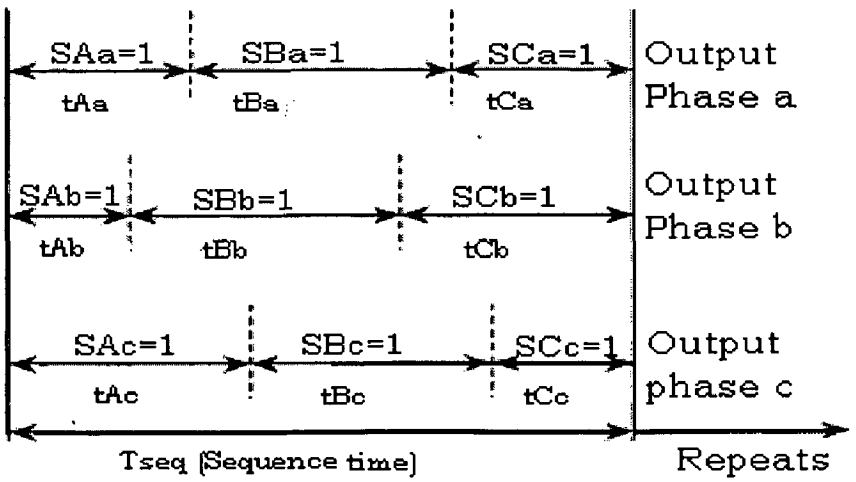

Fig 2.2 General form of switching pattern [5].

Applying Kirchhoff's voltage law to the switch array, it can be easily found that:

$$\begin{bmatrix} V_{aN}(t) \\ V_{bN}(t) \\ V_{cN}(t) \end{bmatrix} = \begin{bmatrix} S_{Aa}(t) & S_{Ba}(t) & S_{Ca}(t) \\ S_{Ab}(t) & S_{Bb}(t) & S_{Cb}(t) \\ S_{Ac}(t) & S_{Bc}(t) & S_{Cc}(t) \end{bmatrix} \tag{2.3}$$

It is worth noting that equation (2.3) is only valid if (2.2) holds. Otherwise, these equations are inconsistent with physical element distribution of Fig 2.1. Applying Kirchhoff's current law to the switch array, it is found that:

$$\begin{bmatrix} i_A(t) \\ i_B(t) \\ i_C(t) \end{bmatrix} = \begin{bmatrix} S_{Aa}(t) & S_{Ab}(t) & S_{Ac}(t) \\ S_{Ba}(t) & S_{Bb}(t) & S_{Bc}(t) \\ S_{Ca}(t) & S_{Cb}(t) & S_{Cc}(t) \end{bmatrix} \tag{2.4}$$

Equation (2.3) and (2.4) are the basis of all modulation methods which consists in selecting appropriate combinations of open and closed switches to generate the desired output voltages. It is important to note that the output voltages V_{jn}, j={a, b, c}, are synthesized using the three input voltages Vi, i={A, B,C} and that the input currents i_i, i={A, B,C} are synthesized using the three output currents i_j, j={a, b, c} which are sinusoidal if the load has a low pass frequency response.

2.3 The Performance Of Matrix Converter

This section gives a short description of what is the performance of a matrix converter. A qualitative analysis of some performance parameters is carried out.

2.3.1 The Output Voltage

Since no energy storage components are present between the input and output side of the matrix converter, the output voltages has to be generated directly from the input voltages. Each output voltage waveform is synthesized by sequential piecewise sampling of the input voltage waveforms. The sampling rate has to be set much higher than both input and output frequencies, and the duration of each sample is controlled in such a way that the average value of the output waveform within each sample period tracks the desired output waveform. As consequence of the

input-output direct connection, at any instant, the output voltages have to fit within the enveloping curve of the input voltage system. Under this constraint, the maximum output voltage the matrix converter can generate without entering the over- modulation range is equal to $\sqrt{3}/2$ of the maximum input voltage: this is an intrinsic limit of matrix converter and it holds for any control law. Entering in the over- modulation range, thus accepting a certain amount of distortion in the output voltages and input currents, it is possible to reach higher voltage transfer ratio.

In Fig.2.3 the output voltage waveform of a matrix converter is shown and compared to the output waveform of a traditional voltage source inverter (VSI). The output voltage of a VSI can assume only two discrete fixed potential values, those of the positive and negative DC-bus. In the case of the matrix converter the output voltages can assume either input voltage a, b or c and their value is not time-invariant: the effect is a reduction of the switching harmonics.

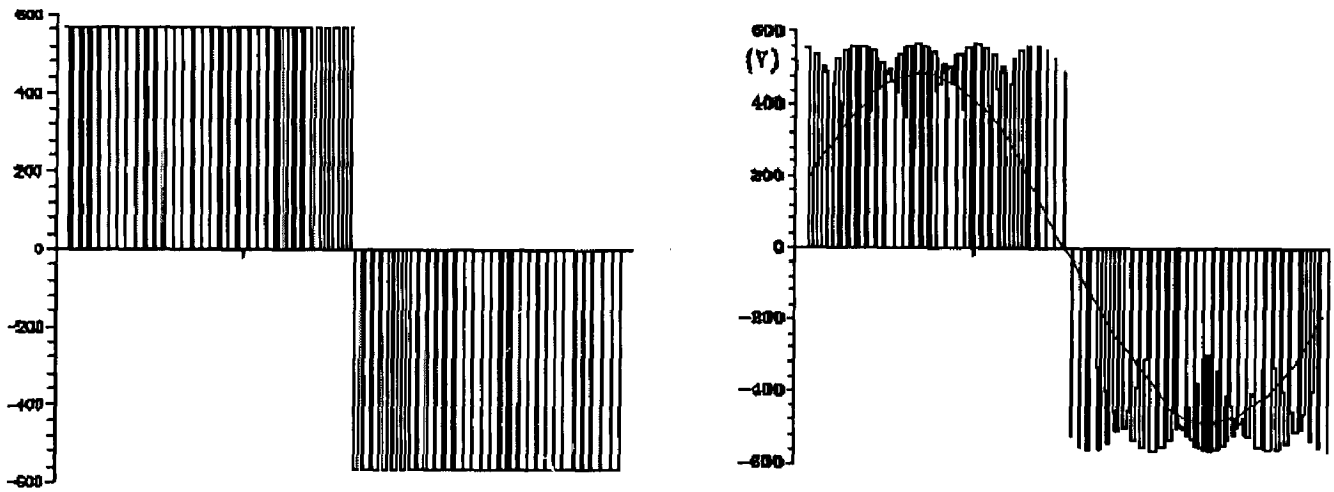

a) VSI *b) Matrix converter*

Fig 2.3: Output voltage waveforms generated by a VSI and a matrix converter

2.3.2 The input current

Likewise to the output voltages, the input currents are directly generated by the output currents, synthesized by sequential piecewise sampling of the output current waveforms. If the switching frequency of the matrix converter is set to a value that is much higher than the input and

output frequency, the input currents drawn by the converter are sinusoidal: their harmonic spectrum consists only of the fundamental desired component plus a harmonic content around the switching frequency. In Fig.2.4 the input current drawn by a matrix converter for a 2 kHz switching frequency is shown. It can be noted that the amplitude of the switching harmonic components is comparable to the fundamental amplitude. It is then obvious that an input filter is needed in order to reduce the harmonic distortion of the input line current to an acceptable level. It follows that care should be used in speaking about matrix converters as an "all silicon" solution for direct AC/AC power conversion, since some reactive components are needed.

The matrix converter performance in terms of input currents represent a significant improvement with respect to the input currents drawn by a traditional VSI converters with a diode bridge rectifier, whose harmonic spectrum shows a high content of low-order harmonics. By the light of the standards related to power quality and harmonic distortion of the power supply this is a very attractive feature of matrix converter.

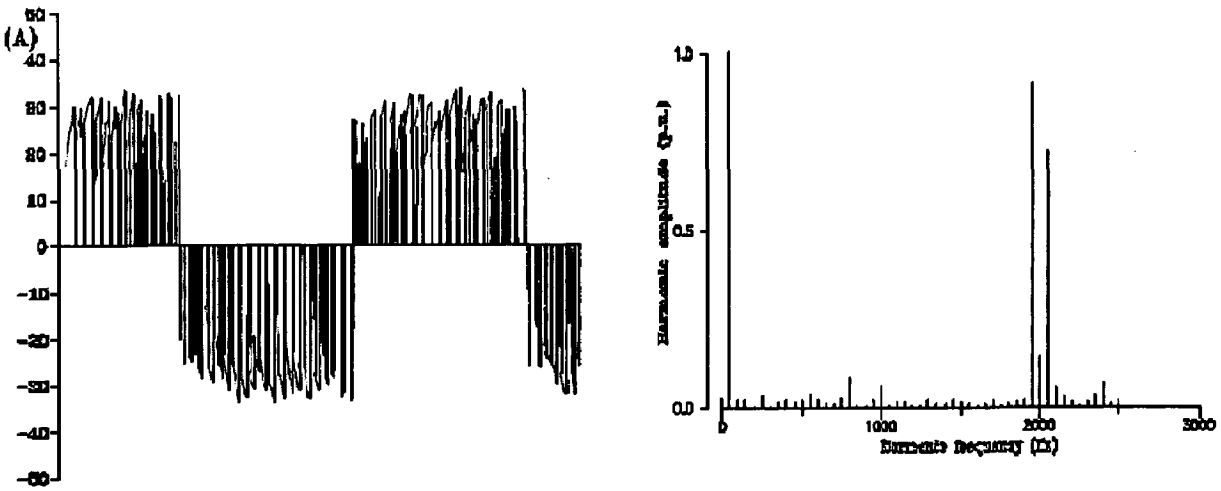

Fig.2.4: Matrix converter input current and harmonic spectrum. Switching frequency 2kHz.

2.3.3 The input power factor control

The input power factor control capability is another attractive feature of matrix converters, which holds for most of the control algorithms.

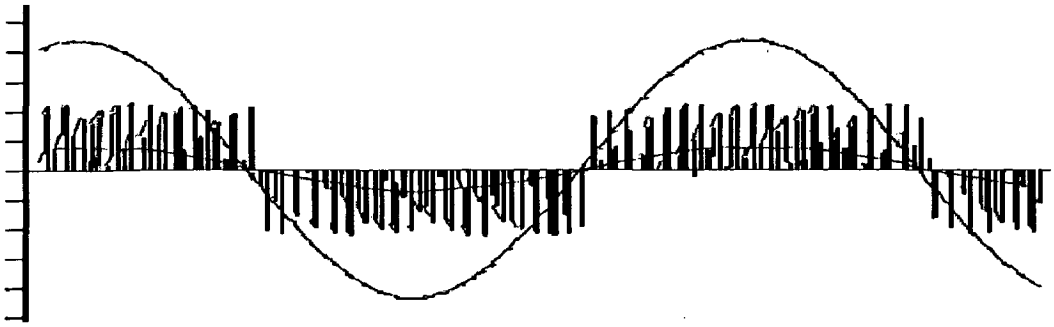

Fig.2.5: Matrix converter input line-to-neutral voltage, instantaneous input Current and its average value. Switching frequency 2 kHz.

2.4 Implementation of the Matrix Converter

Looking at the basic features of the matrix converter that have been briefly described in the previous sections it might be surprising to establish that this converter topology, today, has not found a wide utilization yet. The reasons have to be sought in a number of practical implementation problems that have slowed down the development of this technology.

2.4.1 Bidirectional Switch Realization

The matrix converter requires a bidirectional switch capable of blocking voltage and conducting current in both directions. Unfortunately, there are no such devices currently available, so discrete devices need to be used to construct suitable switch cells. In Fig 2.6 four switching variants can be sub-divided into:

a) Switches with bidirectional operations featured by 4 basic operations.
b) Switches without direction operations featured by 2 basic operations.

Two different stages of gate G :(1: charged 0: uncharged. Index v: forward r: reverse) leads in the case of topology with two transistor/gates to four different states of a bidirectional switch.

I. Forward blocking reverse blocking-that is interruption.
II. Forward conducting reverse blocking-that is ideal diode.
III. Forward blocking reverse conducting -that is ideal reverse diode.
IV. Forward conducting reverse conducting-that is bidirectional close.

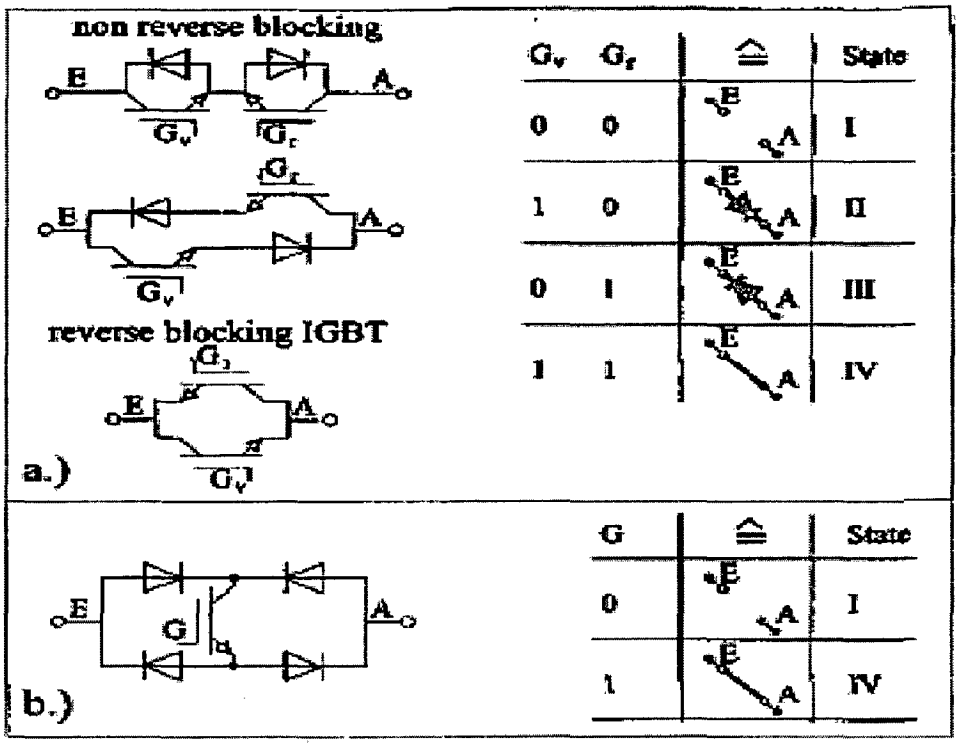

Fig 2.6: Bidirectional switches [20].

2.4.1.1 Diode Bridge Bidirectional Switch Cell

The diode bridge bidirectional switch cell arrangement consists of an insulated gate bipolar transistor (IGBT) at the center of a single-phase diode bridge arrangement as shown in Fig.2.7. The main advantage is that both current directions are carried by the same switching device, therefore, only one gate driver is required per switch cell. Device losses are relatively high since there are three devices in each conduction path. The direction of current through the switch cell cannot be controlled. This is a disadvantage, as many of the advanced commutation methods described later require this.

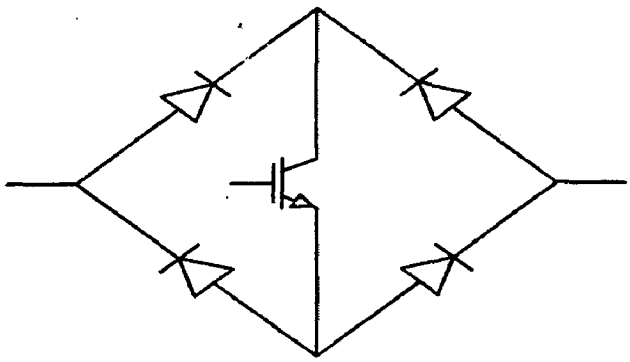

Fig 2.7: Diode bridge bidirectional switch [5]

2.4.1.2 Common Emitter Bidirectional Switch Cell

The common emitter bidirectional switch cell arrangement consists of two diodes and two IGBTs connected in anti parallel as shown in Fig. 2.8(a). The diodes are included to provide the reverse blocking capability. There are several advantages in using this arrangement than diode bridge bidirectional switch cell arrangement. The first is that it is possible to independently control the direction of the current. Conduction losses are also reduced since only two devices carry the current at any one time. One possible disadvantage is that each bidirectional switch cell requires an isolated power supply for the gate drives, but both devices can be driven with respect to the same voltage-the common emitter point.

2.4.1.3 Common Collector Bidirectional Switch Cell

The common collector bidirectional switch cell arrangement is shown in Fig. 2.8(b). The conduction losses are the same as for the common emitter configuration. An often-quoted advantage of this method is that only six isolated power supplies are needed to supply the gate drive signals. However, in practice, other constraints such as the need to minimize stray inductance mean that operation with only six isolated supplies is generally not viable. Therefore, the common emitter configuration is generally preferred for creating the matrix converter bidirectional switch cells.

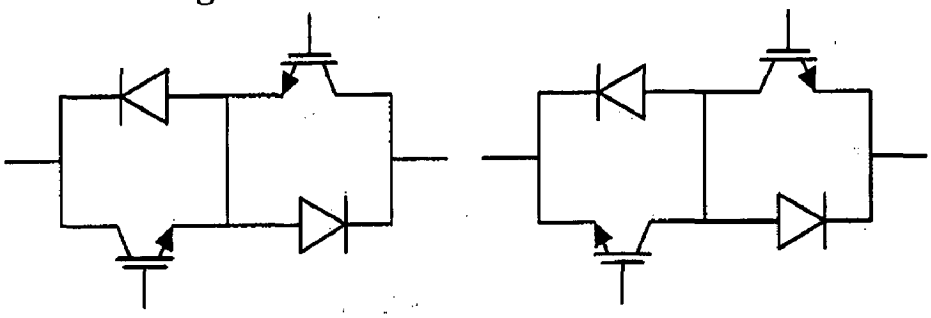

Fig 2.8: (a) Common emitter bidirectional switch
(b) Common collector bidirectional switch [5]

2.4.2 Current Commutation

Reliable current commutation between switches in matrix converters is more difficult to achieve than in conventional VSIs since there

are no natural freewheeling paths. The commutation has to be actively controlled at all times with respect to two basic rules. These rules can be visualized by considering just two switch cells on one output phase of a matrix converter. It is important that no two bidirectional switches are switched on at any instant, as shown pictorially in Fig 2.9(a). This would result in line-to-line short circuits and the destruction of the converter due to over currents. Also, the bidirectional switches for each output phase should not all be turned off at any instant, as shown in Fig.2.9 (b). This would result in the absence of a path for the inductive load current, causing large over voltages. These two considerations cause a conflict since semiconductor devices cannot be switched instantaneously due to propagation delays and finite switching times. Various methods have been proposed to avoid this difficulty and to ensure successful commutation.

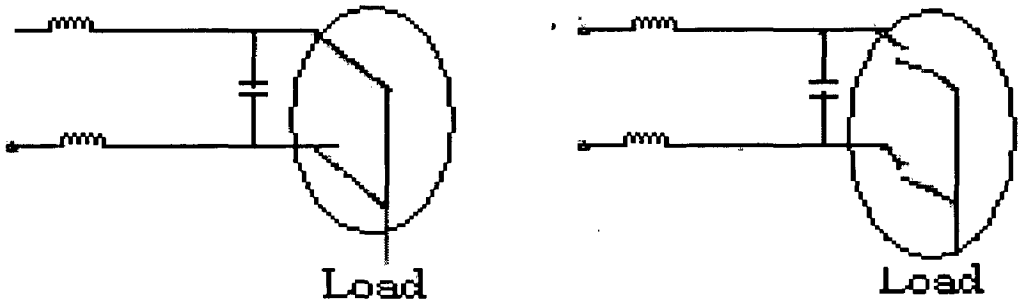

Fig 2.9: (a) Avoid short circuits on the matrix converter input Side
(b) Avoid open circuits on the matrix converter output lines [5]

2.4.2.1 Overlap Time Current Commutation

In overlap current commutation, the incoming cell is fired before the outgoing cell is switched off. This would normally cause a line-to-line short circuit but extra line inductance slows the rise in current so that safe commutation is achieved. This is not a desirable method since the inductors used are large. The switching time for each commutation is also greatly increased which may cause control problems.

2.4.2.2 Dead-Time Current Commutation

Dead-time commutation uses a period where no devices are gated, causing a momentary open circuit of the load. Snubbers or clamping devices are then needed across the switch cells to provide a path for the

load current. This method is undesirable since energy is lost during every commutation and the bidirectional nature of the switch cells further complicates the snubber design. The clamping devices and the power loss associated with them also results in increased converter volume.

2.4.2.3 Semi Soft Current Commutation

Overlap can be used to commutate the load current from one switch to the next switch without creating a short circuit if the incoming and outgoing halves of the bidirectional switches involved in the commutation process are independently controlled. This method of current control will allow zero current switching of the IGBTs if the outgoing device is reverse biased by the turning on the incoming device. This situation will occur when the voltage on the input line of the incoming switch is greater than the voltage on the input line of the outgoing switch in the conduction path. There is a 50% chance of the reverse bias occurring. For this reason an appropriate term for this type of current control is 'semisoft current commutation' (half the switching operation is achieved by natural or soft commutation).

Four Step Semi-Soft Current Commutation

A more reliable method of current commutation , which obeys the rules , use a four step commutation strategy in which the direction of current flow through the commutation strategy in which the direction of current flow through the commutation cells can be controlled . To implement this strategy, the bidirectional switch cell must be designed in such a way as to allow the direction of the current flow in each switch cell to be controlled. Fig.2.10 shows a schematic of a two-phase to single-phase matrix converter. In steady state, both of the devices in the active bidirectional switch cell are gated to allow both directions of current flow. The following explanation assumes that the load current is in the direction shown and that the upper bidirectional switch SW1 is closed. When a commutation to SW2 is required, the current direction is used to determine which device in the active switch is not conducting. This device is then turned off. In this case, device SW1B is turned off. The device that will

conduct the current in the incoming switch is then gated, SW2A in this example. The load current transfers to the incoming device either at this point or when the outgoing device SW1A is turned off. The remaining device in the incoming switch SW2B is turned on to allow current reversals. This process is shown as a timing diagram in Fig 2.11.

This method allows the current to commutate from one switch cell to another without causing a line-to-line short circuit or a load open circuit. One advantage of all these techniques is that the switching losses in the silicon devices are reduced by 50% because half of the commutation process is soft switching and, hence, this method is often called "semi-soft current commutation".

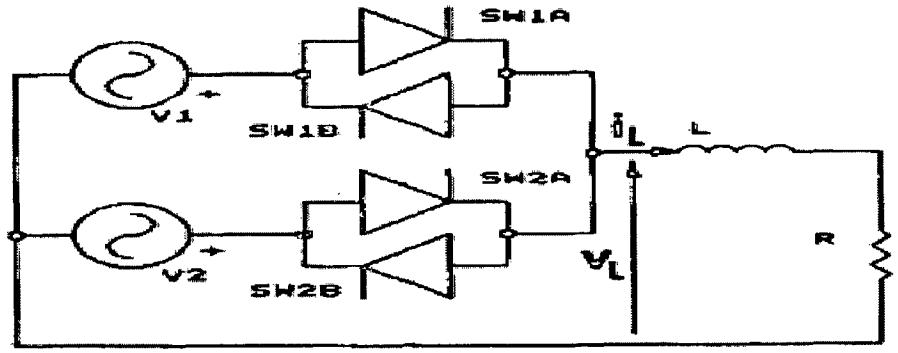

Fig 2.10: Two phase to single phase matrix converter [20]

Table 2.1 shows the legal combination of switch states. Switch states 1 and 2 can exist unconditionally but 3 to 8 are legal only for the sign of load current given in the table. It is not possible to come from conditional state 1 to 2 directly in one step, but it is possible using several conditional state combinations.

Table 2.1: Legal combinations of switch states

No	SW1A	SW1B	SW2A	SW2B	Sign of i_L
1.	1	1	0	0	+-
2.	0	0	1	1	+-
3.	1	0	0	0	+
4.	0	1	0	0	-
5.	0	0	1	0	+
6.	0	0	0	1	-
7.	1	0	1	0	+
8.	0	1	0	1	-

For i_L >0 the following four stepped switching policy is possible:

1. turn off SW1B(go to combination 3)
2. turn on SW2A(go to combination 7)
3. turn off SW1A(go to combination 5)
4. turn on SW2B(go to combination 2).

Analogously, for i_L<0 the following four stepped switching policy is possible:

1. turn off SW1A(go to combination 4)
2. turn on SW2B(go to combination 8)
3. turn off SW1B(go to combination 6)
4. turn on SW2A(go to combination 2).

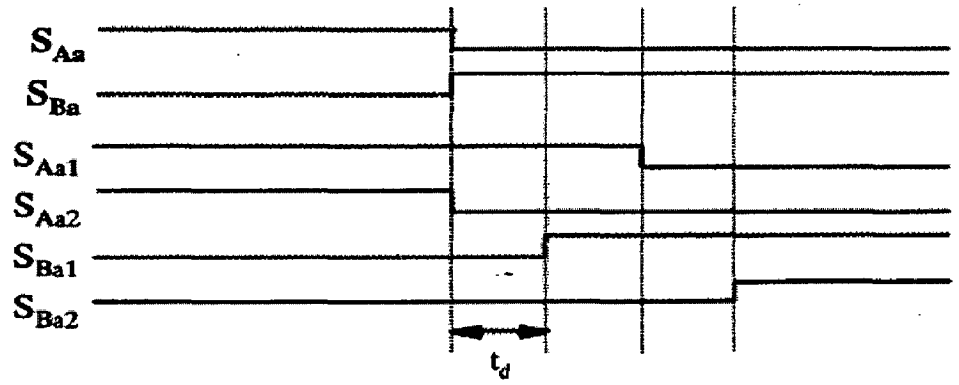

Fig 2.11: Timing diagram [5]

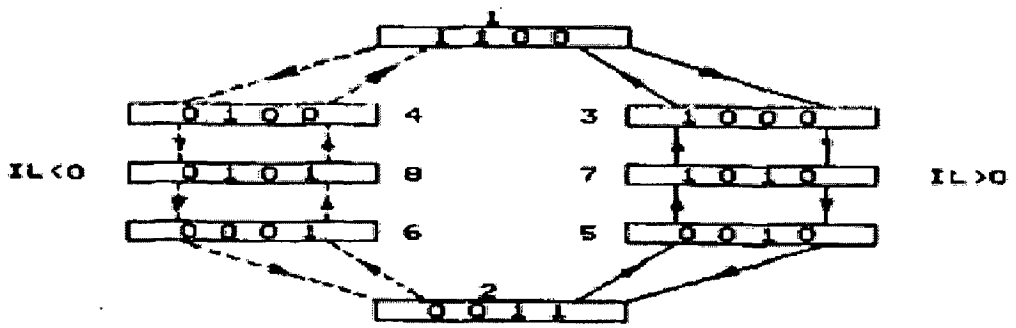

Fig 2.12: Switching diagram [5]

Two-Step Semi-Soft Current Commutation

One popular variation on this current commutation concept is to only gate the conducting device in the active switch cell, which creates a two-step current commutation strategy. In this method only the correct device in the conducting cell is gated. This simplifies the commutation to a 2

step process since only the correct device in the incoming cell is switched on and the outgoing device is switched off. Current reversal is catered for by gating both devices in the conducting cell when the current level falls below threshold level. The non-conducting device is then turned off when the current has risen sufficiently in the opposite direction. The problem with this method is that a commutation between cells cannot occur during a current reversal. Since the direction of current is unknown, the current outgoing device cannot be determined. This method would also be unsuitable if the target output current was to be within the threshold level.

All the current commutation techniques in this category rely on knowledge of the output line current direction. This can be difficult to reliably determine in a switching power converter, especially at low current levels in high-power applications where traditional current sensors such as Hall-effect probes are prone to producing uncertain results. One method that has been used to avoid these potential hazard conditions is to create a "near-zero" current zone where commutation is not allowed to take place, as shown for a two-step strategy in the state representation diagram in Fig. 2.13. However, this method will give rise to control problems at low current levels and at startup.

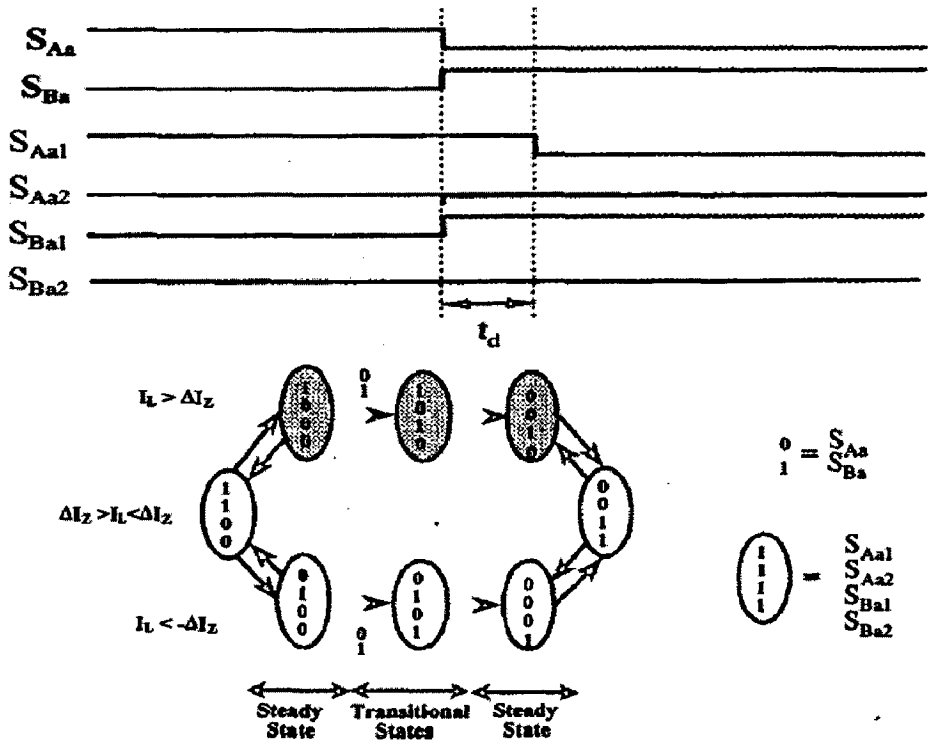

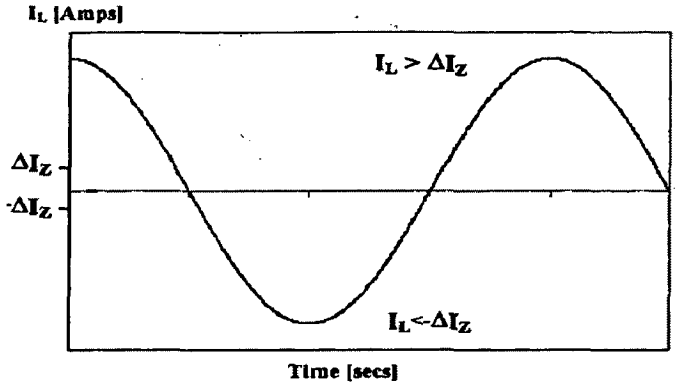

Fig 2.13: Two Step Semisoft Current Commutation between two Bidirectional switches [5]

2.4.3 Input Filter

Filters must be used at the input of the matrix converters to reduce the switching frequency harmonics present in the input current. The requirements for the filter are as follows:

1) To have a cutoff frequency lower than the switching frequency of the converter.
2) To minimize its reactive power at the grid frequency.
3) To minimize the volume and weight for capacitors and chokes.
4) To minimize the filter inductance voltage drop at rated current in order to avoid a reduction in the voltage transfer ratio

The filter does not store energy coming from the load.

2.4.4 Power circuit protection

A critical feature of matrix converter is that current is always commutated from one controlled switch to another. This is in direct contrast to a conventional voltage source inverter where commutation is always from a controlled device to a complementary freewheeling diode or vice versa. In a conventional inverter a time delay can be introduced between the drive signals for complementary devices (in order to avoid simultaneous conduction) safe in the knowledge that the inductive load current will be taken over by a freewheeling diode. There is no such freewheeling path in

the matrix converter but it is still necessary to introduce a delay between drive signals to avoid a short circuit of the input lines. During this delay time the inductive load current is taken over by a snubber circuit which must be chosen to limit the device voltage to an appropriate level. To avoid excessive snubber losses it is important to match the snubber design and delay time setting very carefully.

The absence of freewheeling paths also causes difficulty in protecting the power circuit against fault conditions. For instance, if the devices are turned off in response to a fault condition, such as over current, severe overvoltage and destruction of the power circuit results because of the inductive nature of the load. Therefore a clamp circuit is connected to a matrix converter output as shown in Fig 2.14. The clamp consists of six pulse Diode Bridge feeding a capacitor which absorbs the excess load energy when all the converter devices are gated off.

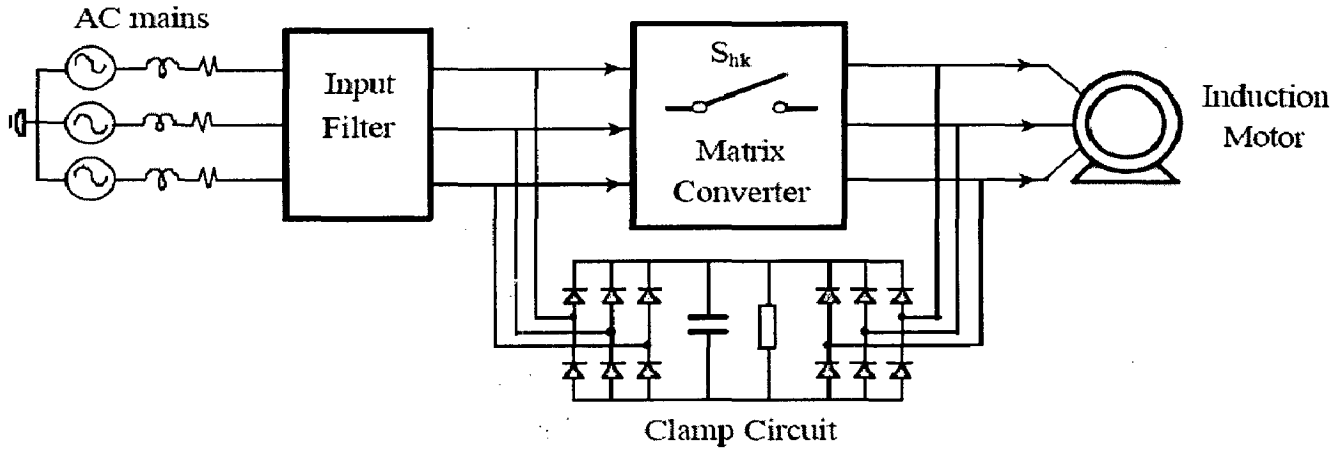

Fig.2.14: Clamp circuit as common protection for all matrix converter Bidirectional switches [5].

This clamp performs essentially the same function as snubber circuits but in practice it has been found that small snubbers are still required to mitigate against the effects of wiring inductance.

When over voltages occurs, the diode conducts and the RC circuit maintains the voltage level at a safe value. In normal operation, the diodes are off and clamp circuit has no influence on the matrix converter operation. It is important to note that the power level is very low for the clamp circuit.

2.4.5 Semiconductor losses

Since a suitable bidirectional semiconductor switch has not yet been developed, so the matrix converter can be realized using a switch constructed from discrete components. The back to back IGBT arrangements are preferred as it allows independent control of the current in both directions with in each switch. This control would not be possible if the diode bridge circuit was used. The diode bridge circuit also has a greater conduction loss since there are two diodes in series with the IGBT. The losses in a matrix converter consist of conduction losses and switching losses. The conduction losses are proportional to the forward voltage drop across the device and the current carried by the device. The conduction loss per switch is calculated as the sum of the conduction losses in the IGBT and in the associated diode. The conduction loss in a matrix converter is therefore slightly greater than in an inverter in which either the IGBT or the diode would carry the load current. The switching losses in the IGBT are due to the finite time taken for the device to change state. The switching losses are also proportional to the switching frequency at which the converter is operating.

2.5 Conclusion

The performance of matrix converter in terms of output voltage, input current and input power factor is better than VSI. The practical realization of a matrix converter requires the use of bi-directional switches. Since a true bi-directional switch does not exist yet, this is generally provided by the use of an antiparallel arrangement of discrete power semiconductor devices plus series diode to provide reverse blocking capability. This implementation implies a higher complexity of the matrix converter as 18 active devices have to be controlled in a three phase to three phase matrix converter but most of all it establishes the commutation problem. In matrix converters, the problem of safely commutate the load current from one bi-directional switch to another basically arises by the absence of natural freewheeling paths..

Chapter 3

Modulation Techniques

This chapter focuses on different matrix converter modulation strategies By means of a simulation model the performance of these strategies have been analyzed under either balanced and sinusoidal or unbalanced and nonsinusoidal supply voltage conditions.

3.1 Introduction

Modulation is the procedure used to generate the appropriate firing pulses to each of the nine bidirectional switches in order to generate the desired output voltage and frequency from fixed frequency and fixed amplitude input voltage.

3.2 Venturini Modulation Method

In this method time windows is considered in which the instantaneous values of the desired output voltages are sampled and the instantaneous input voltages are used to synthesize a signal whose low frequency component is the desired output voltage.

If t_{ij} is defined as the time during which switch $S_{ij\ ON}$ and T as the sampling interval (width of the time window), the synthesis principle described above can be expressed as

$$\overline{v}_{jN}(t) = \frac{t_{Aj}v_A(t) + t_{Bj}v_B(t) + t_{Cj}v_C(t)}{T}; \quad j = \{a, b, c\} \tag{3.1}$$

where $V_{jN}(t)$ is the low frequency component (mean value calculated over one sampling interval) of the j^{th} output pulse and changes in each sampling interval. With this strategy, a high frequency switched output voltage is generated, but the fundamental component of the voltage has the desired waveform. Obviously, $T=t_{Aj}+t_{Bj}+t_{Cj}$ and the following duty cycles can be defined:

$$m_{Aj} = \frac{t_{Aj}}{T}, \quad m_{Bj} = \frac{t_{Bj}}{T}, \quad m_{Cj} = \frac{t_{Cj}}{T} \tag{3.2}$$

Extending equation (3.1) to each output phase and equation (3.2), the following relationship between the input and output voltage and that of the output and input current can be derived.

$$\begin{bmatrix} V_{aN}(t) \\ V_{bN}(t) \\ V_{cN}(t) \end{bmatrix} = \begin{bmatrix} m_{Aa}(t) & m_{Ba}(t) & m_{Ca}(t) \\ m_{Ab}(t) & m_{Bb}(t) & m_{Cb}(t) \\ m_{Ac}(t) & m_{Bc}(t) & m_{Cc}(t) \end{bmatrix};$$

$$V_o(t) = M(t).V_i(t) \tag{3.3}$$

Where $V_o(t)$ is the low frequency output vector, $V_i(t)$ is the instantaneous input voltage and M(t) is the low frequency transfer matrix of the matrix converter.

$$i_i(t) = M^T(t).i_o(t) \tag{3.4}$$

Where $i_i(t)=[i_A(t)\ i_B(t)\ i_C(t)]^T$ is the low frequency input current vector, $i_o(t)=[i_a(t)\ i_b(t)\ i_c(t)]^T$ is the instantaneous output current vector $M^T(t)$ is the transpose of M(t).

Equation (3.3) and (3.4) are basis of the Venturini modulation method and allows us to conclude that the low frequency components of the output voltages are synthesized with the instantaneous values of the input voltages and that the low frequency components of the input current are synthesized with the instantaneous values of the output currents.
Suppose the input voltages are given by

$$v_i(t) = \begin{bmatrix} v_A(t) \\ v_B(t) \\ v_C(t) \end{bmatrix} = \begin{bmatrix} V_i \cos(\omega_i t) \\ V_i \cos(\omega_i t + 2\pi/3) \\ V_i \cos(\omega_i t + 4\pi/3) \end{bmatrix} \tag{3.5}$$

And that due to the low-pass characteristic of the load the output currents are sinusoidal and can be expressed as

$$i_o = I_{om} \begin{bmatrix} \cos(\omega_o t + \emptyset_o) \\ \cos(\omega_o t + \emptyset_o + 2\pi/3) \\ \cos(\omega_o t + \emptyset_o + 4\pi/3) \end{bmatrix} \tag{3.6}$$

Find a modulation matrix such that

$$v_o = qV_{im}\begin{bmatrix}\cos(\omega_o t)\\ \cos(\omega_o t + 2\pi/3)\\ \cos(\omega_o t + 4\pi/3)\end{bmatrix} \tag{3.7}$$

$$i_i = q\cos(\emptyset_o)\, I_{om}\begin{bmatrix}\cos(\omega_i t + \emptyset_i)\\ \cos(\omega_i t + \emptyset_i + 2\pi/3)\\ \cos(\omega_i t + \emptyset_i + 4\pi/3)\end{bmatrix} \tag{3.8}$$

In equation (3.7), q is the voltage gain between the output and input voltages. There are two basic solutions as shown in equation (3.9) and (3.10). The solution in equation (3.9) yields $\emptyset_i = \emptyset_o$ giving the same phase displacement at the input and output ports whereas the solution in equation (3.10) yields $\emptyset_i = \emptyset_o$, giving reversed phase displacement factor control. This basic solution represents a direct transfer function approach and is characterized by the fact that, during each switch sequence time (T), the average output voltage is equal to the demand voltage. For this to be possible, it is clear that the target voltages must fit within the input voltages envelope for any output frequency. This leads to a limitation on maximum voltage ratio.

$$M_1 = \frac{1}{3}\begin{bmatrix}1+2q\cos(\omega_m t) & 1+2q\cos(\omega_m t - 2\pi/3) & 1+2q\cos(\omega_m t - 4\pi/3)\\ 1+2q\cos(\omega_m t - 4\pi/3) & 1+2q\cos(\omega_m t) & 1+2q\cos(\omega_m t - 2\pi/3)\\ 1+2q\cos(\omega_m t - 2\pi/3) & 1+2q\cos(\omega_m t - 4\pi/3) & 1+2q\cos(\omega_m t)\end{bmatrix}$$

With $\omega_m = (\omega_o - \omega_i)$ (3.9)

$$M_1 = \frac{1}{3}\begin{bmatrix}1+2q\cos(\omega_m t) & 1+2q\cos(\omega_m t - 2\pi/3) & 1+2q\cos(\omega_m t - 4\pi/3)\\ 1+2q\cos(\omega_m t - 2\pi/3) & 1+2q\cos(\omega_m t - 4\pi/3) & 1+2q\cos(\omega_m t)\\ 1+2q\cos(\omega_m t - 4\pi/3) & 1+2q\cos(\omega_m t) & 1+2q\cos(\omega_m t - 2\pi/3)\end{bmatrix}$$

With $\omega_m = -(\omega_o + \omega_i)$ (3.10)

However calculating the switch timings directly from these equations is cumbersome for a practical implementation. They are more conveniently expressed directly in terms of the input voltages and the target output voltages assuming unity displacement factor in the following form.

$$m_{Kj} = \frac{t_{Kj}}{T_S} = \frac{1}{3}\left[1 + \frac{2v_k v_j}{V_{im}^2}\right]$$

$$for\ K = A, B, C\ and\ j = a, b, c. \tag{3.11}$$

In this method voltage ratio is limited to 50%.

3.3 Modified Venturini Method

An improvement in the achievable voltage ratio to $\sqrt{3}/2$ (or 87%) is possible by adding common mode voltages to the target outputs as shown in equation (3.12)

$$v_o = qV_{im}\begin{bmatrix} \cos(\omega_o t) - \frac{1}{6}\cos(3\omega_o t) + \frac{1}{2\sqrt{3}}\cos(3\omega_i t) \\ \cos(\omega_o t + 2\pi/3) - \frac{1}{6}\cos(3\omega_o t) + \frac{1}{2\sqrt{3}}\cos(3\omega_i t) \\ \cos(\omega_o t + 4\pi/3) - \frac{1}{6}\cos(3\omega_o t) + \frac{1}{2\sqrt{3}}\cos(3\omega_i t) \end{bmatrix} \quad (3.12)$$

The common mode voltage have no effect on output line to line voltages, but allow target outputs to fit within the input envelope with a value of up to 87% as shown in figure below. In this the modulation function can be expressed as

$$m_{Kj} = \frac{t_{Kj}}{T_S} = \frac{1}{3}\left[1 + \frac{2v_k v_j}{V_{im}^2} + \frac{4q}{3\sqrt{3}}\sin(\omega_i t + \beta_k)\sin(3\omega_i t)\right]$$

$$for\ K = A, B, C\ and\ j = a, b, c.$$

$$\beta_K = 0, 2\pi/3, 4\pi/3 \quad (3.13)$$

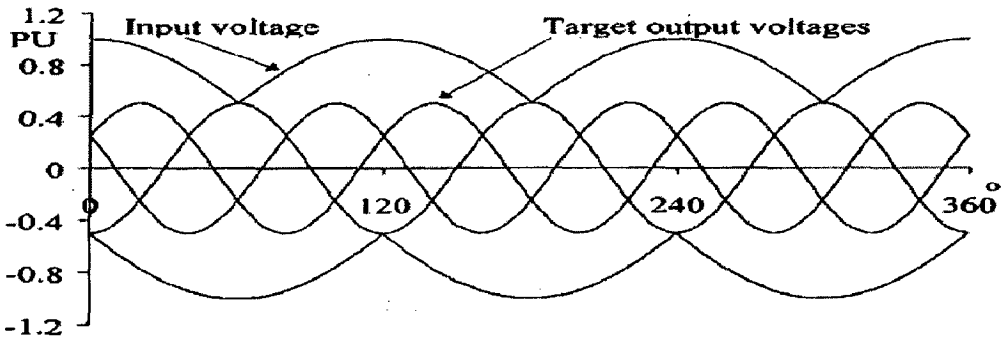

Fig 3.1: Illustrating maximum voltage ratio of 50% [3]

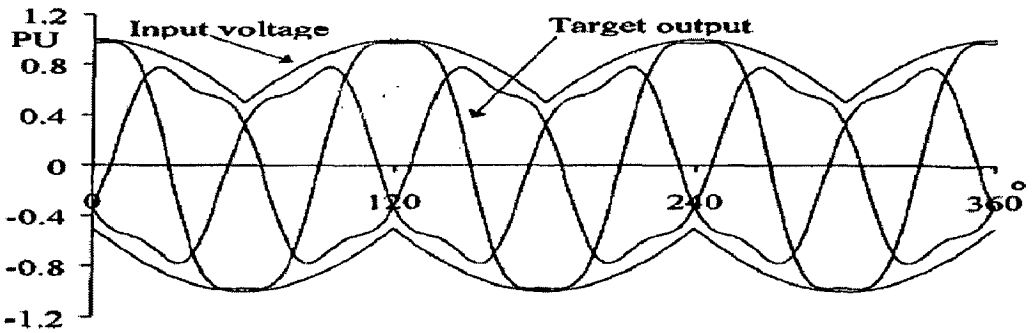

Fig 3.2: Illustrating voltage ratio improvement to 87% [3]

3.4 SPACE VECTOR MODULATION

In this section, the space vector modulation is simultaneously employed in both VSR and VSI parts of the MC. First, the VSI-SVM and VSR-SVM procedures are reviewed, then simultaneous output-voltage and input-current SVM for control of the 3Φ-3Φ MC are performed. Finally, a simple geometric representation in complex plane of the modulation process is given.

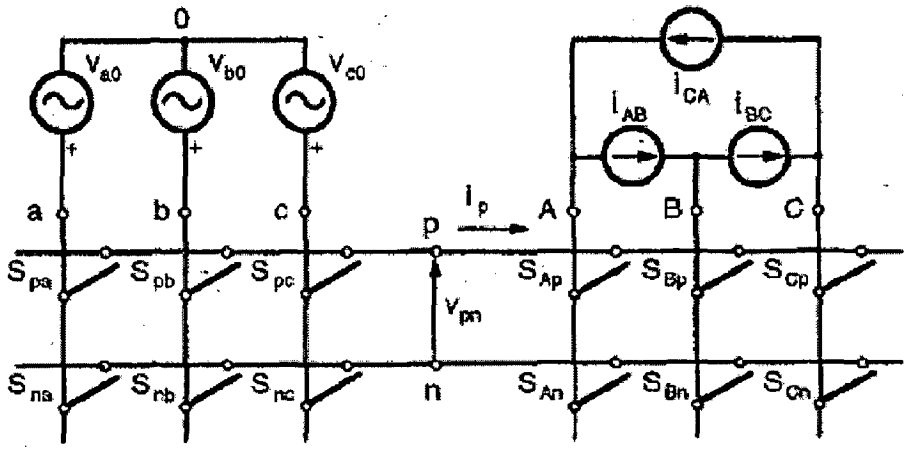

Fig 3.3: Emulation of VSR-VSI conversion [12]

For a matrix converter, the selection of vectors is by no means unique and 512 number of possibilities exist due to 9 bidirectional switches, out of these only 27 possible output vectors for a three-phase matrix converter are considered depending on equation (2.2) can be classified into three groups with the following characteristics.

- *Group I:* Each output line is connected to a different input line. Output space vectors are constant in amplitude, rotating (in either direction) at the supply angular frequency.

- *Group II:* Two output lines are connected to a common input line; the remaining output line is connected to one of the other input lines. Output space vectors have varying amplitude and fixed direction occupying one of six positions regularly spaced 60 apart. The maximum length of these vectors is $2/\sqrt{3}V_{env}$ where V_{env} is the instantaneous value of the rectified input voltage envelope.

• *Group III:* All output lines are connected to a common input line. Output space vectors have zero amplitude (i.e., located at the origin).

In the SVM, the Group I vectors are not used. The desired output is synthesized from the Group II active vectors and the Group III zero vectors. The hexagon of possible output vectors is shown in Fig. 3.2, where the Group II vectors are further subdivided dependent on which output line-to-line voltage is zero.

VSI Output Voltage SVM

Consider the VSI part of the circuit in Fig. 3.3 as a standalone VSI supplied by a dc voltage source, $v_{pn} = V_{dc}$. The VSI switches can assume only six allowed combinations which yield nonzero output voltages, and two combinations with zero output voltages. Hence, the resulting output line-voltage space vector defined by

$$v_{oL} = \frac{2}{3} \cdot \left(v_{AB} + v_{BC} \cdot e^{+j120^0} + v_{CA} \cdot e^{-j120^0}\right) \tag{3.14}$$

can assume only seven discrete values, V_o – V_6 in Fig. 3.4, called voltage switching state vectors (SSV's). The space vector of the desired output line voltages is given by

$$\bar{v}_{oL} = \sqrt{3} \cdot V_{om} \cdot e^{j(\omega_o t - \varphi_o + 30^0)} \tag{3.15}$$

can be approximated by two adjacent SSV's, V_α, and V_β, and the zero voltage vector, V_O, using PWM as shown in Fig. 3.5, where V_{oL} is the sampled value of v_{oL}, at an instant within the switching cycle T_s,. Using the law of sines, the duty cycles of the SSV's are

$$\begin{aligned} d_\alpha &= T_\alpha/T_s = m_v \cdot \sin(60^0 - \theta_{sv}), \\ d_\beta &= T_\beta/T_s = m_v \cdot \sin(\theta_{sv}), \\ d_{ov} &= T_{ov}/T_s = 1 - d_\alpha - d_\beta \end{aligned} \tag{3.16}$$

where m_v is the VSI modulation index

$$0 \le m_v = (\sqrt{3} \cdot V_{om})/V_{dc} \le 1 \tag{3.17}$$

Table 3.1

3Φ-3Φ MC Switching Combinations

Group	A B C	V_{AB} V_{BC} V_{CA}	i_a i_b i_c	S_{Aa} S_{Ab} S_{Ac}	S_{Ba} S_{Bb} S_{Bc}	S_{Ca} S_{Cb} S_{Cc}
I	a b c	V_{ab} V_{bc} V_{ca}	i_A i_B i_C	1 0 0	0 1 0	0 0 1
	a c b	$-V_{ca}$ $-V_{bc}$ $-V_{ab}$	i_A i_C i_B	1 0 0	0 0 1	0 1 0
	b a c	$-V_{ab}$ $-V_{ca}$ $-V_{bc}$	i_B i_A i_C	0 1 0	1 0 0	0 0 1
	b c a	V_{bc} V_{ca} V_{ab}	i_C i_A i_B	0 1 0	0 0 1	1 0 0
	c a b	V_{ca} V_{ab} V_{bc}	i_B i_C i_A	0 0 1	1 0 0	0 1 0
	c b c	$-V_{bc}$ $-V_{ab}$ $-V_{ca}$	i_C i_B i_A	0 0 1	0 1 0	1 0 0
II-A	a c c	$-V_{ca}$ 0 V_{ca}	i_A 0 $-i_A$	1 0 0	0 0 1	0 0 1
	b c c	V_{bc} 0 $-V_{bc}$	0 i_A $-i_A$	0 1 0	0 0 1	0 0 1
	b a a	$-V_{ab}$ 0 V_{ab}	$-i_A$ i_A 0	0 1 0	1 0 0	1 0 0
	c a a	V_{ca} 0 $-V_{ca}$	$-i_A$ 0 i_A	0 0 1	1 0 0	1 0 0
	c b b	$-V_{bc}$ 0 V_{bc}	0 $-i_A$ i_A	0 0 1	0 1 0	0 1 0
	a b b	V_{ab} 0 $-V_{ab}$	i_A $-i_A$ 0	1 0 0	0 1 0	0 1 0
II-B	c a c	V_{ca} $-V_{ca}$ 0	i_B 0 $-i_B$	0 0 1	1 0 0	0 0 1
	c b c	$-V_{bc}$ V_{bc} 0	0 i_B $-i_B$ -	0 0 1	0 1 0	0 0 1
	a b a	V_{ab} $-V_{ab}$ 0	i_B i_B 0	0 0 0	0 1 0	1 0 0
	a c a	$-V_{ca}$ V_{ca} 0	$-i_B$ 0 i_B	1 0 0	0 0 1	1 0 0
	b c b	V_{bc} $-V_{bc}$ 0	0 $-i_B$ i_B	0 1 0	0 0 1	0 1 0
	b a b	$-V_{ab}$ V_{ab} 0	i_B $-i_B$ 0	0 1 0	1 0 0	0 1 0
II-C	c c a	0 V_{ca} $-V_{ca}$	i_C 0 $-i_C$	0 0 1	0 0 1	1 0 0
	c c b	0 $-V_{bc}$ V_{bc}	0 i_C $-i_C$ -	0 0 1	0 0 1	0 1 0
	a a b	0 V_{ab} $-V_{ab}$	i_C i_C 0	1 0 0	1 0 0	0 1 0
	a a c	0 $-V_{ca}$ V_{ca}	$-i_C$ 0 i_C	1 0 0	1 0 0	0 0 1
	b b c	0 V_{bc} $-V_{bc}$	0 $-i_C$ i_C	0 1 0	0 1 0	0 0 1
	b b a	0 $-V_{ab}$ V_{ab}	i_C $-i_C$ 0	0 1 0	0 1 0	1 0 0
III	a a a	0 0 0	0 0 0	1 0 0	1 0 0	1 0 0
	b b b	0 0 0	0 0 0	0 1 0	0 1 0	0 1 0
	c c c	0 0 0	0 0 0	0 0 1	0 0 1	0 0 1

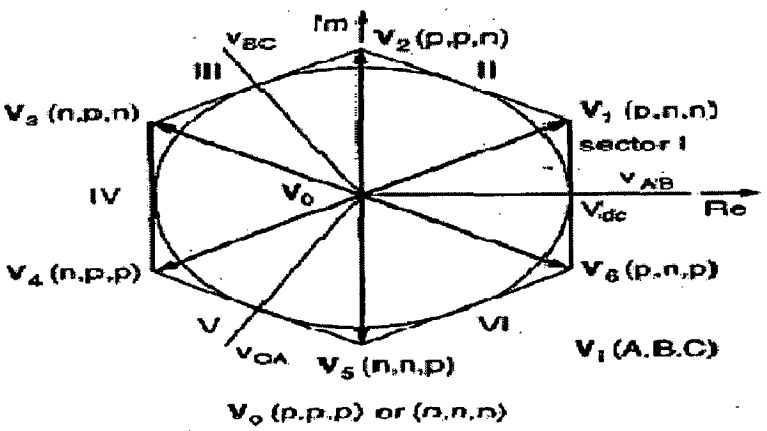

Fig 3.4: VSI hexagon [12]

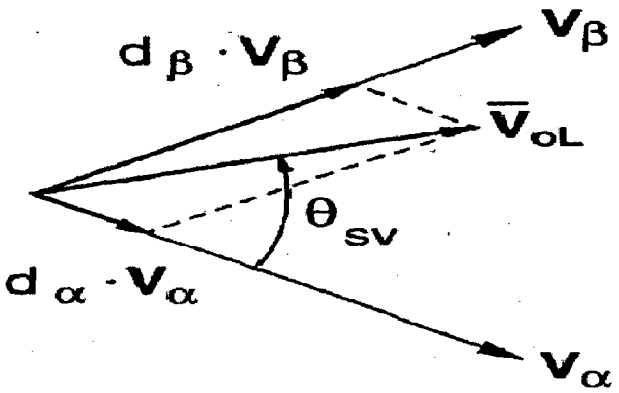

Fig 3.5: VSI SVM vector addition.[12]

The sectors of the VSI hexagon in Fig. 3.4 correspond directly to the six 60°-segments within a period of the desired 3Φ output line voltages shown in Fig. 3.6. The synthesis of the output line voltages for a switching cycle within the first 60°-segment is shown in Fig. 3.7, as an example. The local averaged output line voltages are

$$\begin{bmatrix}\overline{v}_{AB}\\ \overline{v}_{BC}\\ \overline{v}_{CA}\end{bmatrix} = \begin{bmatrix}d_\alpha + d_\beta\\ -d_\alpha\\ -d_\beta\end{bmatrix} \cdot V_{dc}$$

$$= m_v \cdot \begin{bmatrix}\cos(\theta_{sv} - 30^0)\\ -\sin(60^0 - \theta_{sv})\\ -\sin(\theta_{sv})\end{bmatrix} \cdot V_{dc} \qquad (3.18)$$

For the first 60°-segment

$$-30^0 \le \omega_o t - \varphi_o + 30^0 \le +30^0$$

$$\theta_{sv} = (\omega_o t - \varphi_o + 30^0) + 30^0 \qquad (3.19)$$

By substitution of (3.19) in (3.18)

$$\begin{bmatrix}\overline{v}_{AB}\\ \overline{v}_{BC}\\ \overline{v}_{CA}\end{bmatrix} = m_v \cdot \begin{bmatrix}\cos(\omega_o t - \varphi_o + 30^0)\\ \cos(\omega_o t - \varphi_o + 30^0 - 120^0)\\ \cos(\omega_o t - \varphi_o + 30^0 + 120^0)\end{bmatrix} \cdot V_{dc}$$

$$= \overline{T}_{VSI} \cdot V_{dc} \qquad (3.20)$$

The VSI local-averaged input current is determined as

$$\bar{i}_p = T_{VSI}^T \cdot i_{oL} = \frac{\sqrt{3}}{2} \cdot I_{om} \cdot m_v \cdot \cos(\varphi_L) = const \qquad (3.21)$$

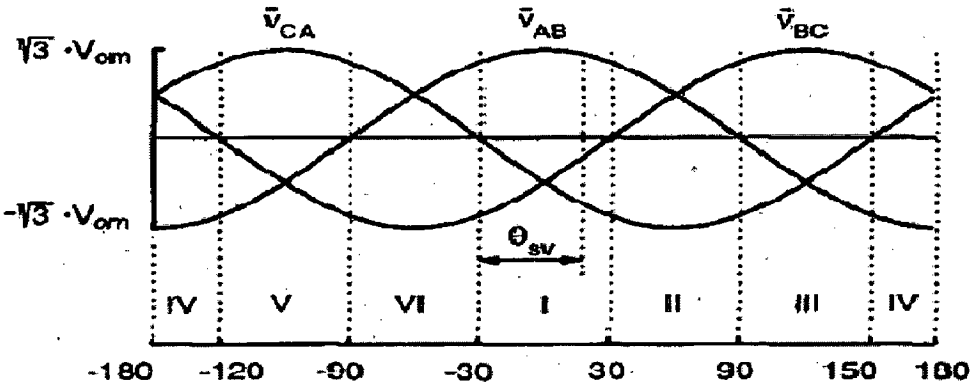

Fig3.6: Output line voltage 60°-segments.[12]

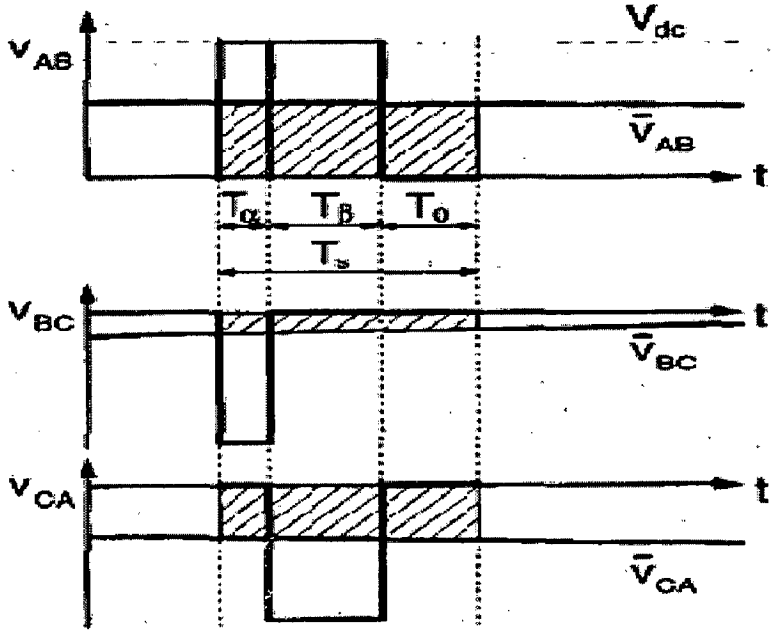

Fig 3.7: Synthesis of VSI output line voltages.[12]

VSR Input Current SVM

Consider the VSR part of the circuit in Fig. 3.3 as a standalone VSR loaded by a dc current generator, $i_p = I_{dc}$. The VSR input-current SVM is completely analogous to the VSI output-voltage SVM. The VSI subscripts α, β and s_v are replaced with the VSR subscripts μ, ν and s_c, respectively. The VSR hexagon is shown in Fig. 3.8. The VSR duty cycles are

$$d_\mu = T_\mu/T_s = m_c \cdot \sin(60^0 - \theta_{sc})$$

$$d_\nu = T_\nu/T_s = m_c \cdot \sin(\theta_{sc})$$

$$d_{oc} = T_{oc}/T_s = 1 - d_\mu - d_\nu \qquad (3.22)$$

where m_c, is the VSR modulation index

$$0 \leq m_c = (I_{im})/I_{dc} \leq 1 \tag{3.23}$$

Examples of the local-averaged input phase currents, for a switching cycle within the first sector of the VSR hexagon, are

$$\begin{bmatrix} \bar{i}_a \\ \bar{i}_b \\ \bar{i}_c \end{bmatrix} = \begin{bmatrix} d_\mu + d_v \\ -d_\mu \\ -d_v \end{bmatrix} \cdot I_{dc}$$

$$= m_c \cdot \begin{bmatrix} \cos(\theta_{sc} - 30^0) \\ -\sin(60^0 - \theta_{sc}) \\ -\sin(\theta_{sc}) \end{bmatrix} \cdot I_{dc} \tag{3.24}$$

By substitution of

$$\theta_{sc} = (\omega_i t - \varphi_i) + 30^0$$
$$-30^0 \leq \omega_o t - \varphi_o + 30^0 \leq +30^0 \tag{3.25}$$

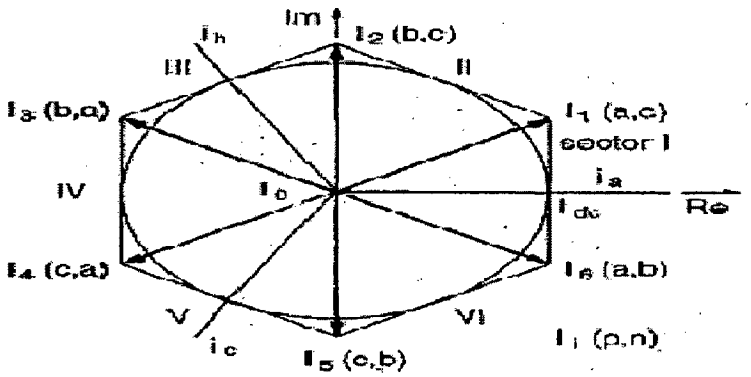

Fig 3.8: VSR hexagon.[12]

for first sector in (3.24), LF transfer matrix of the VSR, T_{VSR}, is defined as

$$\begin{bmatrix} \bar{i}_a \\ \bar{i}_b \\ \bar{i}_c \end{bmatrix} = m_c \cdot \begin{bmatrix} \cos(\omega_i t - \varphi_i) \\ \cos(\omega_i t - \varphi_i - 120^0) \\ \cos(\omega_i t - \varphi_i + 120^0) \end{bmatrix} \cdot I_{dc} = \overline{T}_{VSR} \cdot I_{dc} \tag{3.26}$$

The VSR local averaged output voltage is determined as

$$\bar{v}_{pn} = \overline{T}_{VSR}^{T} \cdot v_{iPh}$$

$$= \frac{3}{2} \cdot m_c \cdot V_{im} \cdot \cos(\varphi_i) = const \tag{3.27}$$

MC Output-Voltage and Input-Current SVM

As the local-averaged output voltage of the SVM VSR, (3.27), and the local-averaged input current of the SVM VSI, (3.21), is constant, from the local-averaged point of view the SVM VSR and the SVM VSI can be directly connected. Substituting v_{pn} from (3.27) for v_{dc} in (3.20) and using T_{VSR} from (3.26), the same expression for the LF transfer matrix of the 3Φ-3Φ, MC is obtained as

$$\overline{T}_{PhL} = m \cdot \begin{bmatrix} \cos(\omega_o t - \varphi_o + 30^0) \\ \cos(\omega_o t - \varphi_o + 30^0 - 120^0) \\ \cos(\omega_o t - \varphi_o + 30^0 + 120^0) \end{bmatrix} \cdot \begin{bmatrix} \cos(\omega_i t - \varphi_i) \\ \cos(\omega_i t - \varphi_i - 120^0) \\ \cos(\omega_i t - \varphi_i + 120^0) \end{bmatrix}^T \quad (3.28)$$

with $m = m_c \cdot m_v$. For simplicity, it is convenient to choose $m_c = 1$ and $m = m_v$. This completes the first step of the HF-synthesis procedure. Since both the VSI and the VSR hexagons contain six sectors, there are 6 x 6 = 36 combinations or operating modes. If at a particular instant, the first output-voltage 60°-segment and the first input-current 60°-segment are active, then by using (3.19) and (3.25), the LF transfer matrix (3.28) becomes

$$\overline{T}_{PhL} = m \cdot \begin{bmatrix} \cos(\theta_{sv} - 30^0) \\ -\sin(60^0 - \theta_{sv}) \\ -\sin(\theta_{sv}) \end{bmatrix} \cdot \begin{bmatrix} \cos(\theta_{sc} - 30^0) \\ -\sin(60^0 - \theta_{sc}) \\ -\sin(\theta_{sc}) \end{bmatrix}^T \quad (3.29)$$

Substituting (27) and (33) in (39), with $m = m_v \cdot m_c$, the local-averaged output line-voltages are

$$\begin{bmatrix} \overline{v}_{AB} \\ \overline{v}_{BC} \\ \overline{v}_{CA} \end{bmatrix} = \begin{bmatrix} d_\alpha + d_\beta \\ -d_\alpha \\ -d_\beta \end{bmatrix} \cdot \begin{bmatrix} d_\mu + d_v \\ -d_\mu \\ -d_v \end{bmatrix}^T \cdot \begin{bmatrix} v_{ao} \\ v_{bo} \\ v_{co} \end{bmatrix} \quad (3.30)$$

Using

$$v_{ab} = v_{ao} - v_{bo} \quad and \quad v_{ac} = v_{ao} - v_{co} \quad (3.31)$$

it is finally obtained

$$\begin{bmatrix} \overline{v}_{AB} \\ \overline{v}_{BC} \\ \overline{v}_{CA} \end{bmatrix} = \begin{bmatrix} d_{\alpha\mu} + d_{\beta\mu} \\ -d_{\alpha\mu} \\ -d_{\beta\mu} \end{bmatrix} \cdot v_{ab} + \begin{bmatrix} d_{\alpha v} + d_{\beta v} \\ -d_{\alpha v} \\ -d_{\beta v} \end{bmatrix} \cdot v_{ac} \quad (3.32)$$

Where

$$d_{\alpha\mu} = d_\alpha \cdot d_\mu = m \cdot \sin(60^0 - \theta_{sv}) \cdot \sin(60^0 - \theta_{sc}) = T_{\alpha\mu}/T_s$$

$$d_{\beta\mu} = d_\beta \cdot d_\mu = m \cdot \sin(\theta_{sv}) \cdot \sin(60^0 - \theta_{sc}) = T_{\beta\mu}/T_s$$

$$d_{\alpha v} = d_\alpha \cdot d_v = m \cdot \sin(60^0 - \theta_{sv}) \cdot \sin(\theta_{sc}) = T_{\alpha v}/T_s$$

$$d_{\beta v} = d_\beta \cdot d_v = m \cdot \sin(\theta_{sv}) \cdot \sin(\theta_{sc}) = T_{\beta v}/T_s \qquad (3.33)$$

As can be seen, the output line voltages are synthesized inside each switching cycle from samples of two input line voltages, v_{ab} and v_{ac}, for the above example. By comparison of (3.32) and (3.18), it can be concluded that simultaneous output-voltage and input-current SVM can be obtained by employing the standard VSI SVM sequentially in two VSI-sub topologies of the 3Φ-3Φ *MC*. When the standard VSI SVM is applied in the first VSI-sub topology, where $v_{pn} = v_{ab}$, the duty cycles of the two adjacent voltage SSV's are $d_{\alpha\mu}$ and $d_{\beta\mu}$, as defined in (3.33). The standard VSI SVM in the second VSI-sub topology, with $v_{pn} = v_{ac}$, results in the SSV duty cycles $d_{\alpha v}$ and $d_{\beta v}$, also defined in (3.33). During the remaining part of the switching cycle

$$d_o = 1 - d_{\alpha\mu} - d_{\beta\mu} - d_{\alpha v} - d_{\beta v} = T_o/T_s \qquad (3.34)$$

the output line voltages are equal to zero, by employing a zero SSV.

A switching sequence within one switching cycle requires decisions on which of the three switching combinations from Group III is used for the zero SSV, and on how the five switching combinations are ordered within the switching cycle. Among the possible combinations, those which require switches to change state only once during a switching cycle should be used. In this paper, the switching sequence $d_{\alpha\mu} \rightarrow d_{\beta\mu} \rightarrow d_{\beta v} \rightarrow d_{\alpha v} \rightarrow d_o$ is used, and the optimum zero SSV is chosen for each of the 36 operating modes.

For example, if at an instant V_{oL} is in the first sector of the MC inverter hexagon, the actual voltage SSV's are $V_\alpha = V_6$ and $V_\beta = V_1$; and if i_{iph} is in the first sector of the MC rectifier hexagon, the actual current SSV's are $I_\alpha = I_6$ and $I_\beta = I_1$. Voltage-current SSV pairs are applied in the following sequence: $I_6 - V_6$, $I_6 - V_1$, $I_1 - V_1$, $I_1 - V_6$, and $I_o - V_o$. To each voltage-current

SSV pair corresponds a switching combination with the on-time determined by (3.33), as shown in Table 3.2. For example, while applying I_6, it follows from Fig 3.6 that p = a and n = b. With simultaneous application of V_6, from Fig 3.2, A = p, B = n, and C = p. Therefore, the voltage-current SSV pair I_6 - V_6 is realized with the switching combination A = a, B = b, and C = a, which is kept ON for the time interval $d_{a\mu} \cdot T_s$. On-times of the individual MC switches can be determined from Table 3.2. The table also shows the resulting output line-voltages and input phase-currents.

Table 3.2

Switching Sequence Example

SSV pair	Switching Combination p n A B C	ON Time	Output Line Voltage V_{AB} V_{BC} V_{CA}	Input Ph current i_a i_b i_c	Switching States $S_{Aa}S_{Ab}S_{Ac}$ $S_{Ba}S_{Bb}S_{Bc}$ $S_{Ca}S_{Cb}S_{Cc}$
I_6-V_6	a b a b a	$d_{a\mu}.T_s$	V_{ab} $-V_{ab}$ 0	$-i_B$ i_B 0	1 0 0 0 1 0 1 0 0
I_6-V_1	a b a b b	$d_{\beta\mu}.T_s$	V_{ab} 0 $-V_{ab}$	i_A $-i_A$ 0	1 0 0 0 1 0 0 1 0
I_1-V_6	a c a c c	$d_{\beta\nu}.T_s$	V_{ac} 0 $-V_{ac}$	i_A 0 $-i_A$	1 0 0 0 0 1 0 0 1
I_1-V_1	a c a c a	$d_{a\nu}.T_s$	V_{ac} $-V_{ac}$ 0	$-i_B$ 0 i_B	1 0 0 0 0 1 1 0 0
I_0-V_0	a a a a a	$d_o.T_s$	0 0 0	0 0 0	1 0 0 1 0 0 1 0 0

3.5 Compensation Structure for Unbalanced and/or Distorted Supply Voltages Using Venturini's Method

Matrix Converter has a inherent capability to compensate for Unbalanced and/or distorted supply voltages by instantaneously controlling the voltage transfer. The momentary amplitude of the three phase input supplies is decided by detecting the supply voltages.

$$V_{imi} = \sqrt{\frac{2}{3}\left(V_a^2(t) + V_b^2(t) + V_c^2(t)\right)} \qquad (3.35)$$

Whenever voltage distortions occur, they are compensated by calculating different switching time periods for each switch by simply adjusting the voltage transfer ratio. In (3.13) if V_{im} is calculated using above formula input voltage unbalance and distortions are instantaneously compensated.

3.6 Compensation Structure for Unbalanced and/or Distorted Supply Voltages Using SVM Method

From (3.27) modulation index in rectifier stage can be related to the amplitude of the input voltages by

$$m_c = \frac{2V_{pn}}{3V_{im}} \tag{3.36}$$

for unity displacement angle. In case of supply voltage disturbances V_{DC} will undergo a change according to the variations of the supply amplitude. Since the output quantities of the matrix converter are drawn by the SVM of the inverter stage based on the fictitious dc link quantities, they will also experience the direct effect on the changed dc link voltage. By modifying m according to the input voltage amplitude output quantities can be compensated. The momentary amplitude of the three phase input supplies is decided by detecting the supply voltages is given by (3.35).

Modulation index becomes

$$m = m_c \cdot m_v \cdot \frac{V_{im}}{V_{imi}} \tag{3.38}$$

3.7 Simulation Results

Extensive simulation is carried out to investigate the performance of the 3-phase to 3-phase Matrix Converter for different frequencies using Venturini and SVM technique.

Venturini Modulation Method

Simulation results of a Matrix Converter loaded with R-L load at V_i = 220V, f_i = 50Hz, f_o = 100Hz, q=.5 are presented in Figs 3.9-3.12. In general neutral of load n is isolated from the neutral of source N. The FFT analysis of output current is shown in Fig 3.12 (c); results show that total harmonic distortion is 1.52%. The main harmonics are located at 100Hz and additional harmonics are around switching frequency.

Load Specifications:

R-L load: R=10Ω, L=50mH.

V_i = 220V, f_i = 50Hz, f_o = 100Hz, q=.5, f_s =5000Hz

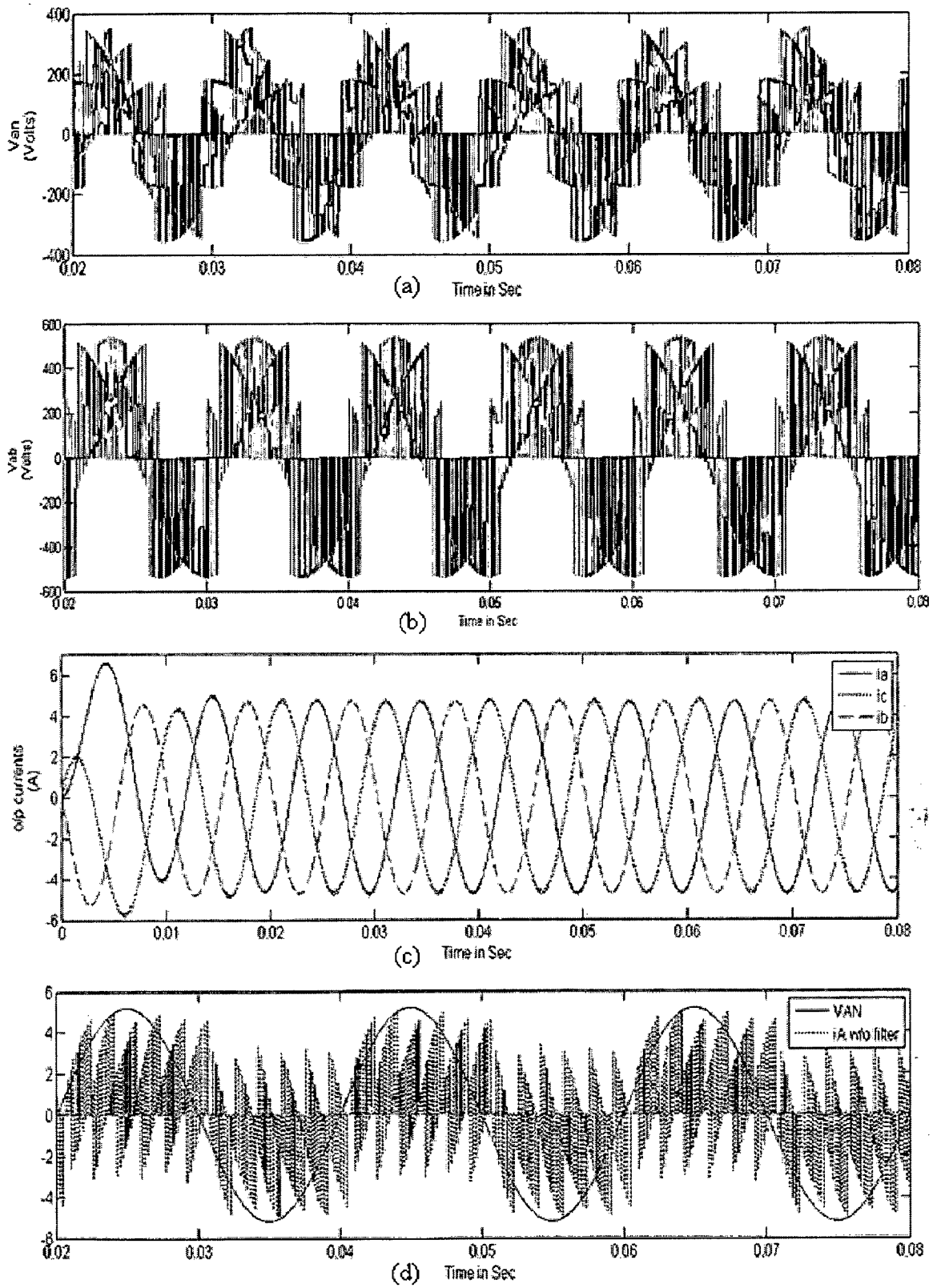

Fig 3.9 (a) Output phase Voltage V_{an} (b) Output line Voltage V_{ab} (c) Output current for all 3-phases (d) Input line current i_A and phase voltage V_{AN} without filter

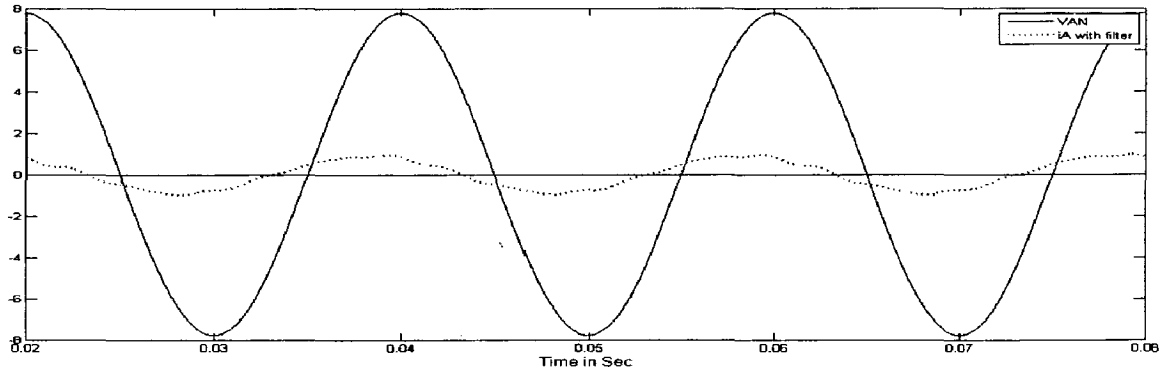

Fig 3.10: Input line current i_A and phase voltage V_{AN} with filter

In Figs 3.9(d)-3.10 voltage scale is 60V/div and current is 1A/div.

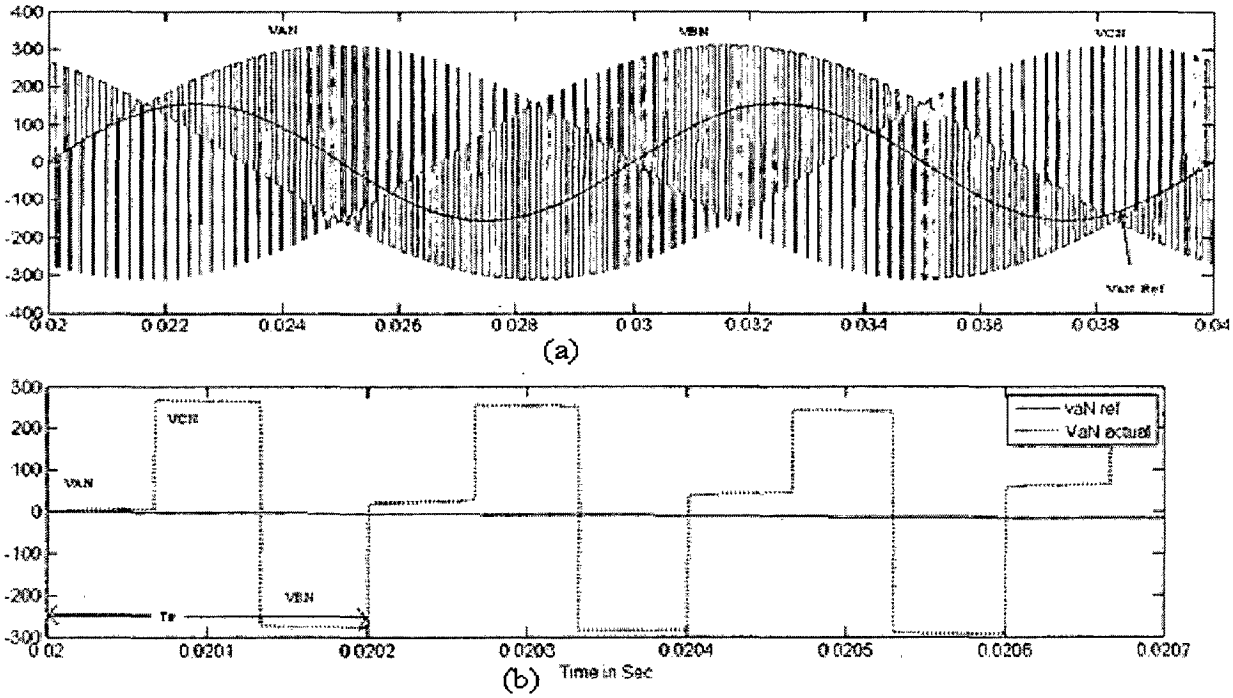

Fig 3.11 (a) Output phaseVoltage V_{aN}
(b) Working principle of an MC for generation of V_{aN}

Fig 3.9 (d) shows that the input current generated by the matrix converter has the form of several pulses with high di/dt, making it necessary to introduce an input filter to avoid the generation of overvoltages. The parameters of the filter for simulation are Filter inductor =40mH, Filter capacitor = 5μF. The frequency spectrum in Fig 3.12 (a) confirms the

presence of high-order harmonics in the input current i_A without filter with THD of 230.72%. Fig 3.10 shows that the source current i_A is free of high-frequency harmonics, due to the action of the input filter, which also is confirmed by Fig 3.12 (b) where THD is 6.87%.

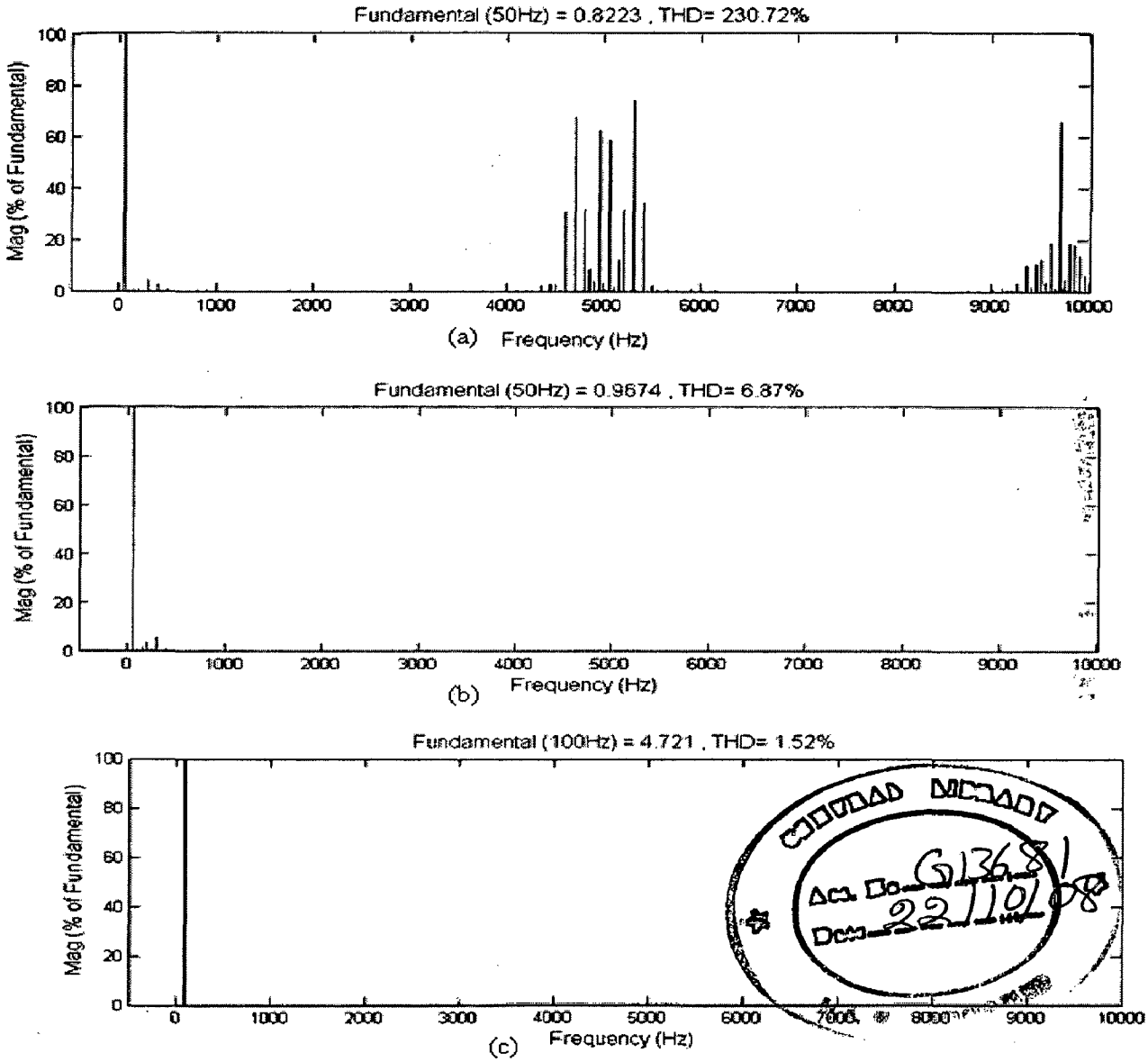

Fig 3.12: (a) FFT of input current without filter (b) FFT of input current with filter (c) FFT of output line current i_a

Simulation results of a Matrix Converter loaded with R-L load at V_i = 220V, f_i = 50Hz, f_o = 25Hz, q=.5 are presented in Figs 3.13-3.15. In general neutral of load n is isolated from the neutral of source N. The FFT analysis of output current is shown in Fig 3.15 (c); results show that total

harmonic distortion is 0.74%. The main harmonics are located at 25Hz and additional harmonics are around switching frequency.

Load Specifications:

R-L load: R=10Ω, L=50mH.

V_i = 220V, f_i = 50Hz, f_o = 25Hz, q=.5, f_s =5000Hz

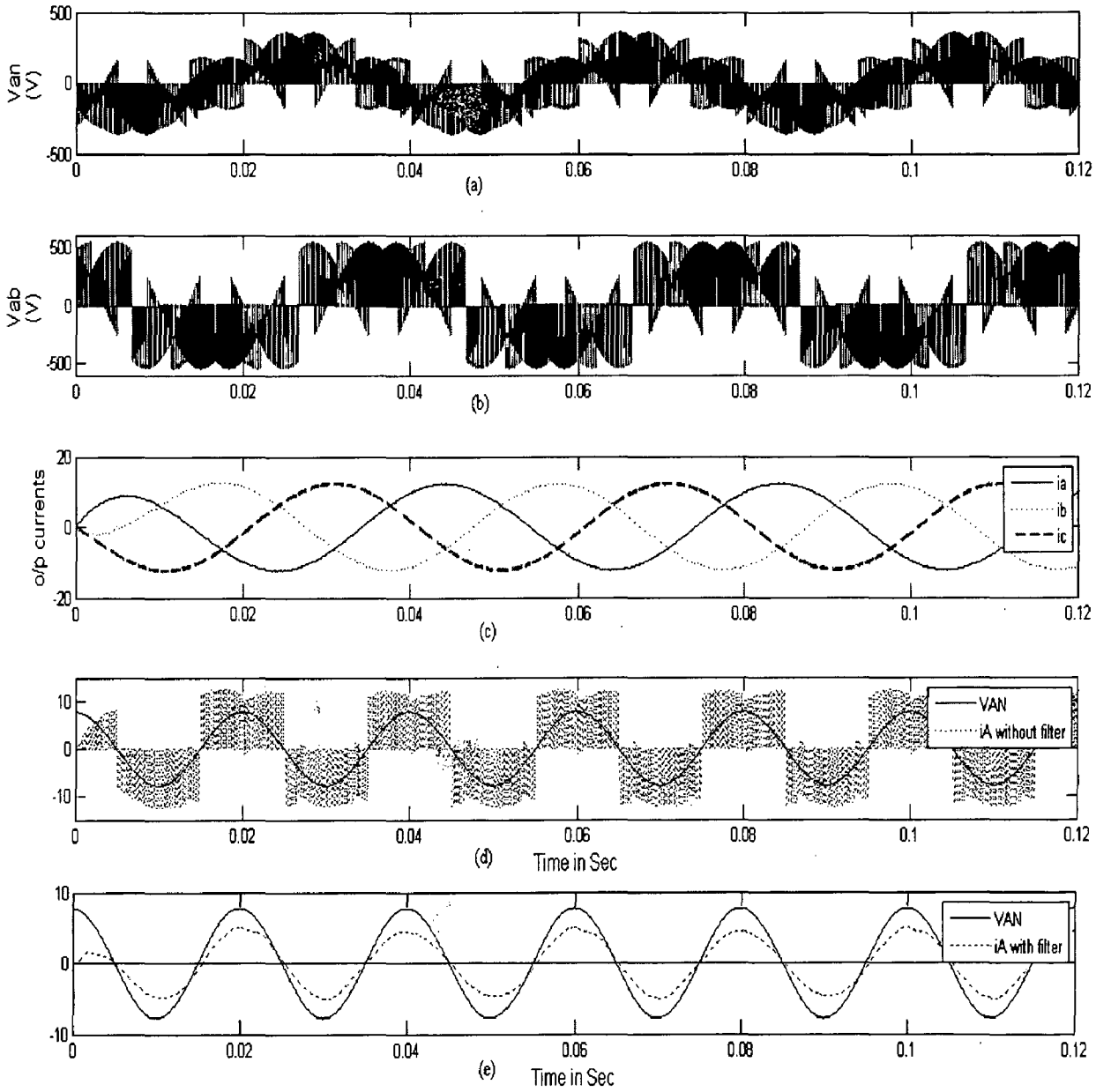

Fig 3.13 (a) Output phase Voltage V_{an} (b) Output line Voltage V_{ab} (c) Output current for all 3-phases (d) Input line current i_A and phase voltage V_{AN} without filter (e) Input line current i_A and phase voltage V_{AN} with filter

In Figs 5.13 (d)-(e) voltage scale is 40V/div and current is 1A/div.

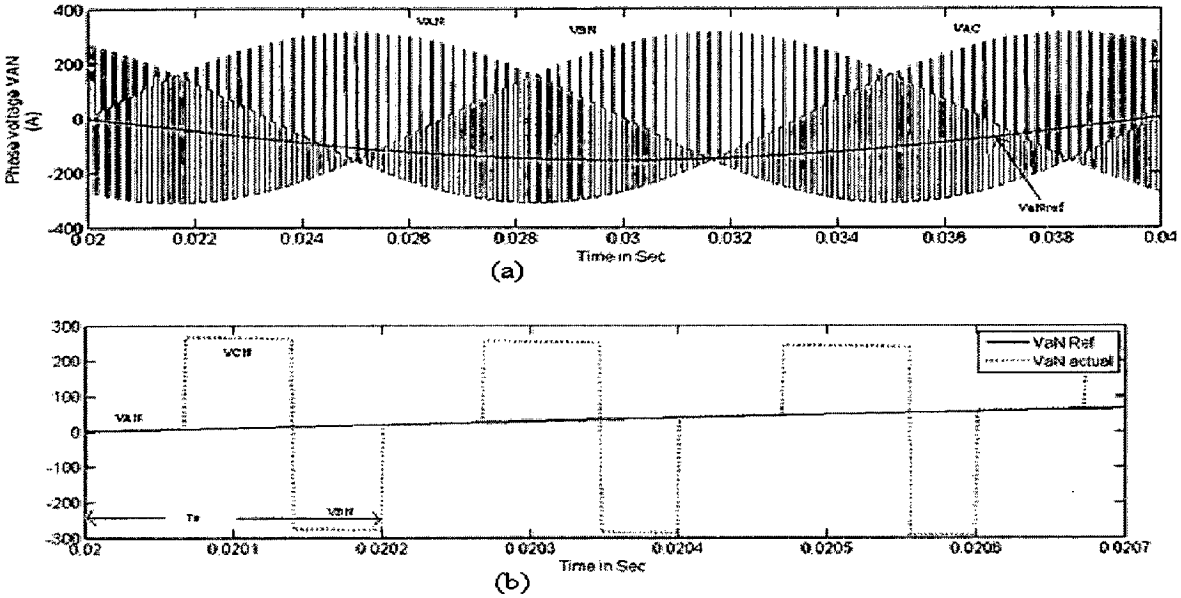

Fig 3.14 (a) Output phaseVoltage V_{aN}

(b) Working principle of an MC for generation of V_{aN}

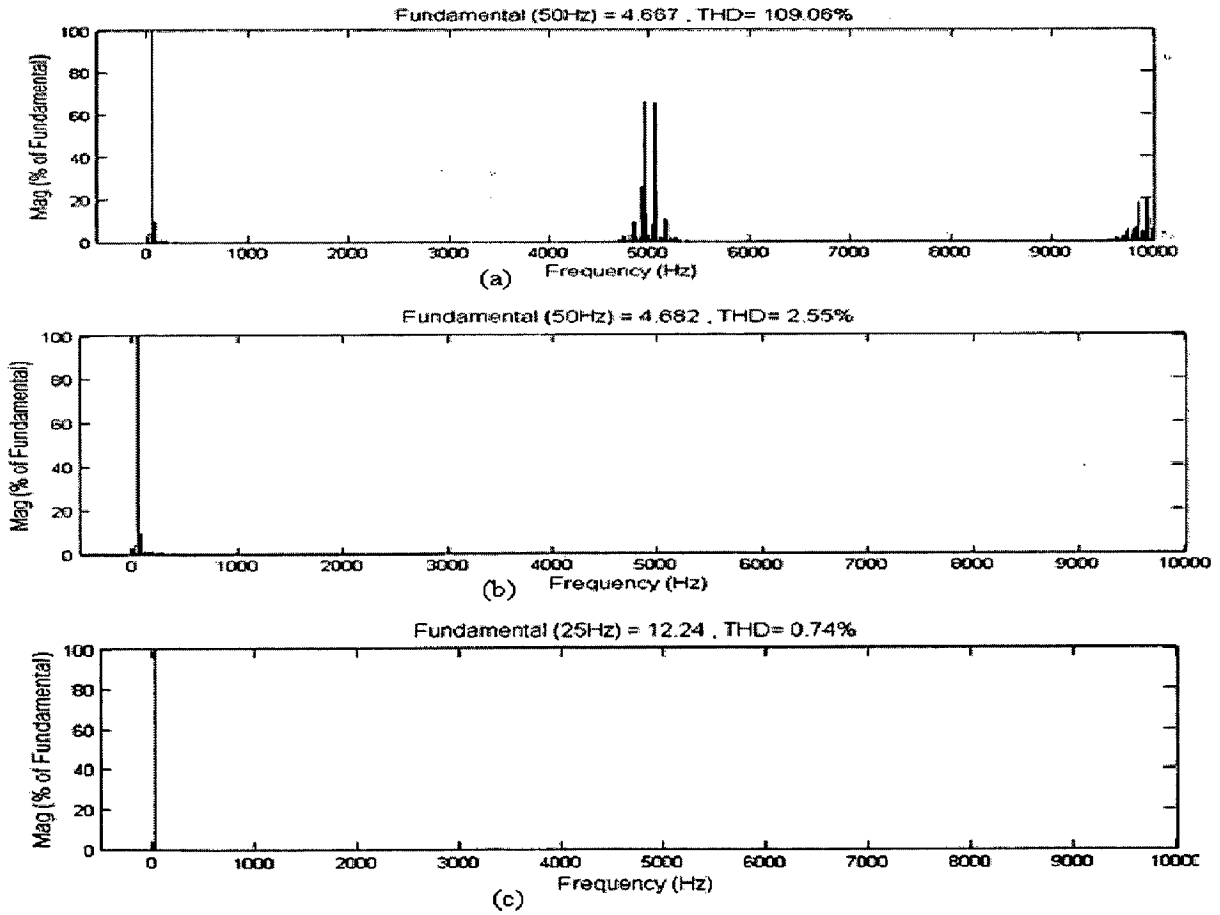

Fig 3.15: (a) FFT of input current without filter (b) FFT of input current with filter (c) FFT of output line current i_a

Fig 3.16 illustrate the simulation results for a step change in output frequeny instantaneously from 100Hz to 25Hz at t=.1s with R-L load(R=10Ω, L=50mH) at amplitude of input voltage V_i = 220V, f_i = 50Hz, q=.5, f_s =5000Hz

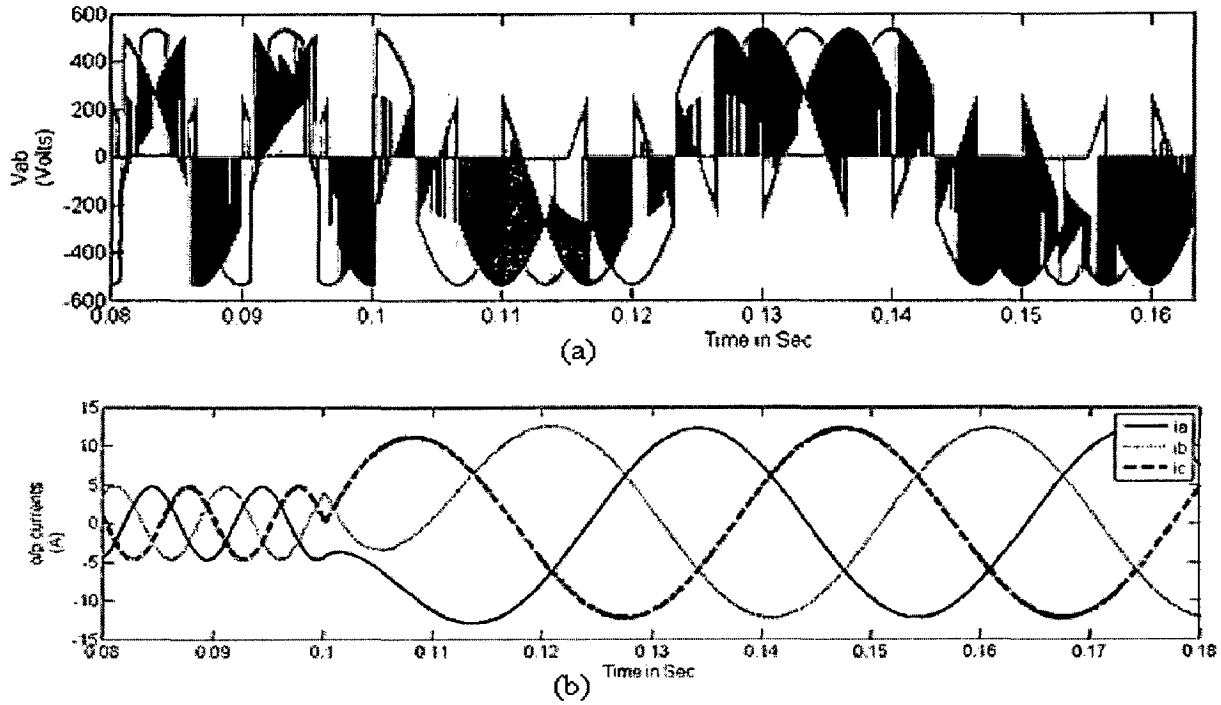

Fig 3.16: (a) Output line voltage Vab for step change in output frequency from 100Hz to 25Hz at t=.1s (b) Output line currents for step change in output frequency from 100Hz to 25Hz at t=.1s

Modified Venturini Method:

In the Venturini Method the maximum voltage transfer ratio is 0.5, this limitation can be overcome by Modified Venturini Method. Simulation results of a Matrix Converter loaded with R-L load at V_i = 220V, f_i = 50Hz, f_o = 40Hz, q=.8 are presented in Figs 3.17.In this method output phase voltages are little bit distorted but line voltages and currents are not distorted.

Load Specifications:

R-L load: R=10Ω, L=50mH.

V_i = 220V, f_i = 50Hz, f_o = 40Hz, q=.8, f_s =5000Hz

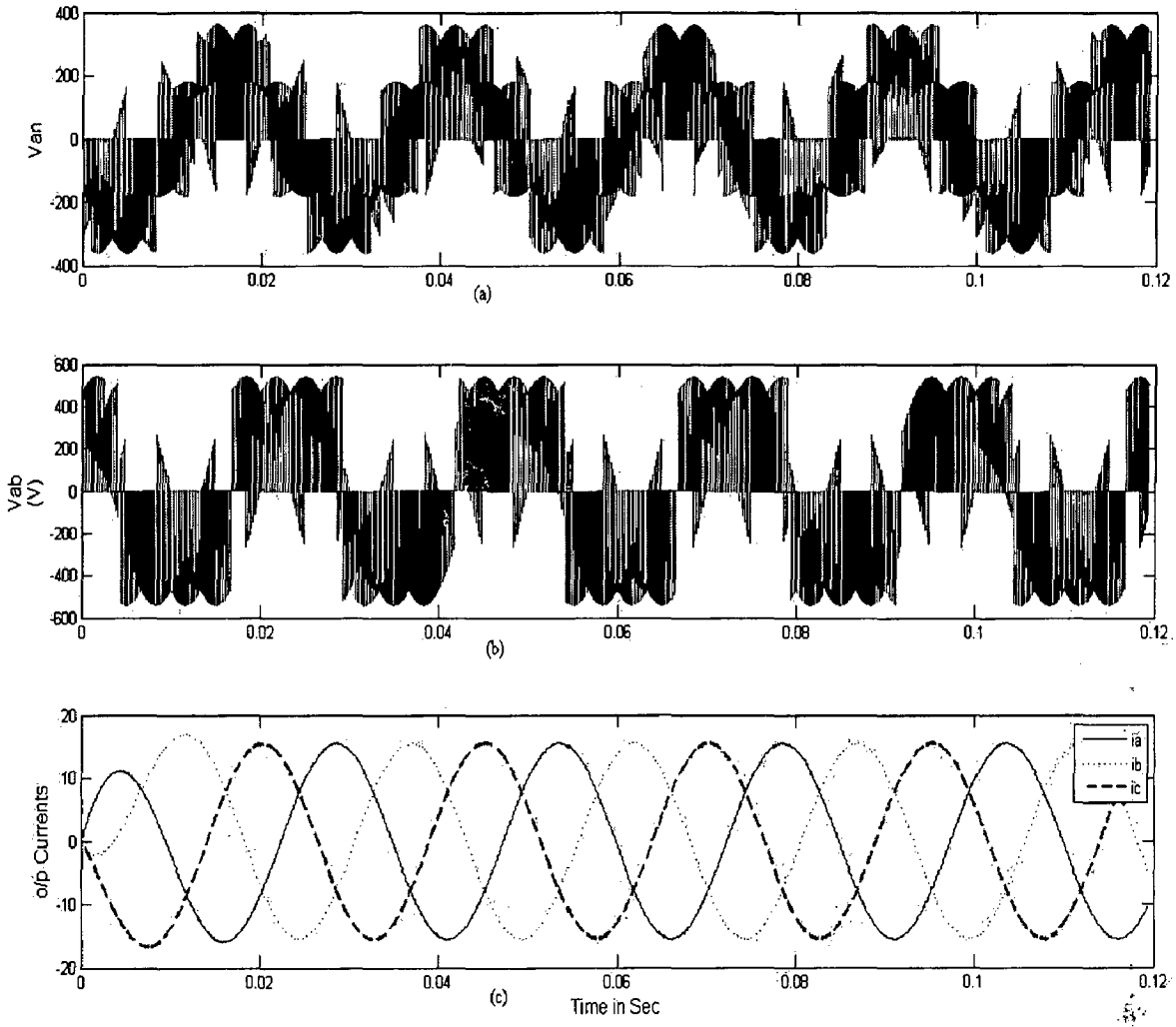

Fig 3.17 (a) Output phase Voltage V_{an} (b) Output line Voltage V_{ab} (c) Output current for all 3-phases

Compensation Using Venturini Method

Simulation results of a Matrix Converter loaded with R-L load at V_i = 220V, f_i = 50Hz, f_o = 40Hz, q=.6 are presented in Figs 3.18-3.19. In Fig 3.18 compensation for voltage sag is shown and in Fig 3.19 compensation for input voltage harmonics are shown. Results show that output currents are not affected by input voltage distortions.

Load Specifications:

R-L load: R=10Ω, L=50mH.

V_i = 220V, f_i = 50Hz, f_o = 40Hz, q=.6, f_s =5000Hz

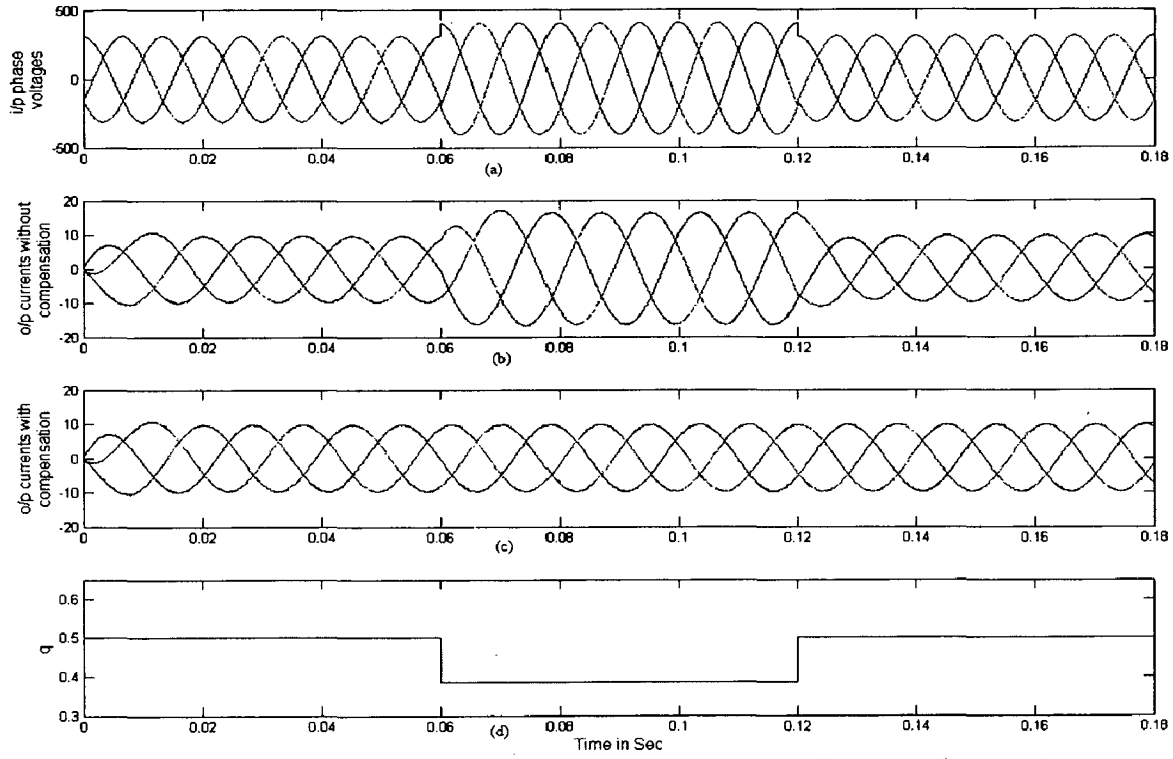

Fig 3.18: Simulated results of matrix converter when input voltages have sudden 30% balanced voltage swell (fo=40Hz, fs=5KHz, q=0.6)

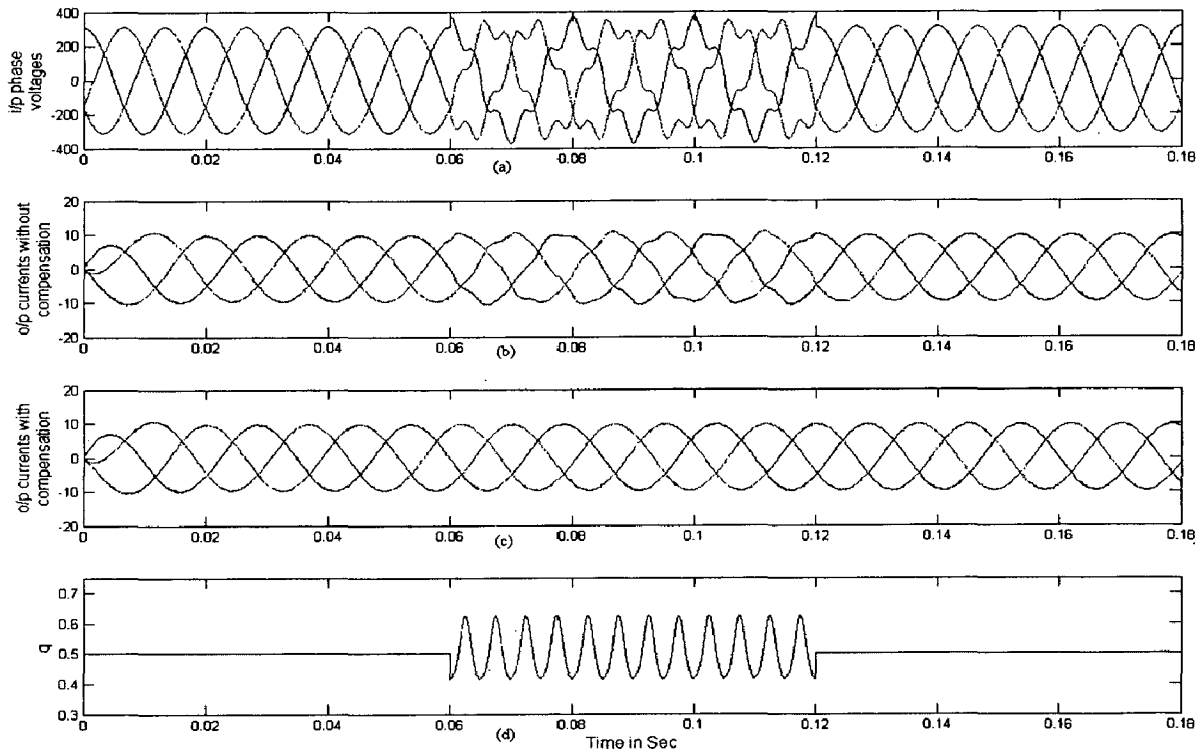

Fig 3.19: Simulated results of matrix converter when input voltages have 5th order harmonics with magnitude 20% of fundamental (fo=40Hz, fs=5KHz q=0.6)

SVM Method

Simulation results of a Matrix Converter loaded with R-L load at V_i = 220V, f_i = 50Hz, f_o = 100Hz, q=0.8 are presented in Figs 3.20-3.28. In this technique the q can be greater than 0.5.In this technique input power factor can be controlled. Fig 3.23-3.25 shows the input phase voltage and current with 0^0,30^0 lag, 30^0 lead phase difference.

Load Specifications:

R-L load: R=10Ω, L=50mH.

V_i = 220V, f_i = 50Hz, f_o = 100Hz, q=.8, f_s =5000Hz

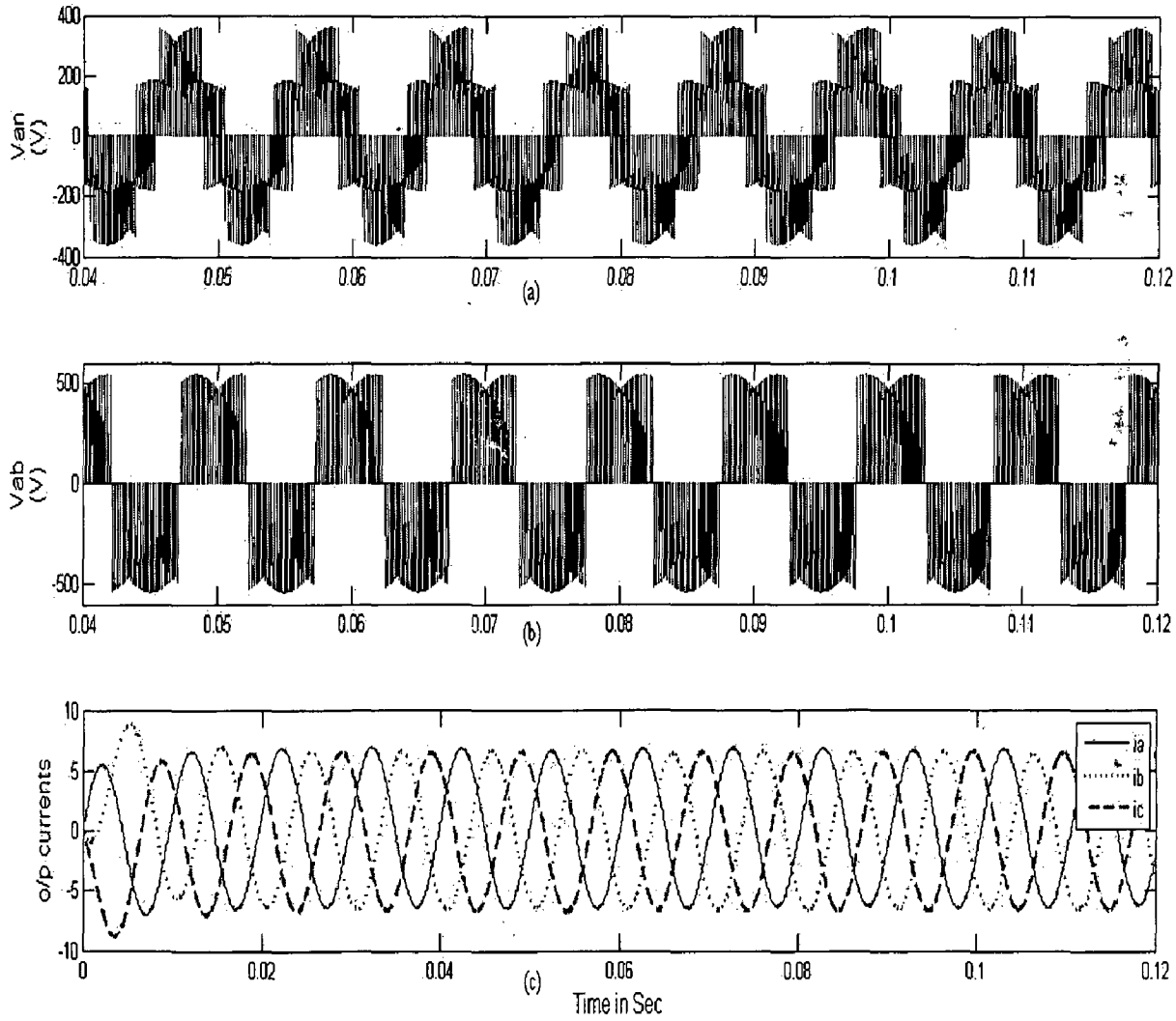

Fig 3.20 (a) Output phase Voltage V_{an} (b) Output line Voltage V_{ab} (c) Output current for all 3-phases

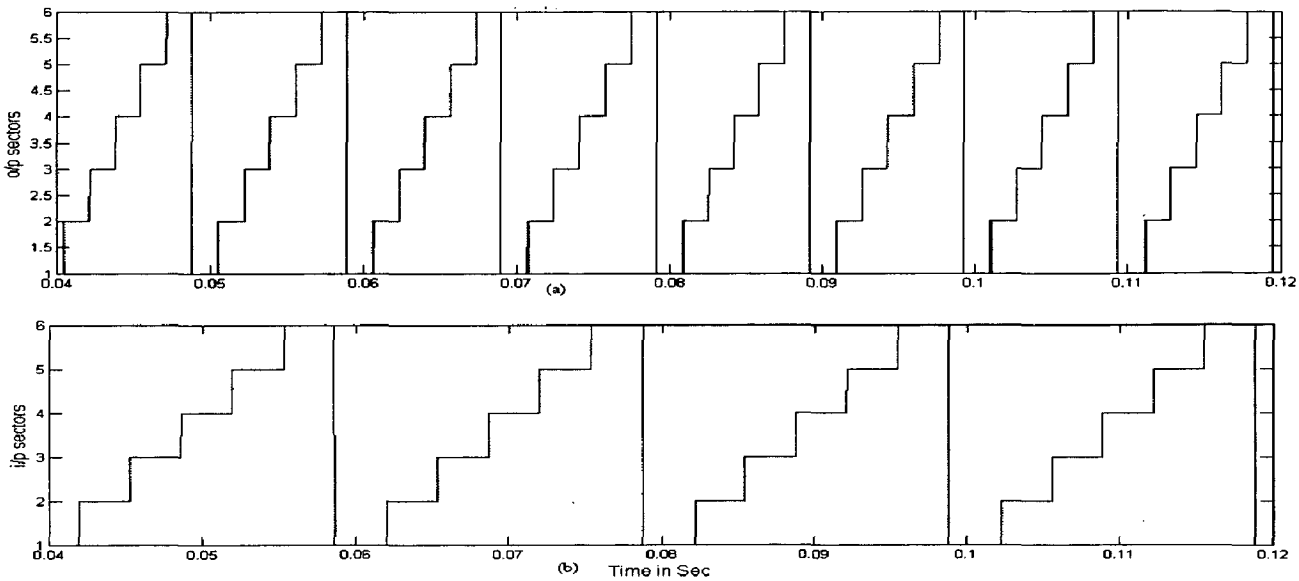

Fig 3.21: (a) Output voltage sectors (b) Input current sectors

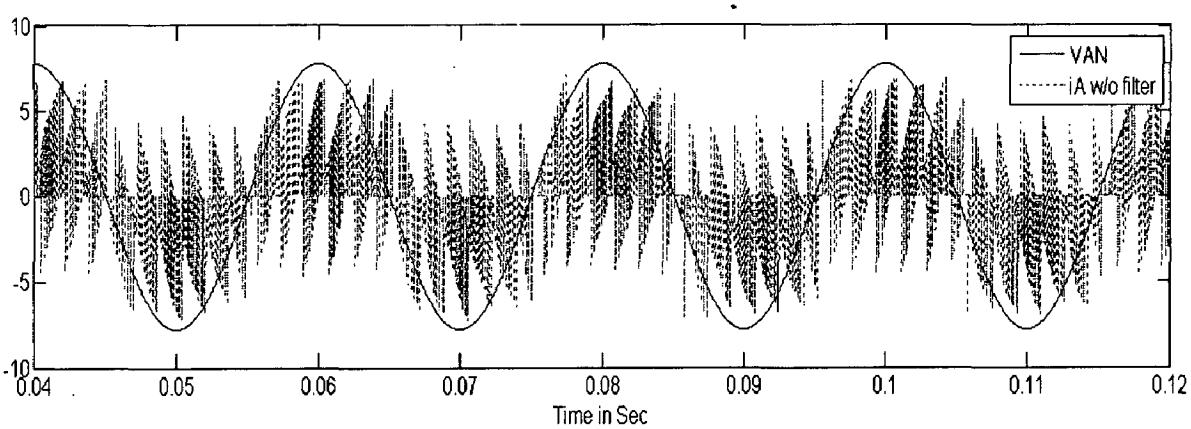

Fig 3.22: Input line current i_A and phase voltage V_{AN} without filter

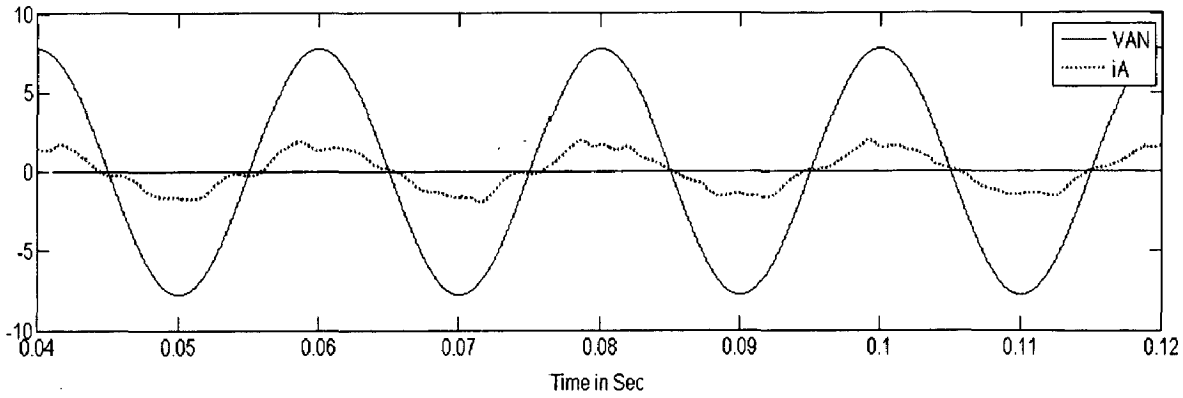

Fig 3.23: Input line current i_A and phase voltage V_{AN} with filter and phase difference (φ_i=0)

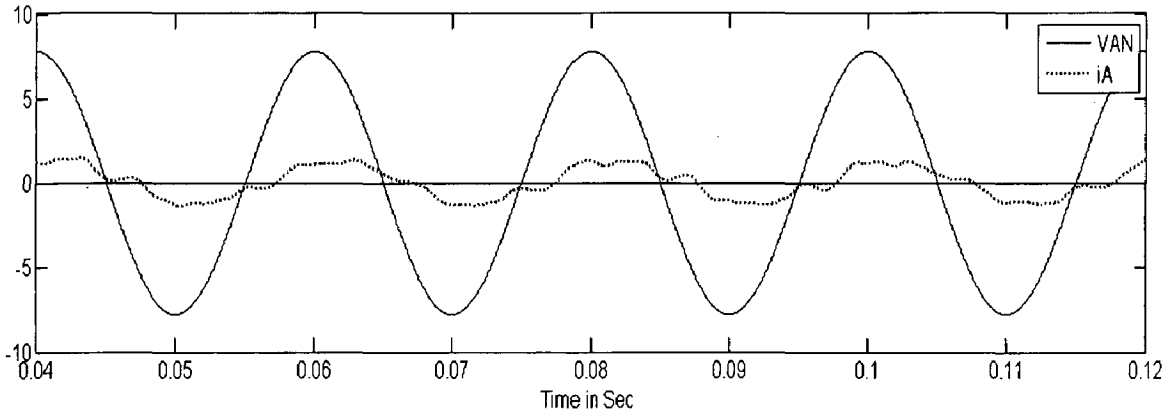

Fig 3.24: Input line current i_A and phase voltage V_{AN} with filter and phase difference (φ_i=30° lag)

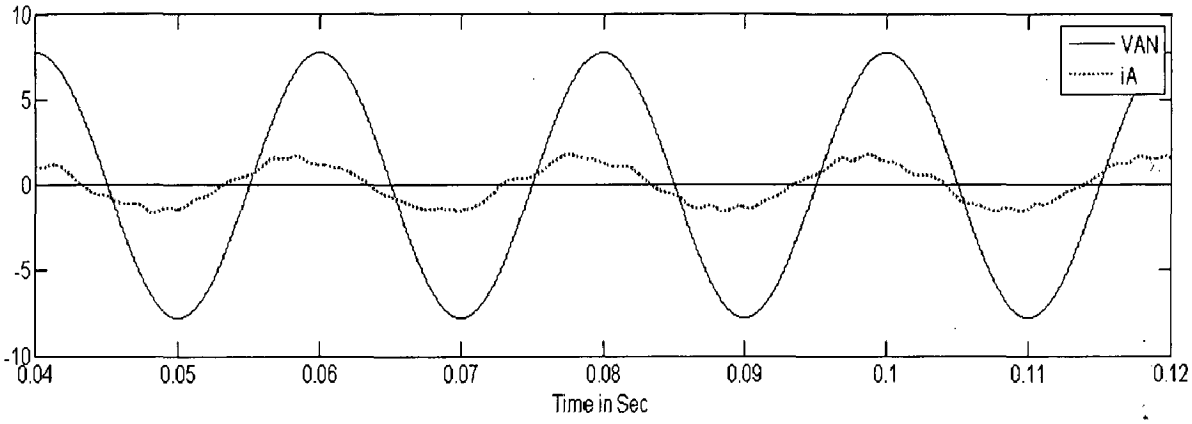

Fig 3.25: Input line current i_A and phase voltage V_{AN} with filter and phase difference (φ_i=30° lead)

In Figs 3.22-3.25 voltage scale is 40V/div and current is 1A/div.

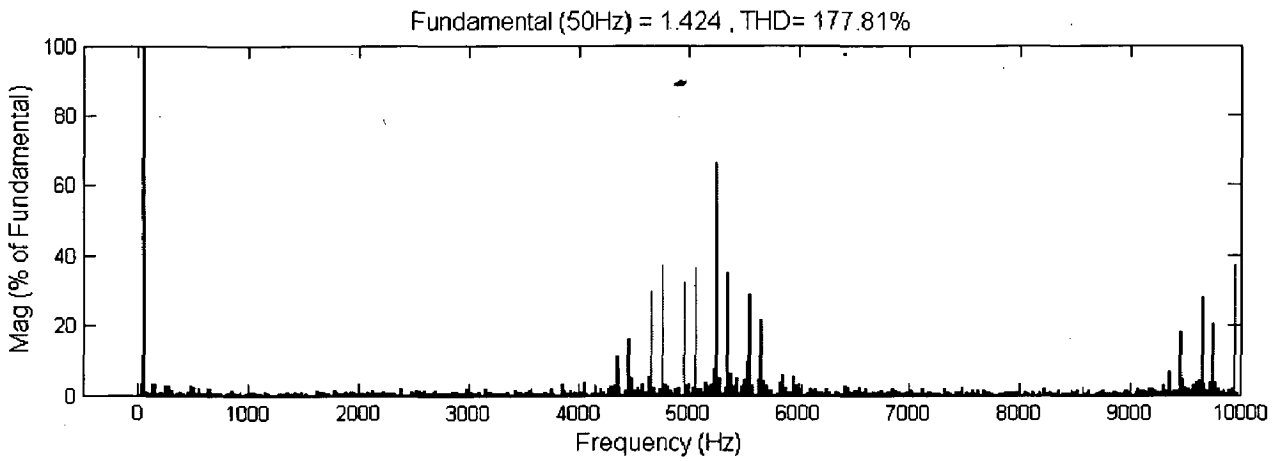

Fig 3.26: FFT of input current without filter

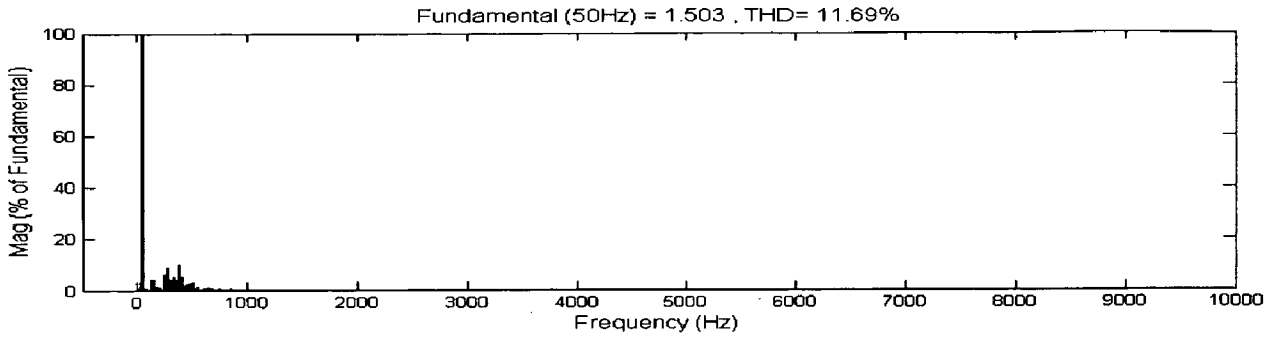

Fig 3.27: FFT of input current with filter

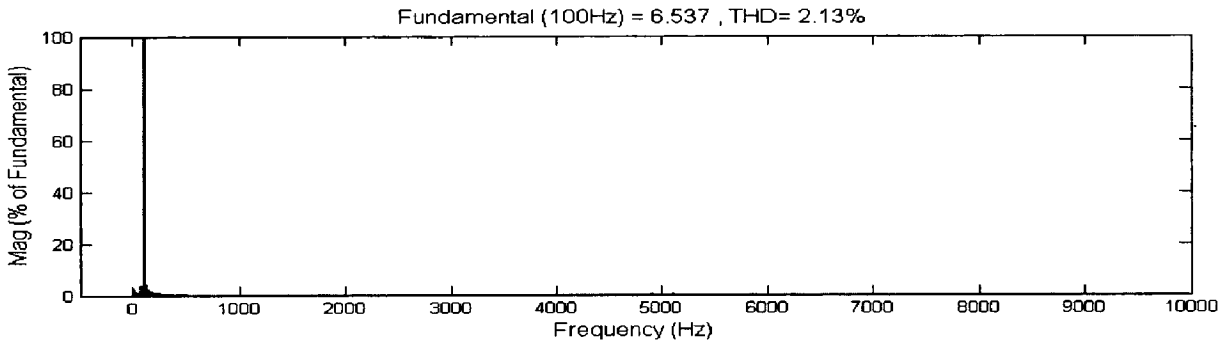

Fig 3.28: FFT of output line current i_a

Simulation results of a Matrix Converter loaded with R-L load at V_i = 220V, f_i = 50Hz, f_o = 25Hz, q=.8 are presented in Figs 3.29-3.32.

Load Specifications:

R-L load: R=10Ω, L=50mH.

V_i = 220V, f_i = 50Hz, f_o = 25Hz, q=.8, f_s =5000Hz

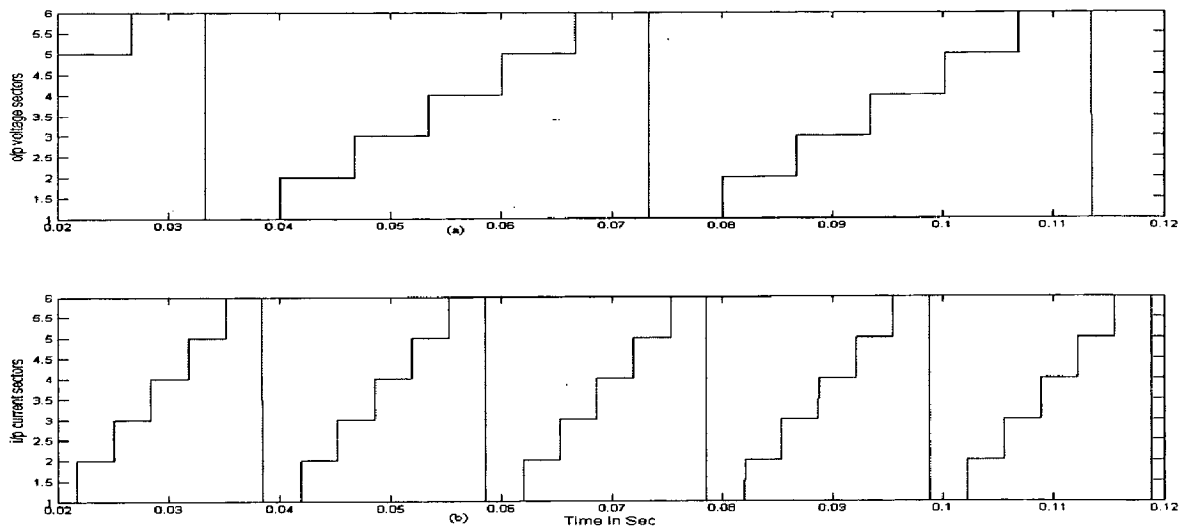

Fig 3.29: (a) Output voltage sectors (b) Input current sectors

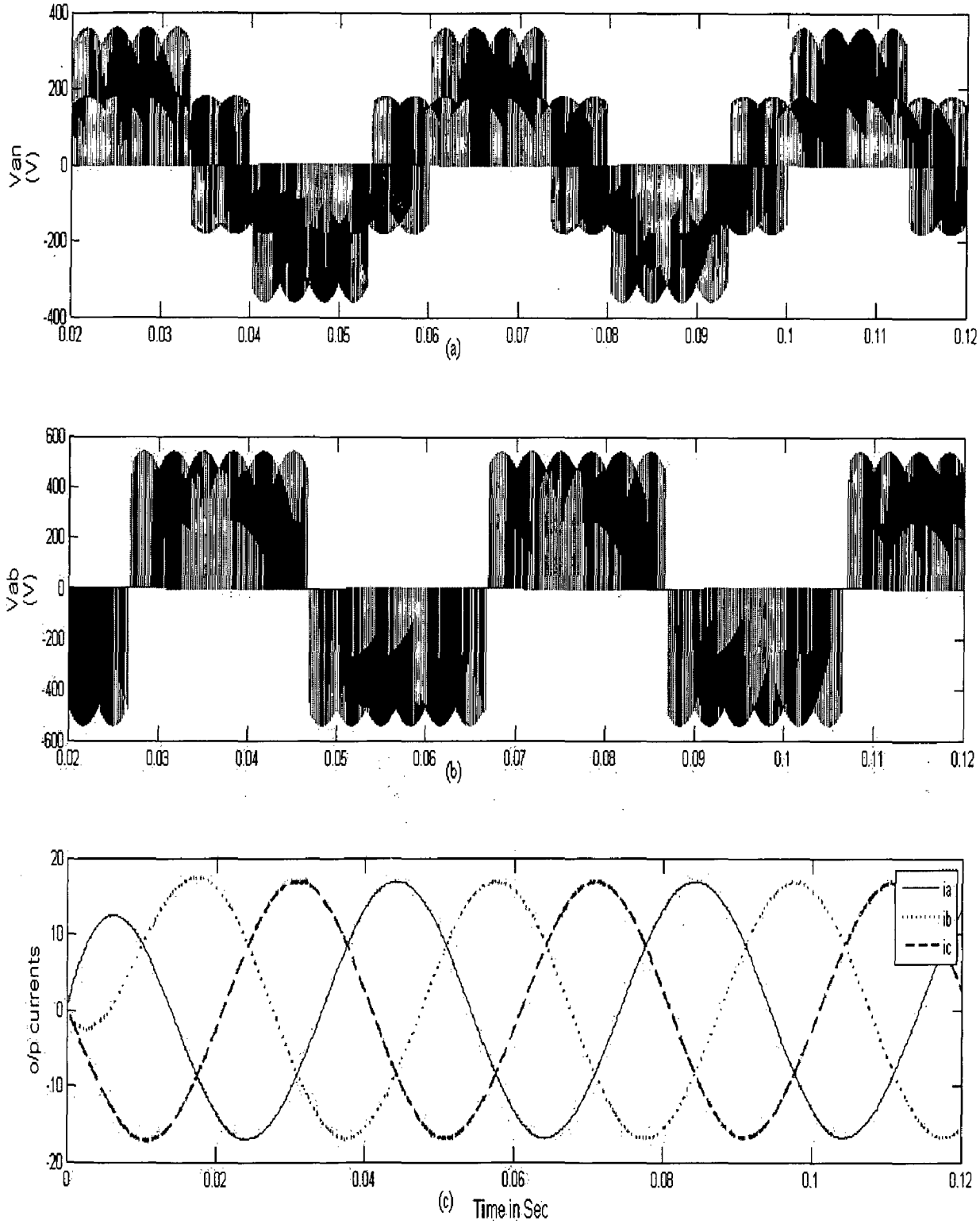

Fig 3.30 (a) Output phase Voltage V_{an} (b) Output line Voltage V_{ab} (c) Output current for all 3-phases

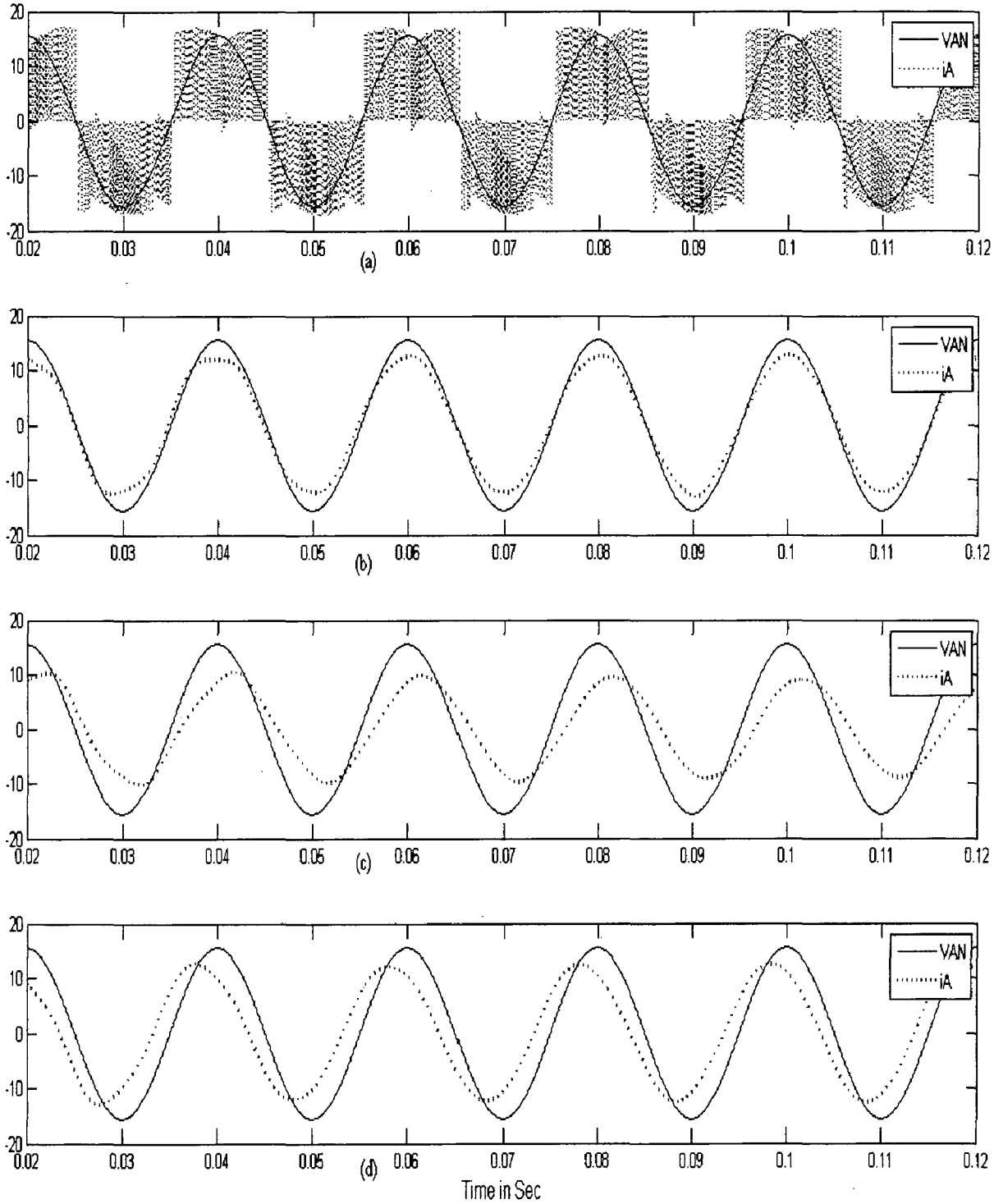

Fig 3.31: (a) Input line current i_A and phase voltage V_{AN} without filter (b) Input line current i_A and phase voltage V_{AN} with filter and phase difference (φ_i=0) (c) Input line current i_A and phase voltage V_{AN} with filter and phase difference (φ_i=30° lag) (d) Input line current i_A and phase voltage V_{AN} with filter and phase difference (φ_i=30° lead)

In Figs 3.31 voltage scale is 20V/div and current is 1A/div.

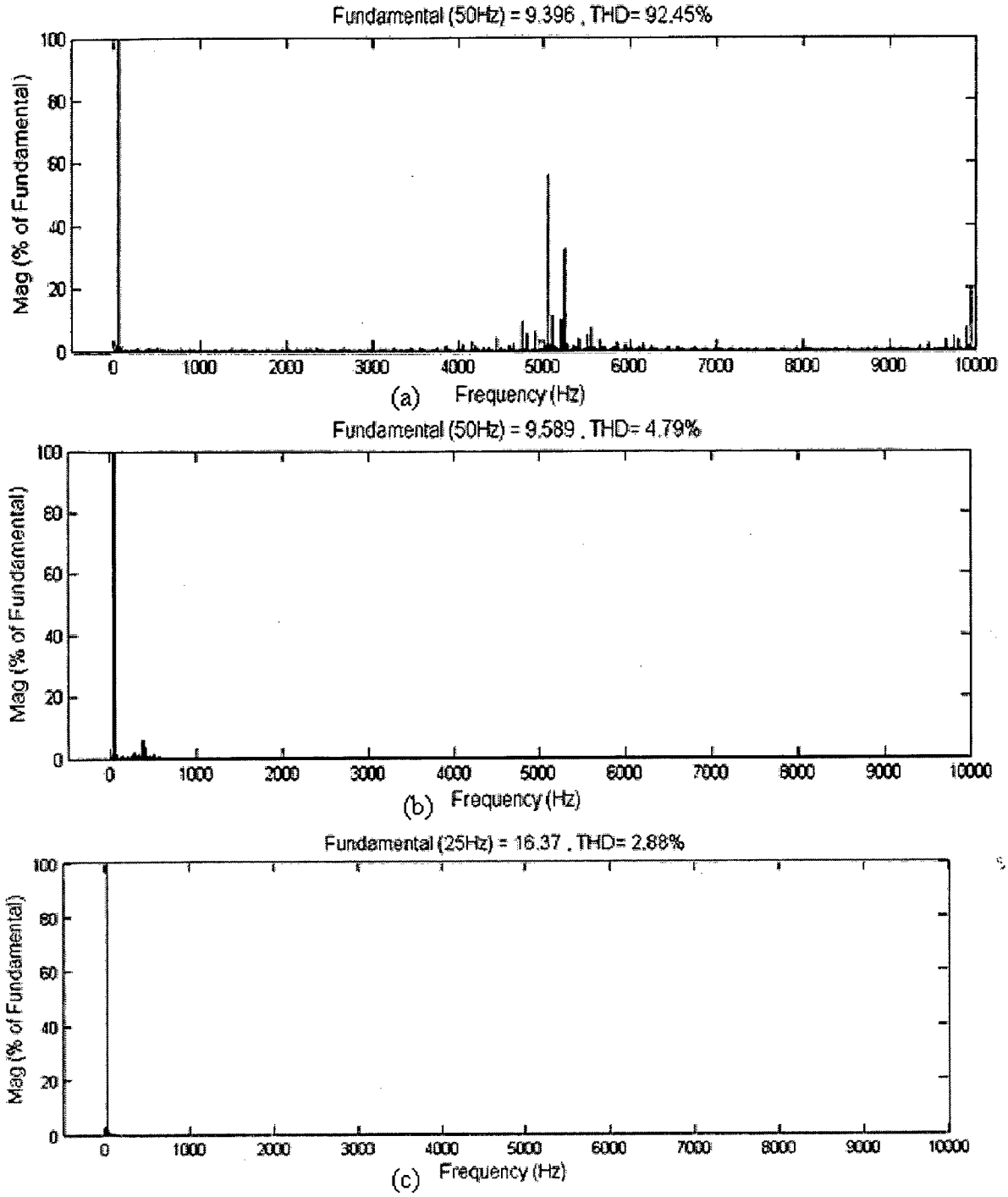

Fig 3.32: (a) FFT of input current without filter (b) FFT of input current with filter (c) FFT of output line current i_a

Fig 3.33 illustrate the simulation results for a step change in output frequeny instantaneously from 100Hz to 25Hz at t=.1s with R-L load(R=10Ω, L=50mH) at amplitude of input voltage V_i = 220V, f_i = 50Hz, q=.8, f_s =5000Hz

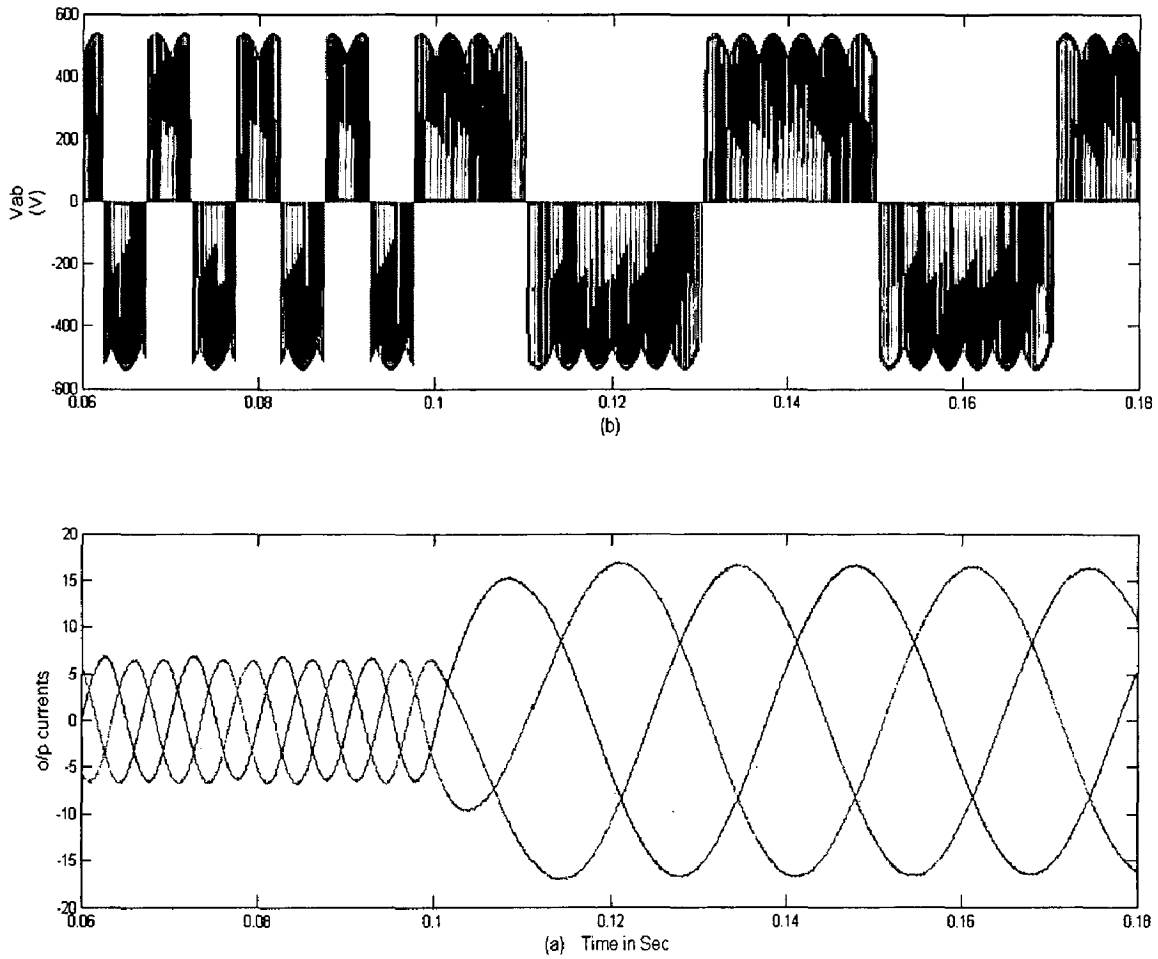

Fig 3.33: (a) Output line voltage Vab for step change in output frequency from 100Hz to 25Hz at t=.1s (b) Output line currents for step change in output frequency from 100Hz to 25Hz at t=.1s

Compensation Using SVM Method

Simulation results of a Matrix Converter loaded with R-L load at V_i = 220V, f_i = 50Hz, f_o = 40Hz, m=.6 are presented in Figs 3.34-3.35. In Fig 3.34 compensation for voltage sag is shown and in Fig 3.35 compensation for input voltage harmonics are shown. Results show that output currents are not affected by input voltage distortions.

Load Specifications:

R-L load: R=10Ω, L=50mH.
V_i = 220V, f_i = 50Hz, f_o = 40Hz, q=.6, f_s =5000Hz

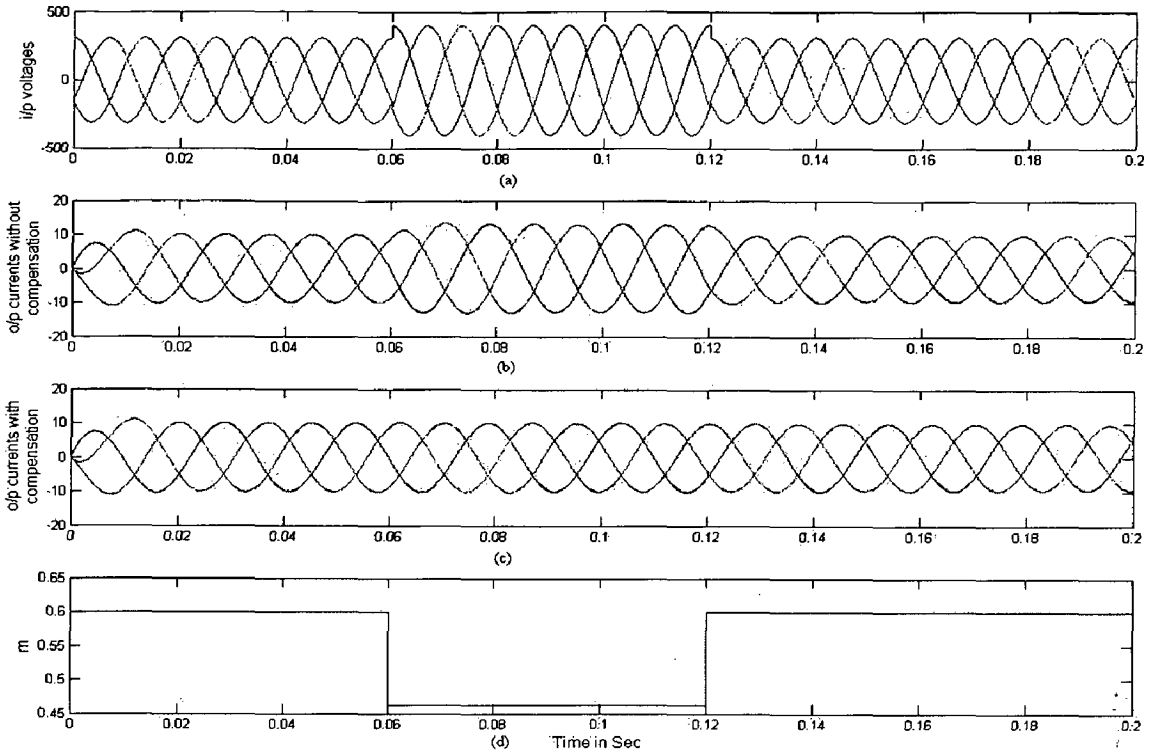

Fig 3.34: Simulated results of matrix converter when input voltages have sudden 30% balanced voltage swell (fo=40Hz, fs=5KHz, q=0.6)

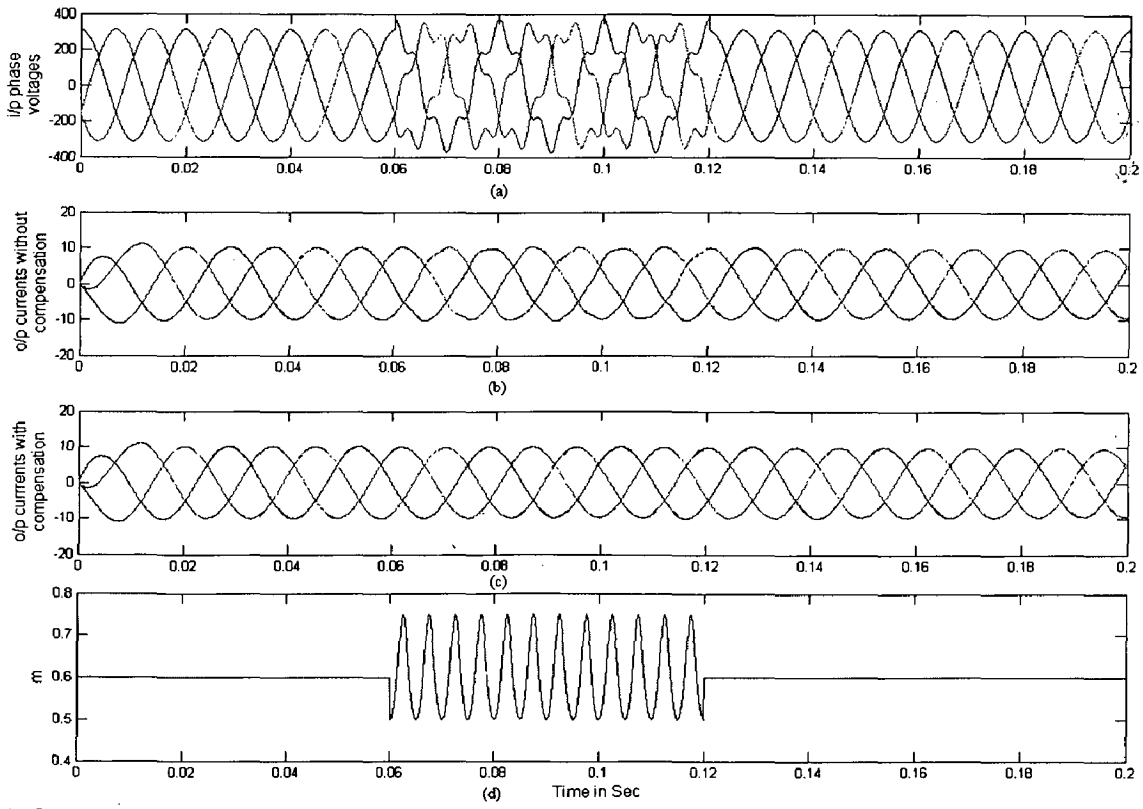

Fig 3.35: Simulated results of matrix converter when input voltages have 5th order harmonics with magnitude 20% of fundamental (fo=40Hz, fs=5KHz q=0.6)

3.8 Conclusions

Three modulation strategies for matrix converters have been presented. The simulation results for the three methods are presented and it is shown that input current power factor is unity and output current harmonics are very small. Methods to compensate for input voltage unbalance and distortions are presented. Results show that output quantities are not affected by input voltage distortions by using the compensation techniques.

Chapter 4

Field Oriented and Direct Torque Control Using Matrix Converters

In this chapter, after a short introduction to the Field Oriented Control (FOC) and Direct Torque Control (DTC) scheme of induction machines, are presented control methods for matrix converters which allow, under the constraint of unity input power factor, the generation of the voltage vectors required to implement these schemes. The performance of the proposed control methods are analyzed and discussed on the basis of simulation results in Chapter 5.

4.1 Introduction

Ac drives using induction machines are now finding increasing acceptance in various industrial variable-speed applications because of the performance they can provide. The development of high-performance control strategies for ac drives, driven by industry requirements, has followed a rapid evolution during the last two decades. It is now recognized that the two high-performance control strategies for induction motor drives are field-oriented control (FOC) and direct torque control (DTC).

FOC technique was firstly proposed F. Blaschke in 1971 and DTC technique was firstly proposed by Takahashi in 1984. These control strategies are different on the operation principle but their objectives are the same. They aim both to control effectively the motor torque and flux in order to force the motor to accurately track the command trajectory regardless of the machine and load parameter variation or any extraneous disturbances. Both control strategies have been successfully implemented in industrial products. The supporters of field-oriented control and direct torque control claim the superiority of their strategy versus the other. Up to now, the question has not been clearly answered.

4.2 Field-oriented control system

Fig. 4.1 shows a block diagram of an indirect field-oriented control system for an induction motor. In this system, the d-q coordinates reference frame is locked to the rotor flux vector rotating at the stator frequency ω_e as shown in Fig. 4.2. This results in a decoupling of the variables so that flux and torque can be separately controlled by stator direct-axis current i_{ds} and quadrature-axis current i_{qs} respectively. The stator quadrature-axis reference i_{qs}^* is calculated from torque reference input T_e^* as:

$$i_{qs}^* = \frac{2}{3} \cdot \frac{2}{p} \cdot \frac{L_r}{L_m} \cdot \frac{T_e^*}{|\Psi_r|_{est}} \tag{4.1}$$

where $|\Psi_r|_{est}$ the estimated rotor flux linkage given by:

$$|\Psi_r|_{est} = \frac{L_m i_{ds}}{1 + \tau_r s} \tag{4.2}$$

The stator direct-axis current reference i_{ds}^* is obtained from rotor flux reference input $|\Psi_r|^*$:

$$i_{ds}^* = \frac{|\Psi_r|^*}{L_m} \tag{4.3}$$

The rotor flux position θ_e, required for coordinates transformation is generated from the rotor speed ω_m and slip frequency ω_{sl}:

$$\theta_e = \int (\omega_m + \omega_{sl}) dt \tag{4.4}$$

The latter is calculated from the stator reference current i_{qs}^* and the motor parameters:

$$\omega_{sl} = \frac{L_m}{|\Psi_r|_{est}} \cdot \frac{R_r}{L_r} \cdot i_{qs}^* \tag{4.5}$$

The i_{qs}^* and i_{ds}^* current references are converted into phase current references i_a^*, i_b^*, i_c^* for the current regulators. The regulators process the measured and reference currents to produce the inverter gating signals S_a, S_b, S_c.

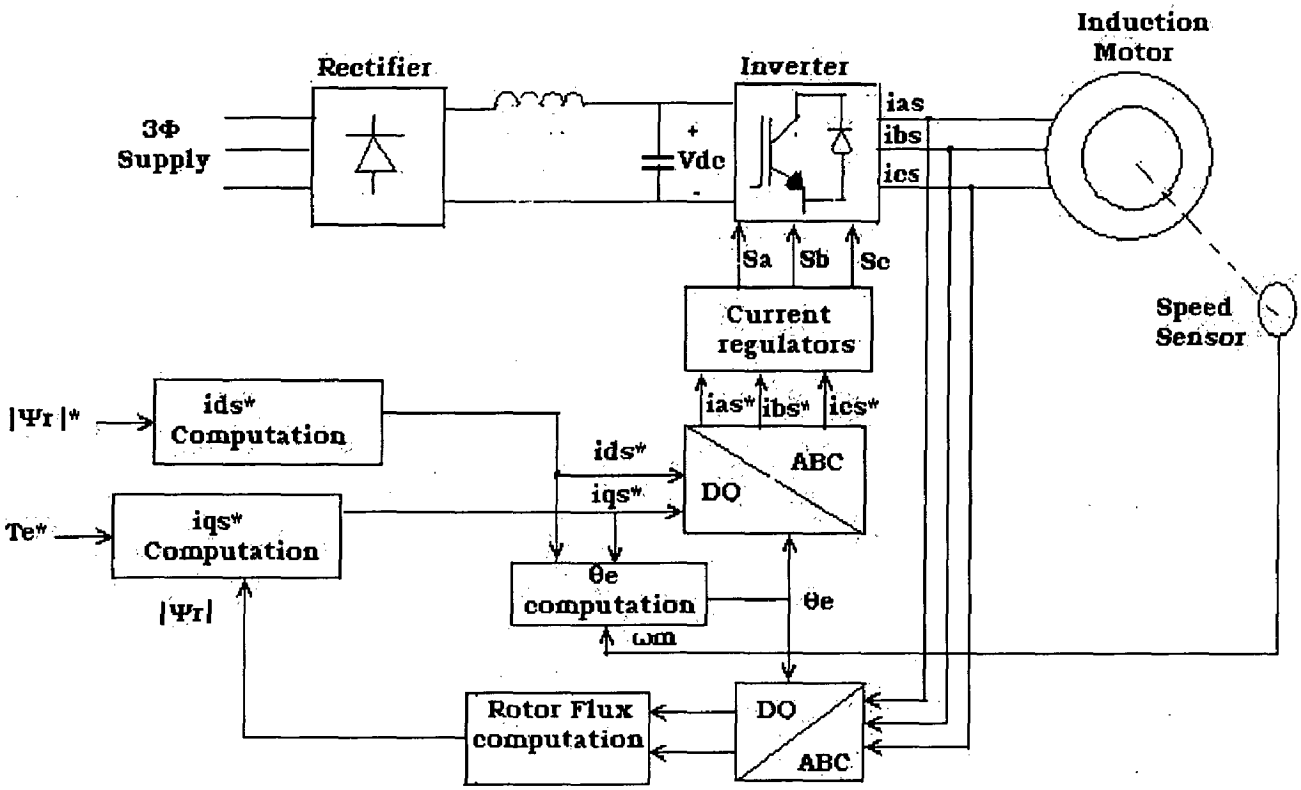

Fig 4.1: Indirect field-oriented control of an induction motor

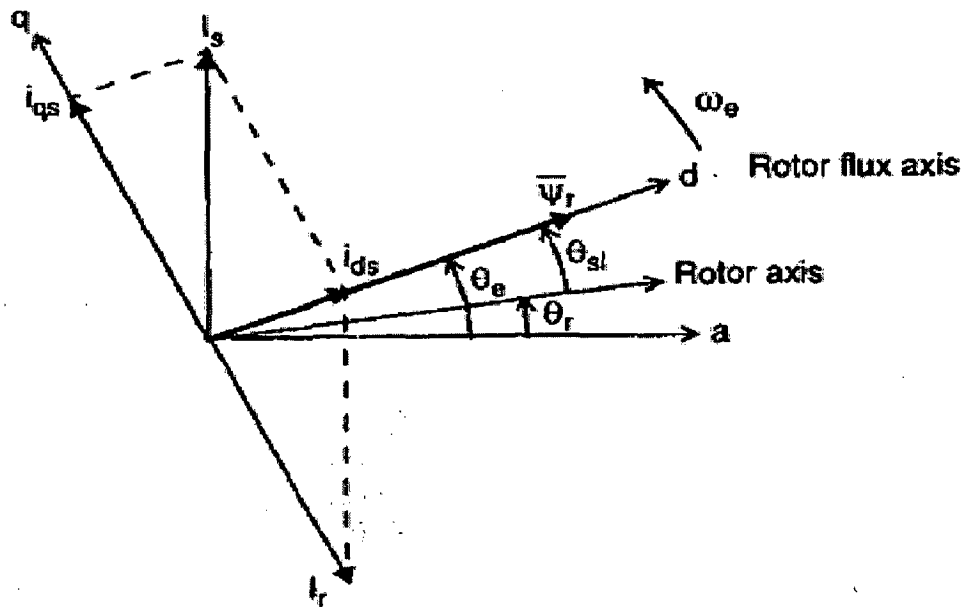

Fig4.2: Field-oriented control principle.

4.3 Direct torque control system

This technique allows to independently control the motor flux, which can be the stator, the rotor or the magnetizing flux, and the electromagnetic torque, at the same time.

If the stator flux is assumed as reference, the estimated values of flux and torque can be calculated just taking into account the stator currents and voltages. Furthermore, the stator resistance is the only motor parameter needed. This is a feature which significantly contributes to the DTC scheme robustness.

The torque control is achieved by quickly changing the position of the stator flux space vector φ_s with respect to the rotor flux space vector φ_r. In fact, for a symmetrical three-phase induction machine, the electromagnetic torque T_{em} is proportional to the scalar product of the stator flux vector φ_s and the rotor flux vector φ_r, referred to a stationary stator reference frame. The following relation holds:

$$T_{em} = \frac{3}{2} pA[\overline{\varphi}_s \cdot j\overline{\varphi}_r]$$

$$A = \frac{M}{L_s L_r - M^2} \tag{4.6}$$

where L_S is the stator self- inductance coefficient, L_R is the rotor self-inductance coefficient in a stator reference frame, M is the mutual inductance coefficient and p the number of poles pairs.

Now, it can be demonstrated that the stator and rotor flux vectors φ_s and φ_r are related by the following expression:

$$\dot{\overline{\varphi}}_r B + \overline{\varphi}_r(1 - jB\omega_m) = \frac{M}{L_s}\overline{\varphi}_s$$

$$B = \left[L_R - \frac{M^2}{L_s}\right]\frac{1}{R_R} \tag{4.7}$$

where $\dot{\bar{\varphi}}_r$ is the time derivative of the rotor flux space vector, R_R is the rotor resistance in the stator frame and ω_m is the mechanical angular velocity of the rotor. Equation (4.7) shows that there is a low-pass filter relation between φ_s and φ_r. This means that the rotor flux vector follows the stator flux vector variations with a finite time delay. The DTC capability to have rapid instantaneous torque variations is based right on this time delay.

The control quantities through which the DTC tracks the reference flux and torque are the radial $\Delta\varphi_{sr}$ and the tangential $\Delta\varphi_{st}$ components of the stator flux variation $\Delta\varphi_s$ impressed by the inverter voltage vector applied to the motor. The expression of the stator flux vector variation $\Delta\varphi_s$ in terms of its radial and tangential components is given by

$$\Delta\bar{\varphi}_s = \Delta\bar{\varphi}_{sr} + \bar{\varphi}_{st} = \bar{\varphi}_{sr}\hat{r} + \bar{\varphi}_{st}\hat{t} \qquad (4.8)$$

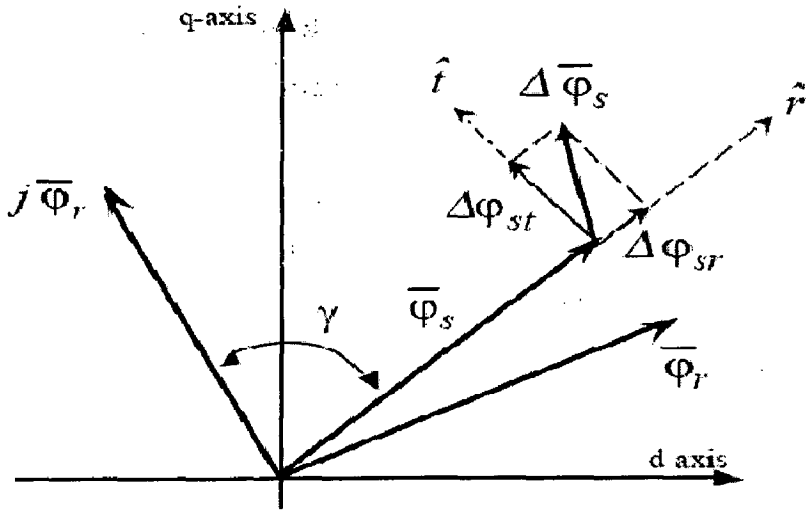

Fig 4.3: Representation of the torque generation operating principle. The stator flux vector variation $\Delta\varphi_s$ is resolved in its radial $\Delta\varphi_{sr}$ and tangential $\Delta\varphi_{st}$ vector components.

As it can be sensed by Fig.4.3, the radial component controls the stator flux vector amplitude while the tangential component controls the stator flux vector angular position and hence the torque.

In Fig 4.4 the schematic circuit of a voltage source inverter is represented along with the voltage vectors corresponding to the eight

different switching configurations that it can assume. Two of them determine zero voltage vectors, v_0 and v_7 , while the remaining generates six equally spaced voltage vectors having the same magnitude. Equation (4.9) gives the general expression for a VSI voltage vector, where U_{DC} is the DC link voltage.

$$\bar{v}_k = \frac{2}{3} U_{DC} e^{j(k-1)\frac{\pi}{3}} \quad k = 1,2,\dots 6 \tag{4.9}$$

In Fig 4.4 it is also shown how the d-q stator reference frame is divided in sectors. Now, for the induction motor stator winding the following equation in terms of space vectors can be written with reference to a stator frame:

$$\bar{v}_s = R_s \bar{i}_s + \frac{d\bar{\varphi}_s}{dt} \tag{4.10}$$

where v_s and i_s are the stator voltage and current space vectors respectively. If it is assumed, for simplicity, to neglect the voltage drop on the stator resistance R_s and to consider a short finite time Δt, representing the control cycle period, equation (4.10) reduces to the following equation

$$\Delta\bar{\varphi}_s = \bar{v}_s \Delta t \tag{4.11}$$

Some remarks can be made with regard to equation (4.11)

First, it shows that the applied inverter voltage vector, $v_k = v_s$, directly impresses the stator flux space vector. This means that the required stator flux vector locus will be obtained by using the opportune inverter output voltage vectors and hence inverter configurations.

Second, equation (4.11) shows that the stator flux space vector moves by the discrete amount $\Delta\varphi_s$ in the direction of the voltage vector applied by the inverter. The amplitude of the variation depends on the DC link voltage, by way of equation (5.4). For a given DC link voltage level, setting the control cycle period Δt the minimum stator flux vector variation $\Delta\varphi_s$ is defined. Substituting equation (4.11) in equation (4.8) the following is obtained

$$\Delta\varphi_{sr}\hat{r} + \Delta\varphi_{st}\hat{t} = \bar{v}_s \Delta t = (v_{sr}\hat{r} + v_{st}\hat{t})\Delta t \tag{4.12}$$

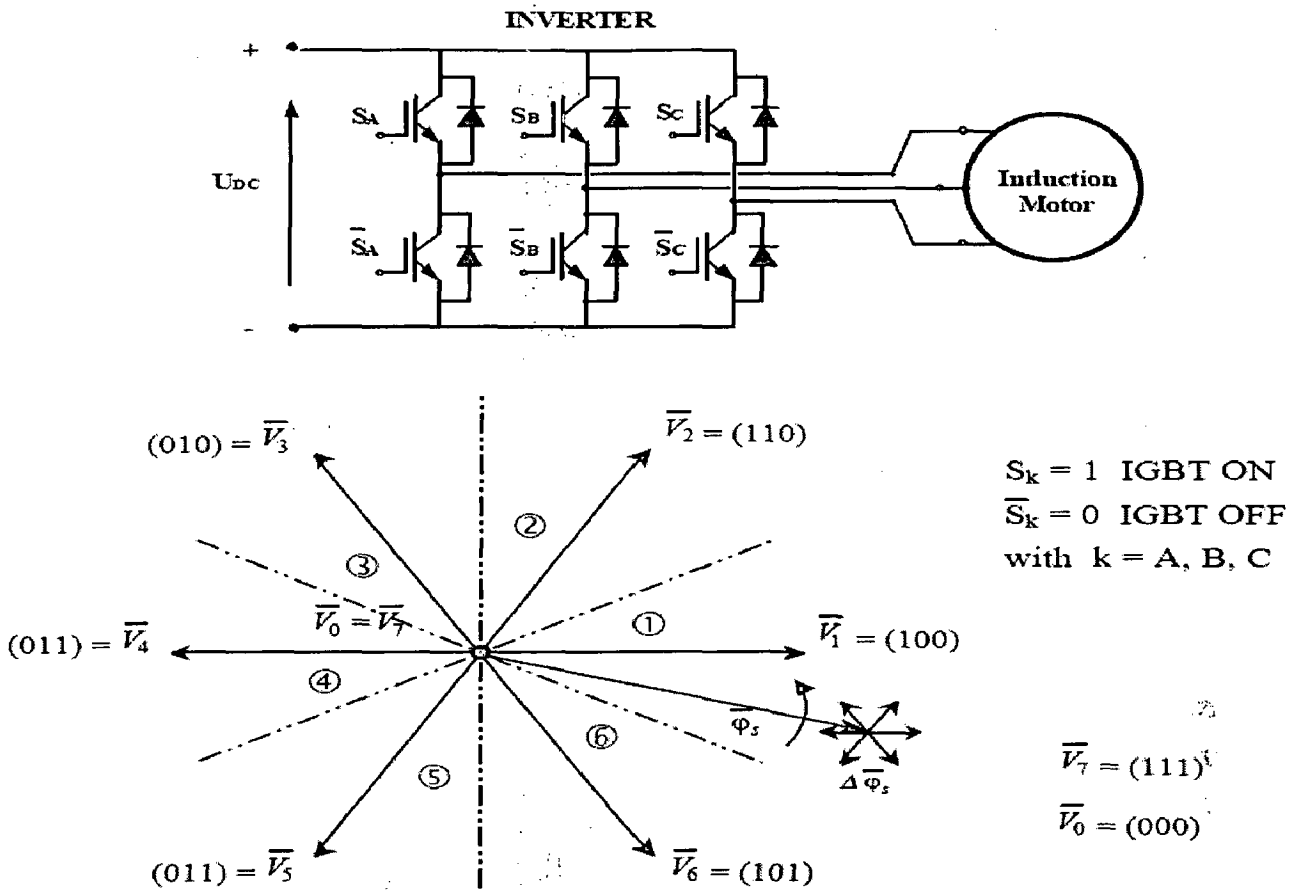

Fig 4.4: Schematic circuit of a voltage source inverter and relevant switching configurations voltage vectors [42]

Equation (4.11) explicitly states that the decoupled control of the stator flux and the electromagnetic torque can be carried out by way of the selection of the opportune inverter voltage vector, and hence switching configuration. It is worth noting that due to the fixed direction of the inverter voltage vectors and to the rotating motion of the stator flux vector φ_s in the d-q stator frame, for each inverter voltage vectors the amplitude of its radial and tangential components will be variable within a sector.

At each cycle period, hereinafter indicated by t_C, the selection of the proper inverter voltage vector is made in order to maintain the estimated torque and stator flux within the limits of two hysteresis bands. More precisely, the vector choice is made on the basis of the position of the stator flux vector and the instantaneous errors in torque and stator flux magnitude.

As an example, considering the stator flux vector laying in sector 1, as shown in Fig 4.4, the voltage vectors V_2 and V_6 can be selected in order to increase the flux while V_3 and V_5 can be applied to decrease the flux. Among these, V_2 and V_3 determine a torque increase, while V_5 and V_6 a torque decrease. The zero voltage vectors are selected when the output of the torque comparator is zero, irrespective to the stator flux condition. Using the basic switching table given in Table 4.1 it is possible to implement DTC scheme having good performance.

Advantages of the basic DTC scheme are:

1. Simplicity, as no coordinate transformation is required.
2. High dynamic.
3. Robustness.
4. Sensor less operation.

Disadvantages of basic DTC are:

1. Difficulty to control the torque and the flux at very low speed
2. Higher current and torque ripple
3. High noise level at low speed.
4. Inherent variable switching frequency.
5. Lack of direct current control.

Table 4.1

Basic DTC inverter configuration selection table.

Sector of $\overline{\varphi}_s$	C_φ= -1			C_φ= 1		
	C_T=-1	C_T= 0	C_T= 1	C_T=-1	C_T= 0	C_T= 1
①	V_2	V_7	V_6	V_3	V_0	V_5
②	V_3	V_0	V_1	V_4	V_7	V_6
③	V_4	V_7	V_2	V_5	V_0	V_1
④	V_5	V_0	V_3	V_6	V_7	V_2
⑤	V_6	V_7	V_4	V_1	V_0	V_3
⑥	V_1	V_0	V_5	V_2	V_7	V_4

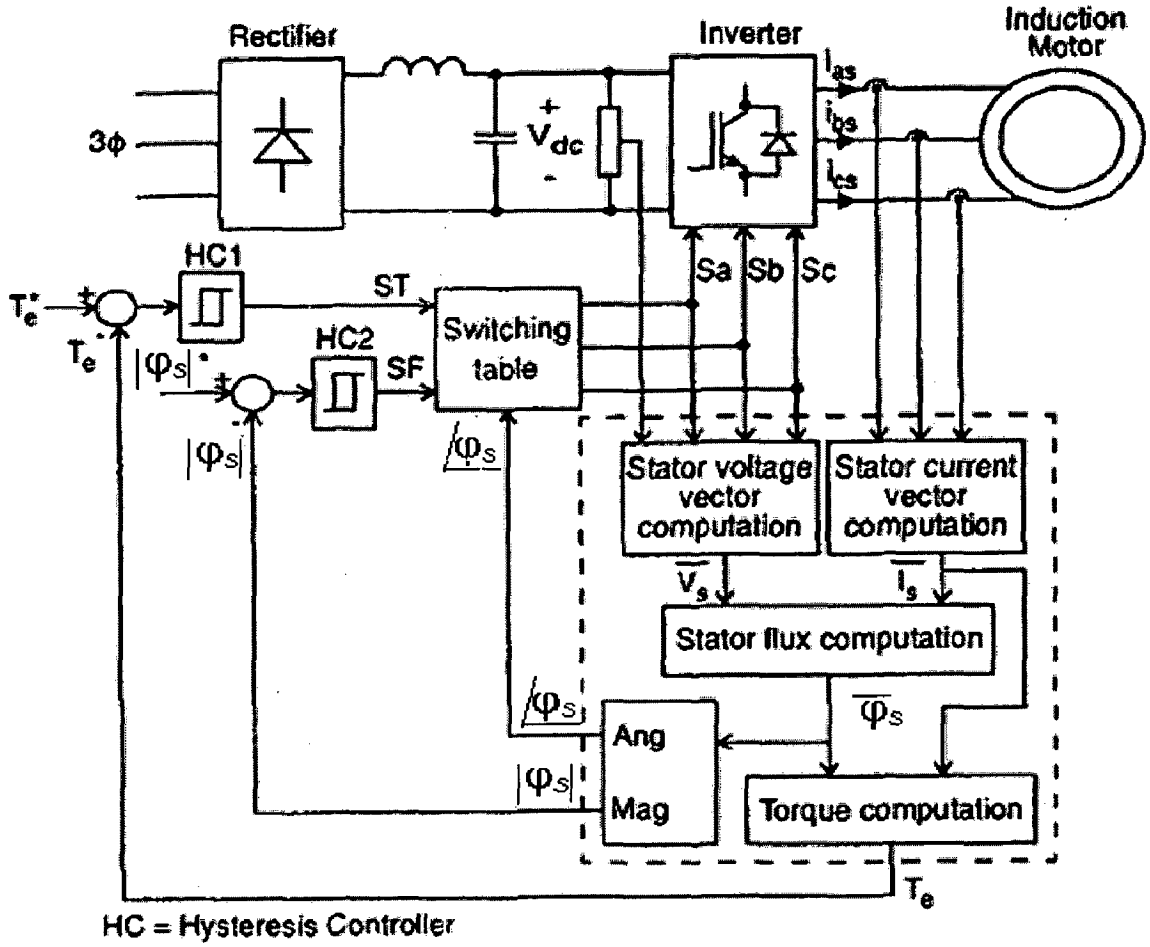

Fig 4.5: Direct torque control of an induction motor

4.4 The Use of Matrix Converter in FOC

The converter is controlled using the Venturini control algorithm as discussed in chapter 3; the modulation index calculation for each bidirectional switch is summarized in (4.13). The vector control scheme gives the three target output voltages for the Venturini control algorithm (v_a, v_b, and v_c), as shown in Fig 4.6.

$$m_{Kj} = \frac{t_{Kj}}{T_S} = \frac{1}{3}\left[1 + \frac{2v_k v_j}{V_{im}^2} + \frac{4q}{3\sqrt{3}}\sin(\omega_i t + \beta_k)\sin(3\omega_i t)\right]$$

$$for\ K = A, B, C\ and\ j = a, b, c.$$

$$\beta_k = 0, 2\pi/3, 4\pi/3 \qquad (4.14)$$

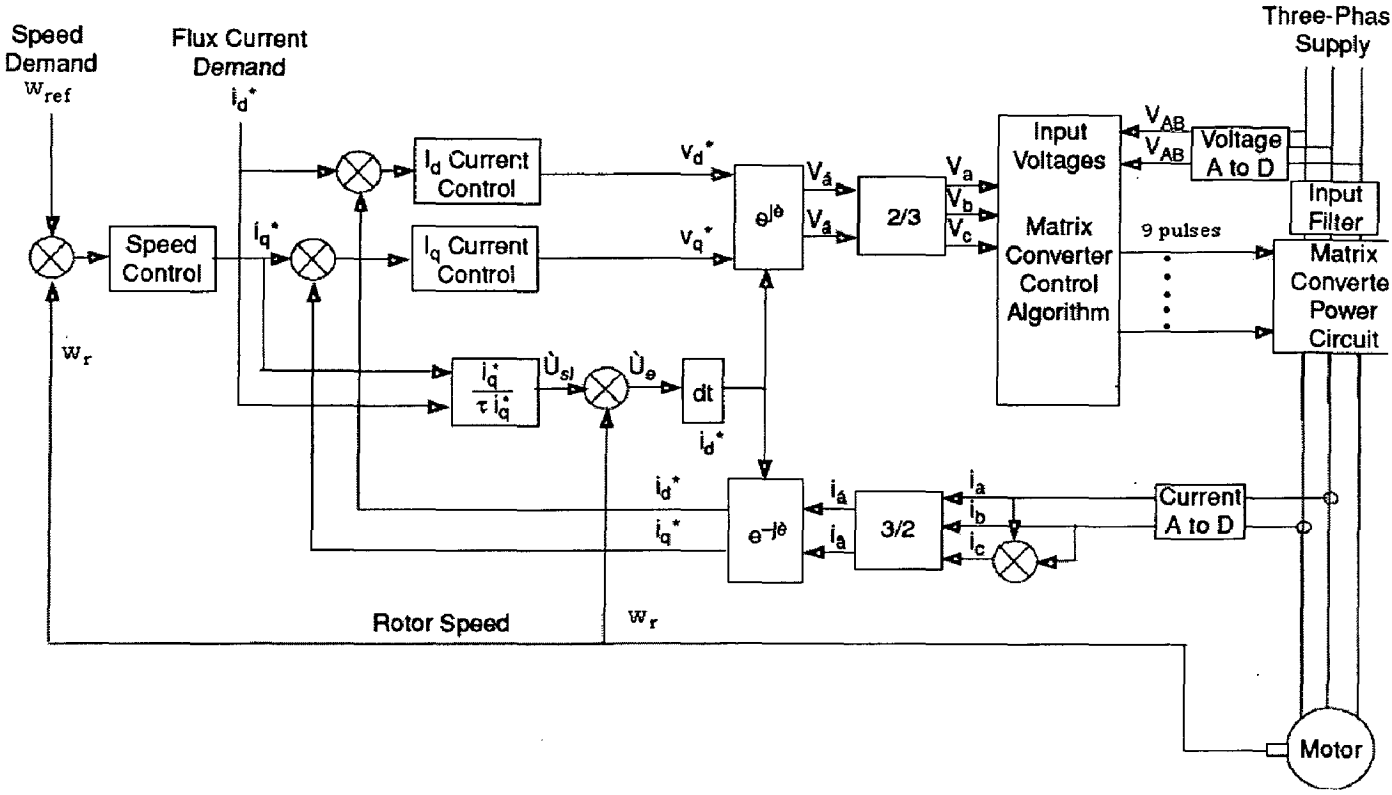

Fig 4.6: Matrix converter closed-loop vector control scheme.[44]

4.5 The Use of Matrix Converter in DTC

The proposed control method relies on a space vector representation of the matrix converter switching configurations. As for the SVM modulation strategies presented in chapter 3, this control method make use of the active and zero configurations only, which are quoted in Table 4.2. It has to be highlighted that with respect to Table 3.1 of chapter 3, in Table 4.2 the output line-to-neutral voltage space vector e_o is considered. For the output line-to-neutral voltage vector e_o and the matrix converter input current vector i_i the following expressions hold.

$$\bar{e}_o = \frac{2}{3}\left(e_{oA} + e_{oB}e^{j2\pi/3} + e_{oC}e^{j4\pi/3}\right) = e_o(t)e^{j\alpha_o(t)} \tag{4.14}$$

$$\bar{i}_i = \frac{2}{3}\left(i_{ia} + i_{ib}e^{j2\pi/3} + i_{ic}e^{j4\pi/3}\right) = i_i(t)e^{j\beta_i(t)} \tag{4.15}$$

In Fig 4.7 the output line-to-neutral voltage and the input current vectors for the active configurations are respectively shown. In the same way as for matrix converter space vector modulated control method,

the reference control quantities are the output voltage vector and the input current vector phase displacement with respect to the input line-to-neutral voltage vector. But the choice of the switching configuration to apply is made on a totally different basis.

Table 4.2

Switching configurations of the MC used in the proposed DTC control scheme.

Switching Configuration	A B C	v_{AB}	v_{BC}	v_{CA}	i_a	i_b	i_c	e_o	α_o	i_i	β_i
+1	*a b b*	v_{ab}	0	$-v_{ab}$	i_A	$-i_A$	0	$2/3\ v_{ab}$	0	$2\sqrt{3}\ i_A$	$-\pi/6$
-1	*b a a*	$-v_{ab}$	0	v_{ab}	$-i_A$	i_A	0	$-2/3\ v_{ab}$	0	$-2\sqrt{3}\ i_A$	$-\pi/6$
+2	*b c c*	v_{bc}	0	$-v_{bc}$	0	i_A	$-i_A$	$2/3\ v_{bc}$	0	$2\sqrt{3}\ i_A$	$\pi/2$
-2	*c b b*	$-v_{bc}$	0	v_{bc}	0	$-i_A$	i_A	$-2/3\ v_{bc}$	0	$-2\sqrt{3}\ i_A$	$\pi/2$
+3	*c a a*	v_{ca}	0	$-v_{ca}$	$-i_A$	0	i_A	$2/3\ v_{ca}$	0	$2\sqrt{3}\ i_A$	$7\pi/6$
-3	*a c c*	$-v_{ca}$	0	v_{ca}	i_A	0	$-i_A$	$-2/3\ v_{ca}$	0	$-2\sqrt{3}\ i_A$	$7\pi/6$
+4	*b a b*	$-v_{ab}$	v_{ab}	0	i_B	$-i_B$	0	$2/3\ v_{ab}$	$2\pi/3$	$2\sqrt{3}\ i_B$	$-\pi/6$
-4	*a b a*	v_{ab}	$-v_{ab}$	0	$-i_B$	i_B	0	$-2/3\ v_{ab}$	$2\pi/3$	$-2\sqrt{3}\ i_B$	$-\pi/6$
+5	*c b c*	$-v_{bc}$	v_{bc}	0	0	i_B	$-i_B$	$2/3\ v_{bc}$	$2\pi/3$	$2\sqrt{3}\ i_B$	$\pi/2$
-5	*b c b*	v_{bc}	$-v_{bc}$	0	0	$-i_B$	i_B	$-2/3\ v_{bc}$	$2\pi/3$	$-2\sqrt{3}\ i_B$	$\pi/2$
+6	*a c a*	$-v_{ca}$	v_{ca}	0	$-i_B$	0	i_B	$2/3\ v_{ca}$	$2\pi/3$	$2\sqrt{3}\ i_B$	$7\pi/6$
-6	*c a c*	v_{ca}	$-v_{ca}$	0	i_B	0	$-i_B$	$-2/3\ v_{ca}$	$2\pi/3$	$-2\sqrt{3}\ i_B$	$7\pi/6$
+7	*b b a*	0	$-v_{ab}$	v_{ab}	i_C	$-i_C$	0	$2/3\ v_{ab}$	$4\pi/3$	$2\sqrt{3}\ i_C$	$-\pi/6$
-7	*a a b*	0	v_{ab}	$-v_{ab}$	$-i_C$	i_C	0	$-2/3\ v_{ab}$	$4\pi/3$	$-2\sqrt{3}\ i_C$	$-\pi/6$
+8	*c c b*	0	$-v_{bc}$	v_{bc}	0	i_C	$-i_C$	$2/3\ v_{bc}$	$4\pi/3$	$2\sqrt{3}\ i_C$	$\pi/2$
-8	*b b c*	0	v_{bc}	$-v_{bc}$	0	$-i_C$	i_C	$-2/3\ v_{bc}$	$4\pi/3$	$-2\sqrt{3}\ i_C$	$\pi/2$
+9	*a a c*	0	$-v_{ca}$	v_{ca}	$-i_C$	0	i_C	$2/3\ v_{ca}$	$4\pi/3$	$2\sqrt{3}\ i_C$	$7\pi/6$
-9	*c c a*	0	v_{ca}	$-v_{ca}$	i_C	0	$-i_C$	$-2/3\ v_{ca}$	$4\pi/3$	$-2\sqrt{3}\ i_C$	$7\pi/6$
0_a	*a a a*	0	0	0	0	0	0	0	--	0	--
0_b	*b b b*	0	0	0	0	0	0	0	--	0	--
0_c	*c c c*	0	0	0	0	0	0	0	--	0	--

The control of the output voltage is based on the classical DTC scheme described in section 4.3. As a consequence , at each cycle period the optimum vector, among the eight generated by a VSI, is selected in

switching Table 4.1 accordingly to the position of the stator flux vector and the output signals C_φ and C_T of the stator flux and torque hysteresis comparators. In Figs 4.8 and 4.9 the two- level stator flux and the three-level electromagnetic torque hysteresis comparators are respectively shown.

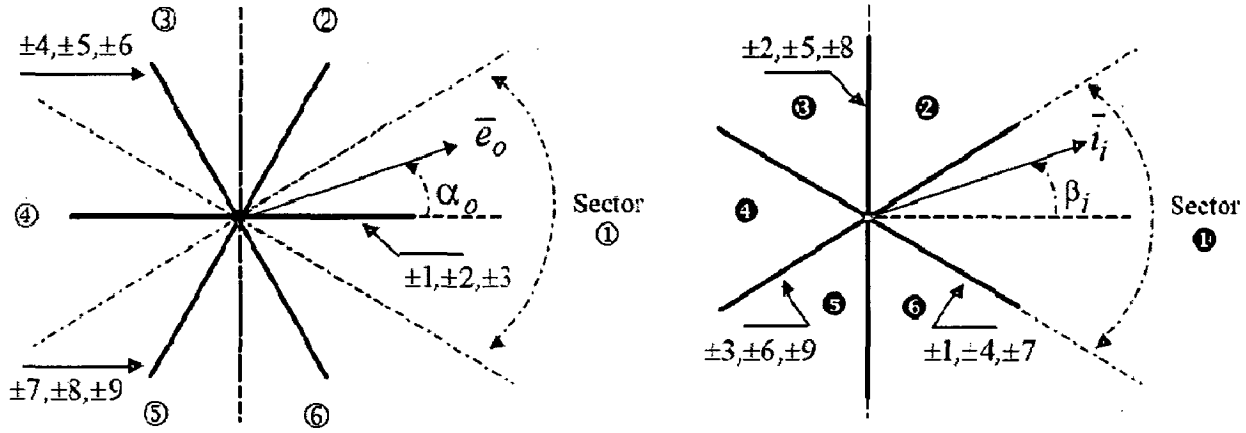

Fig 4.7: Output voltage and Input current vectors for active configurations and reference output voltage and input current vector respectively [42]

Once the classical DTC control scheme has selected the optimum vector to be applied to the machine, it is a matter of determining the correspondent matrix converter switching configuration. If it is assumed, for example, that the VSI output vector V_1 has been chosen, looking at Table 4.2 and Figs 4.4 and 4.7, it can be seen that matrix converter can generate the same vector by means of the switching configurations ±1, ±2 and ±3. But not all of them can be usefully employed to provide vector V_1.

In fact, at any instant, the magnitude and the direction of their corresponding output voltage vectors depend on the position of the input line-to-neutral voltage vector e_i. Among the 6 vectors, those having the same direction of $V1$ and the maximum magnitude are considered.

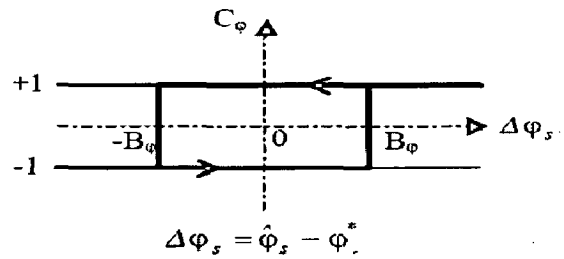

Fig: 4.8 Two-level stator flux hysteresis comparator.

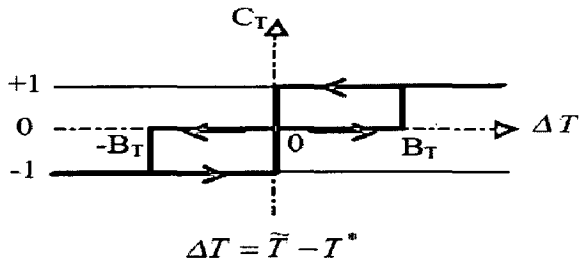

Fig: 4.9 Three-level torque hysteresis comparator.

If it is assume, for example, that vector e_i is in sector 1, the switching configurations to be used are +1 and –3. In fact, looking at Fig 4.10 and Table 4.2 it can be seen that within sector 1 these two switching configurations are those which complies with the above mentioned selection criteria.

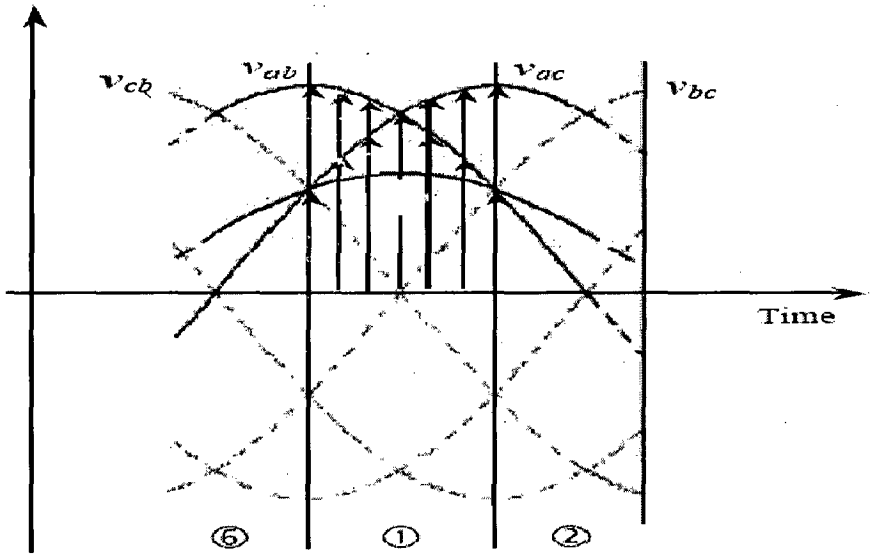

Fig 4.10: Representation of the input line-to-line voltages in the time domain for sector 1 of the input line-to-neutral voltage vector [42]

It has been verified that, whatever is the sector which the vector e_i is in; the matrix converter makes always available two switching configurations for each VSI output vector chosen by the classical DTC scheme.

Such redundancy gives the opportunity to control a further variable in addition to the stator flux and the electromagnetic torque. In the proposed control method the average value of the sine of the displacement angle ψ_i between the input current vector and the corresponding input line-to- neutral voltage vector has been chosen as third variable. This variable will be indicated by $<sin\ \psi_i>$.

If the constraint to comply with is an unity input power factor, such aim can be achieved keeping the value of $<sin\ \psi_i>$ to zero. The variable $<sin\ \psi_i>$ is directly controlled by the hysteresis comparator shown in Fig

4.11. The average value of $sin\ \psi_i$ is obtained applying a low pass filter to its instantaneous estimated value.

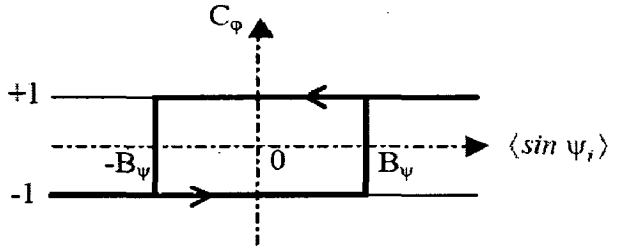

$$\Delta\psi_i = \langle sin\ \psi_i \rangle - \langle sin\ \psi_i \rangle^*$$

Fig 4.11: Hysteresis comparator of $<sin\ \psi_i>$ *the value.*

The control of the input power factor is possible because the input current vector for switching configurations +1 and –3 have different directions, as it can be seen from Table 4.2 and shown in Fig 4.12.

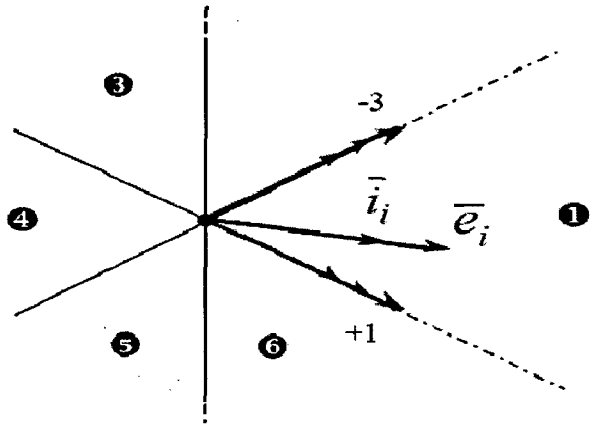

Fig 4.12: Representation of an unity control of the input power factor. [42]

Keep going with the previous example, it is assumed by Fig 4.12 that the reference input displacement angle is set to zero. As a consequence the reference value of $<sin\ \psi_i>$ is also set to zero, $<sin\ \psi_i>^* = 0$

Now, if the estimated value of $<sin\ \psi_i>$ is positive, $C_\Psi = +1$, which means that the input current vector i_i is lagging the voltage vector e_i, then the configuration –3 has to be applied. On the contrary, if the estimated value of $<sin\ \psi_i>$ is negative, $C_\Psi = -1$, which means that the input current vector i_i is leading the voltage vector e_i, the configuration +1 has to be applied.

The switching table based on these principles is shown in Table 4.3. The first column on the left hand side contains the voltage vectors selected by the basic DTC scheme in order to keep the stator flux and torque within the limits of the corresponding hysteresis bands.

The other six bold columns are related to the sector of the matrix converter input current vector i_i. Depending on the output value of the C_ψ hysteresis comparator, the left or the right column has to be used in selecting the switching configuration of the matrix converter.

Table 4.3
Matrix Converter Switching Table for DTC control [42]

	❶		❷		❸		❹		❺		❻	
C_ψ	+1	-1	+1	-1	+1	-1	+1	-1	+1	-1	+1	-1
V_1	-3	1	2	-3	-1	2	3	-1	-2	3	1	-2
V_2	9	-7	-8	9	7	-8	-9	7	8	-9	-7	8
V_3	-6	4	5	-6	-4	5	6	-4	-5	6	4	-5
V_4	3	-1	-2	3	1	-2	-3	1	2	-3	-1	2
V_5	-9	7	8	-9	-7	8	9	-7	-8	9	7	-8
V_6	6	-4	-5	6	4	-5	-6	4	5	-6	-4	5

Input Current Vector sector number

$\langle sin\ \psi_i \rangle$ *Hysteresis comparator*

Voltage Vectors selected by the basic DTC

When a zero voltage vector is required from Table 4.1, the zero configuration of the matrix converter which minimizes the number of commutations is selected.

The output of the hysteresis regulator C_ψ, together with the sector number of the input current vector and the voltage vector required by the DTC, are the input to the matrix converter switching configuration selection algorithm represented by Table 4.3.

It is worth noting that the sectors were related the input line-to-neutral voltage vector e_i. The matrix converter switching configurations

selected on the basis of the e_i or i_i vectors sector are identical only in the case of unity input power factor. In the case of an input power factor different from unity, for a proper control of the matrix converter input current, the switching configuration selection has to be referred to the sector of the i_i vector.

But likewise to the space vector modulated matrix converter, if the input power factor is controlled to be less than unity, a reduction in the voltage transfer ratio is the result, which in the DTC application turns into a reduction of the dynamic performance of the drive. In Fig 4.13 it is shown the block diagram of the proposed DTC control scheme for the matrix converter.

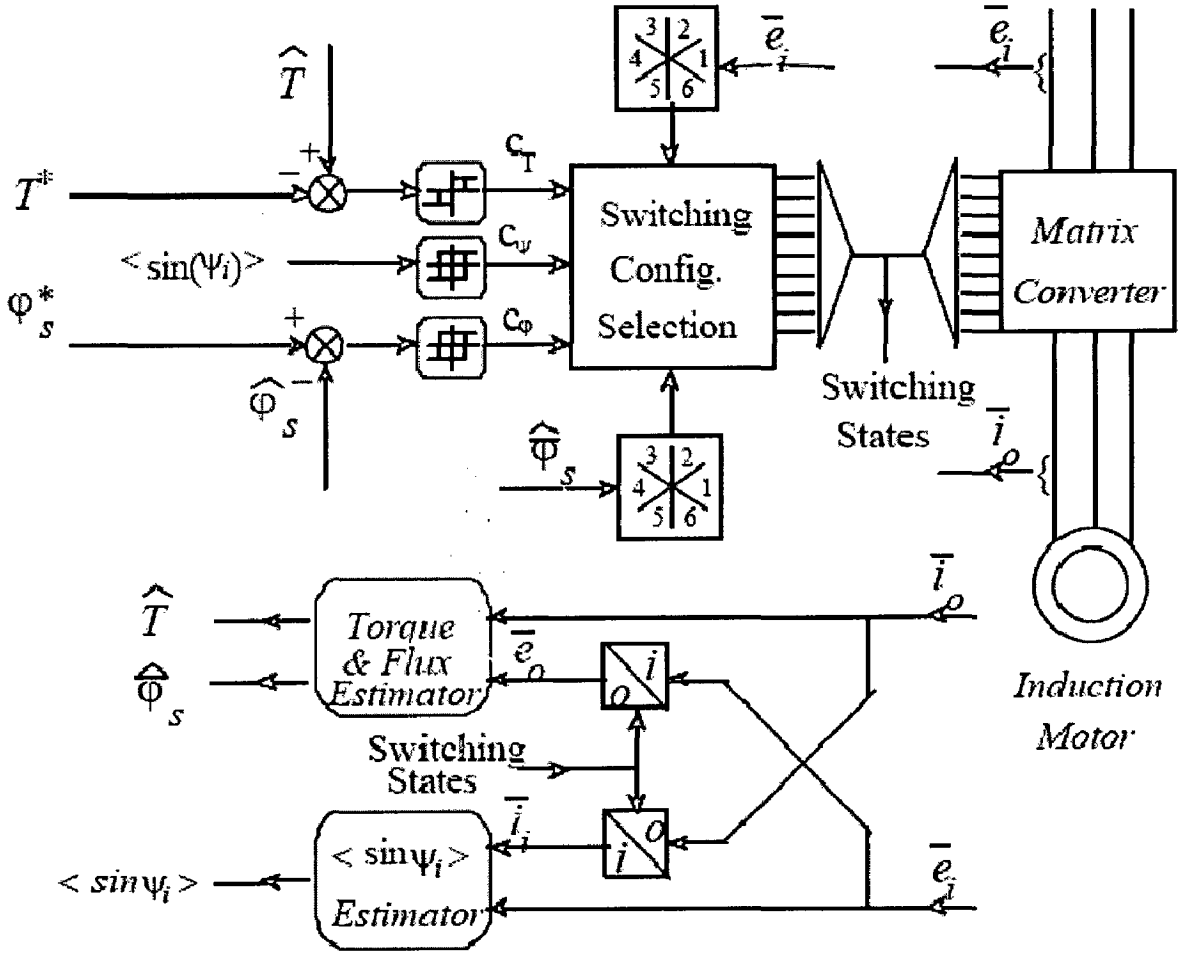

Fig 4.13: Block diagram of the proposed DTC scheme for matrix converter.[42]

With reference to Fig 4.13, in the lower part of the diagram the estimators of the electromagnetic torque, the stator flux and the average value of $<sin\ \psi_i>$ are represented. It is evident that these estimators require the knowledge of input and output voltages and currents. However, only the input voltages and the output currents are measured in each cycle period, because the other quantities can be calculated on the basis of the actual switching configuration of the matrix converter which is known.

The Direct Torque Control (DTC) is a high-dynamic and high performance control technique for induction motor drives which has been developed as possible alternative solution to DC servo drives.

In direct-torque-controlled adjustable speed drives the motor flux and the electromagnetic torque are the reference quantities which are directly controlled by the applied inverter voltage vector. At any cycle period, accordingly to the position of the motor flux space vector and the output signals of a flux and a torque hysteresis comparators the most opportune inverter switching state is selected.

4.6 Conclusions

Control methods based on Field oriented control and classical direct torque control technique has been presented for a matrix converter induction motor drive.

Chapter 5

Simulation Results

Extensive simulation is carried out to investigate the performance of the 3-phase to 3-phase Matrix Converter for different frequencies using Venturini and SVM technique in Chapter 3. In this chapter simulations are carried out for DTC and FOC for Induction Motor drives using Matrix Converter.

5.1 Introduction

Simulations are developed using MATLAB and its Power system blockset in SIMULINK.

5.2 FOC And DTC Using Matrix Converter

A detailed comparison between the two solutions has been carried out by numerical simulations. The characteristics of the motor under test are shown in appendix.

5.2.1: Steady-State Performance

The steady-state performance of DFOC and DTC schemes has been compared. The considered operating conditions are related to rotor speed values of 2000 RPM, 1000 RPM and 200 RPM and torque values of 2.2 Nm, 1.1 NM, and 0 Nm. As it is possible to see, in all the operating conditions the behavior of FOC scheme is characterized by lower values of the three-phase rms current ripple with respect to the DTC scheme. The torque and the stator current waveforms obtained with FOC scheme are shown in Figs 5.1-5.6 respectively. Figs 5.7-5.12 shows the same quantities obtained when using DTC scheme. Under the assumption that same mean switching frequency the amplitude of torque ripple in DTC is slightly higher than FOC.

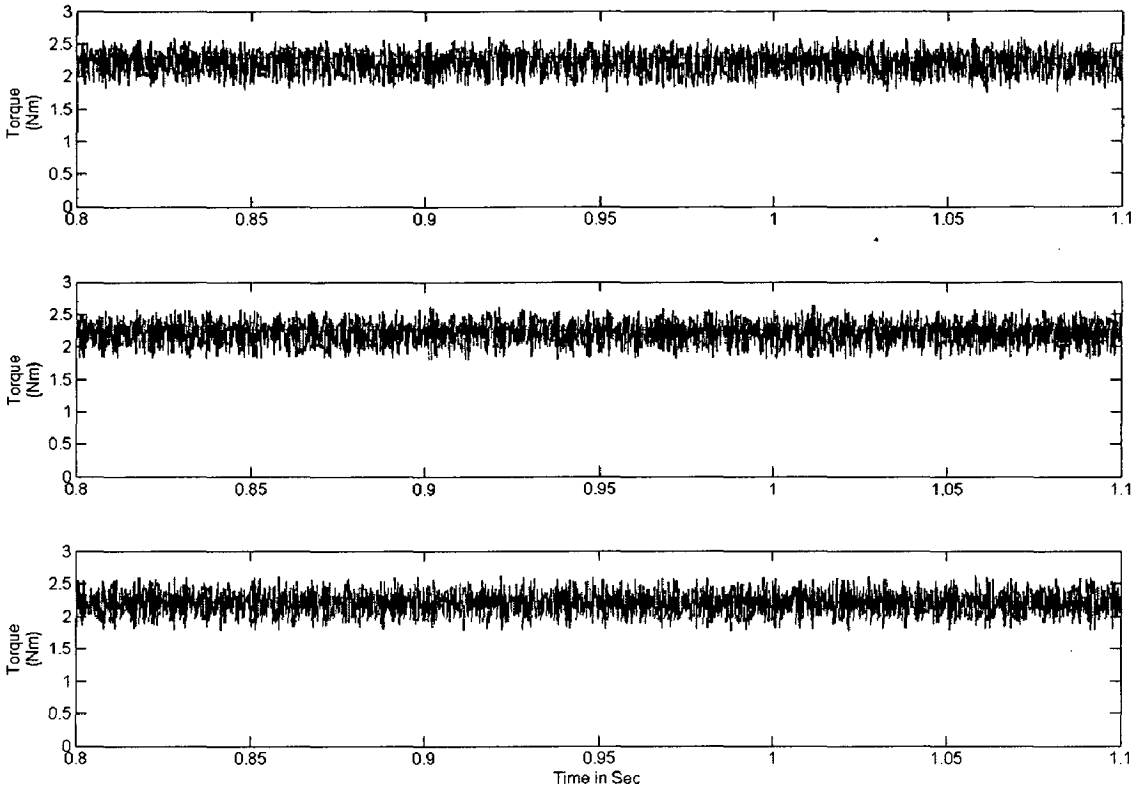

Fig 5.1: Torque (FOC), 2000, 1000, 200 rpm and load torque 2.2 Nm

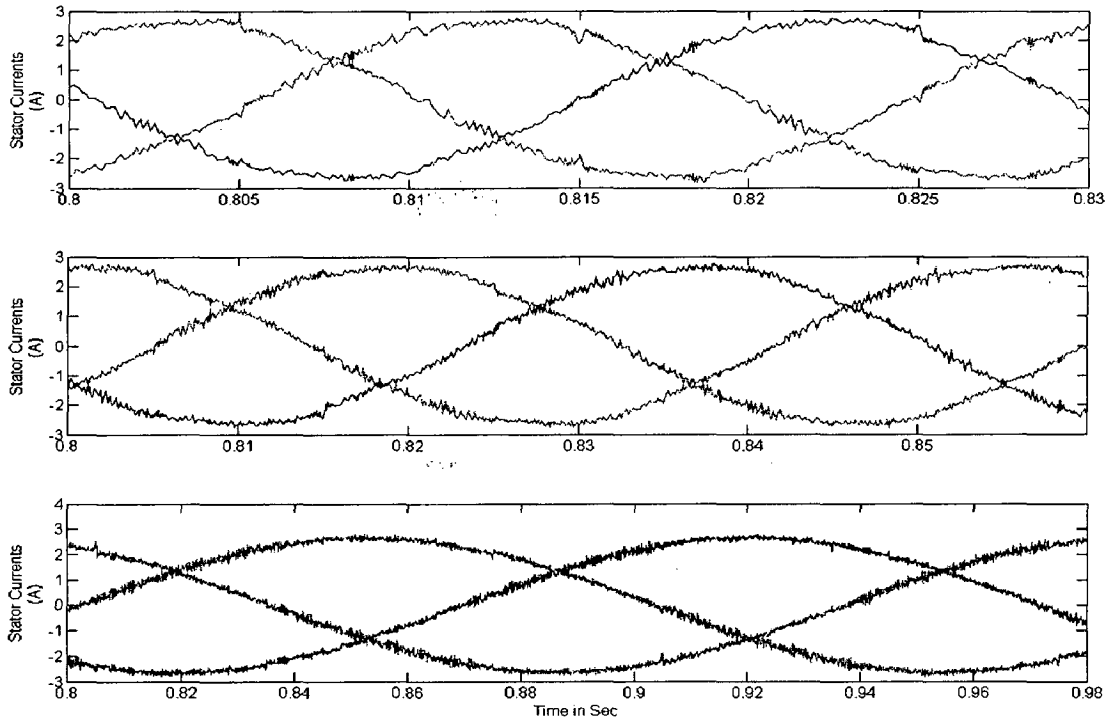

Fig 5.2: Stator Currents (FOC), 2000, 1000, 200 rpm and load torque 2.2 Nm

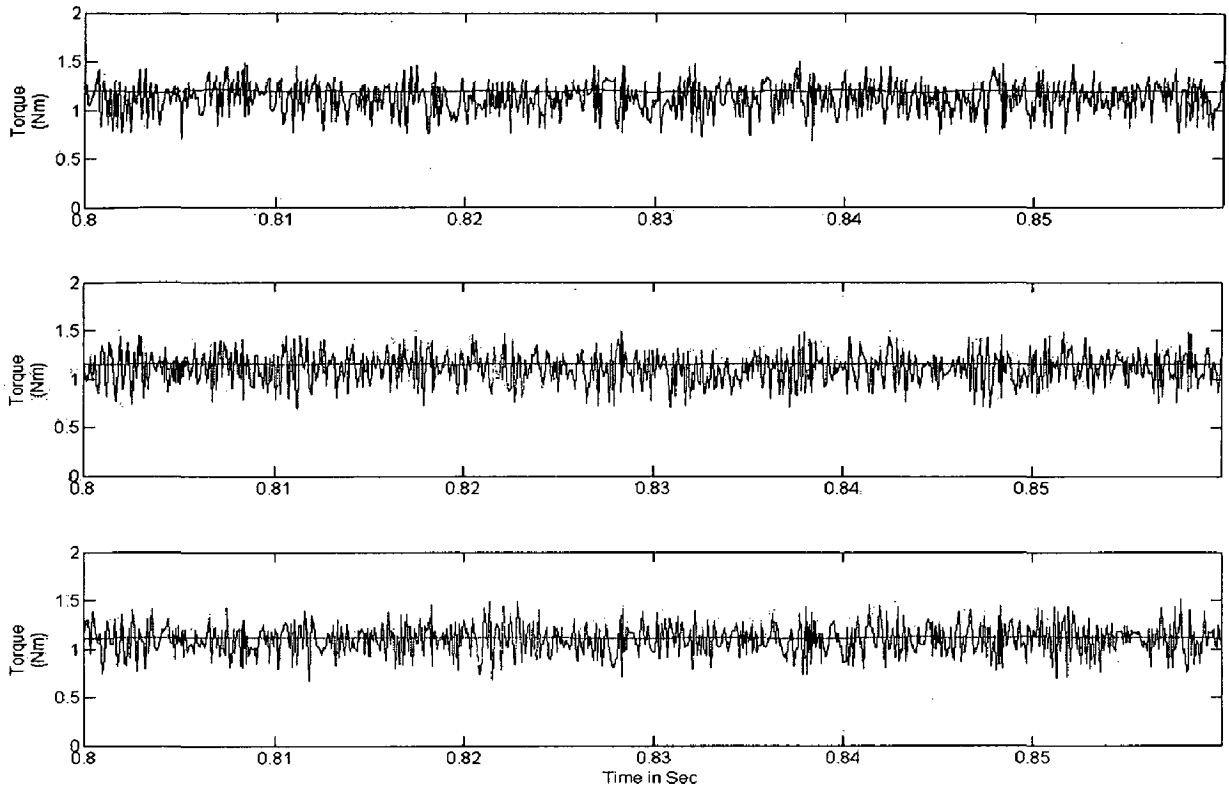

Fig 5.3: Torque (FOC), 2000, 1000, 200 rpm and load torque 1.1 Nm

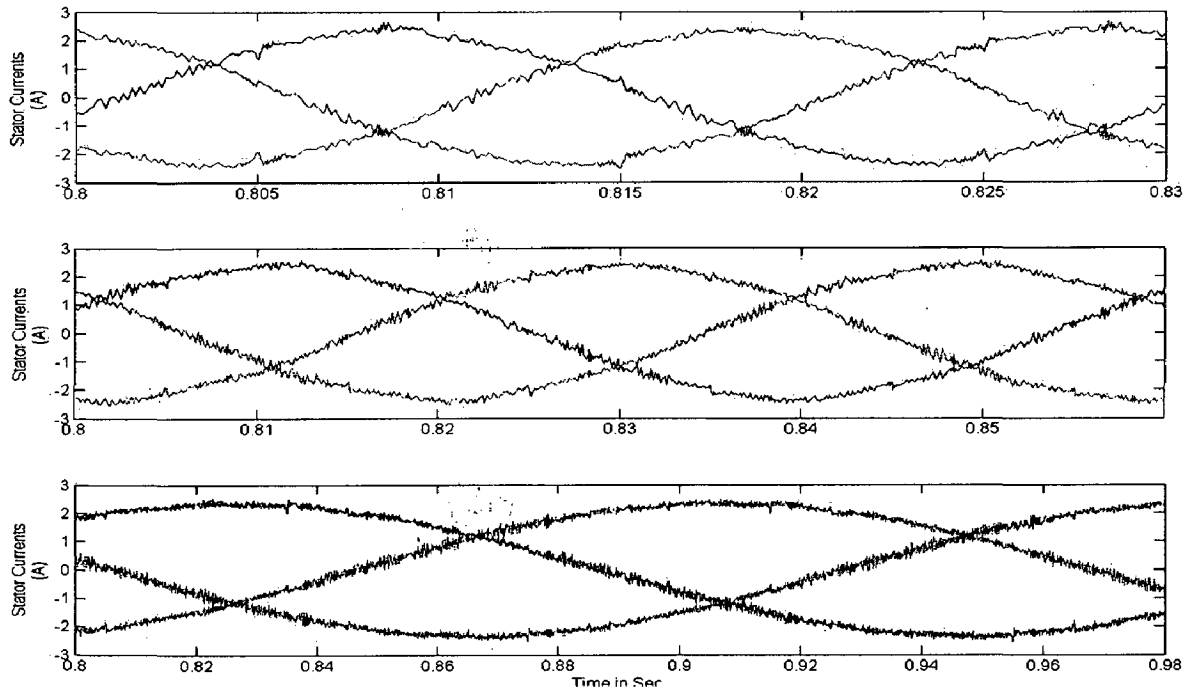

Fig 5.4: Stator Currents (FOC), 2000, 1000, 200 rpm and load torque 1.1 Nm

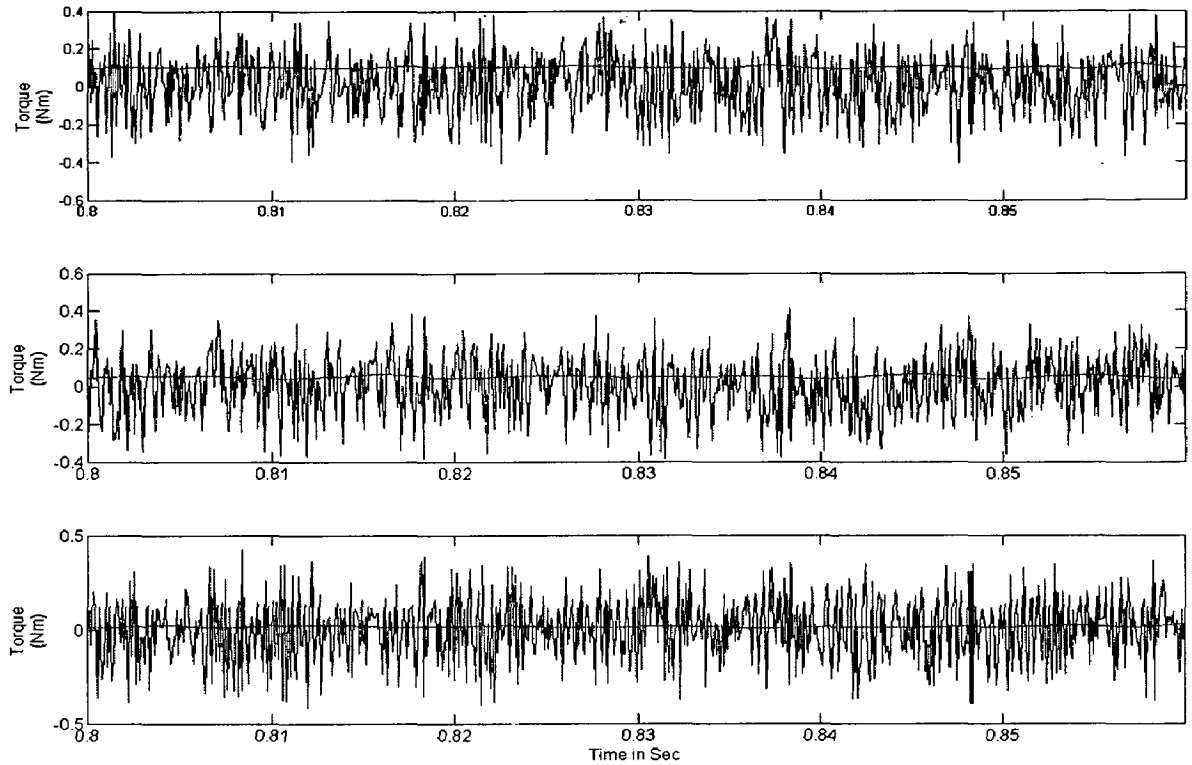

Fig 5.5: Torque (FOC), 2000, 1000, 200 rpm and load torque 0 Nm

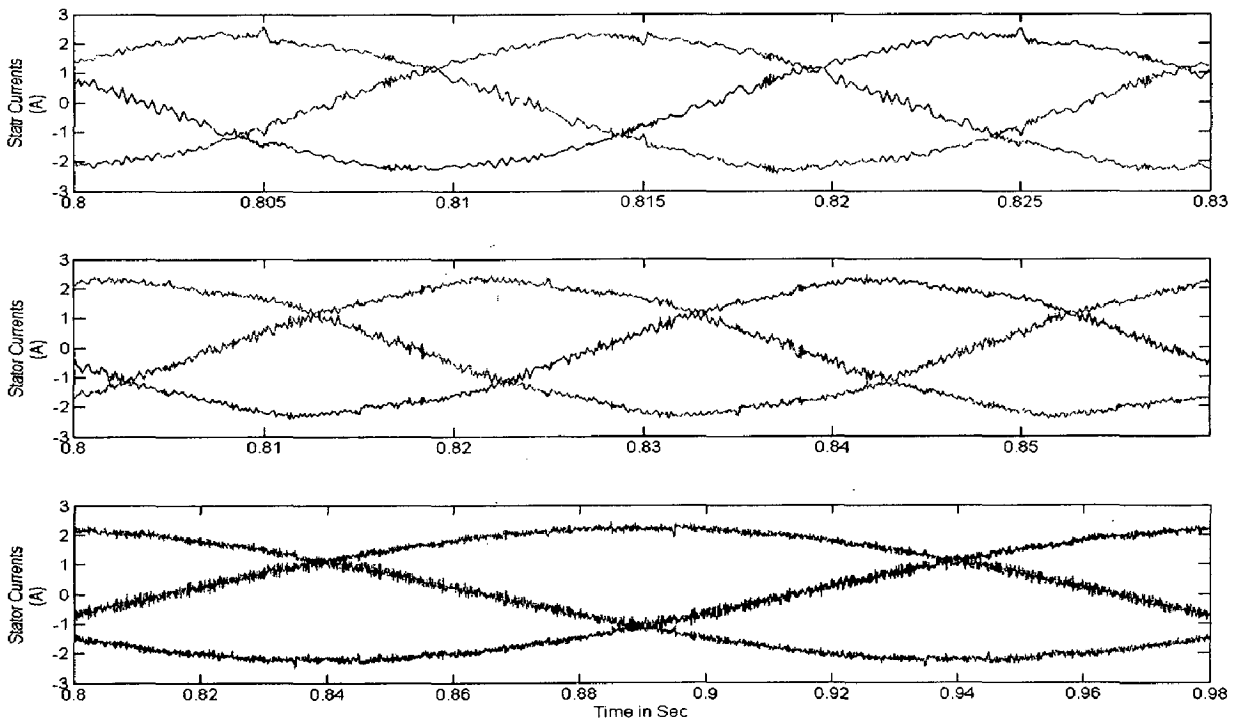

Fig 5.6: Stator Currents (FOC), 2000, 1000, 200 rpm and load torque 0 Nm

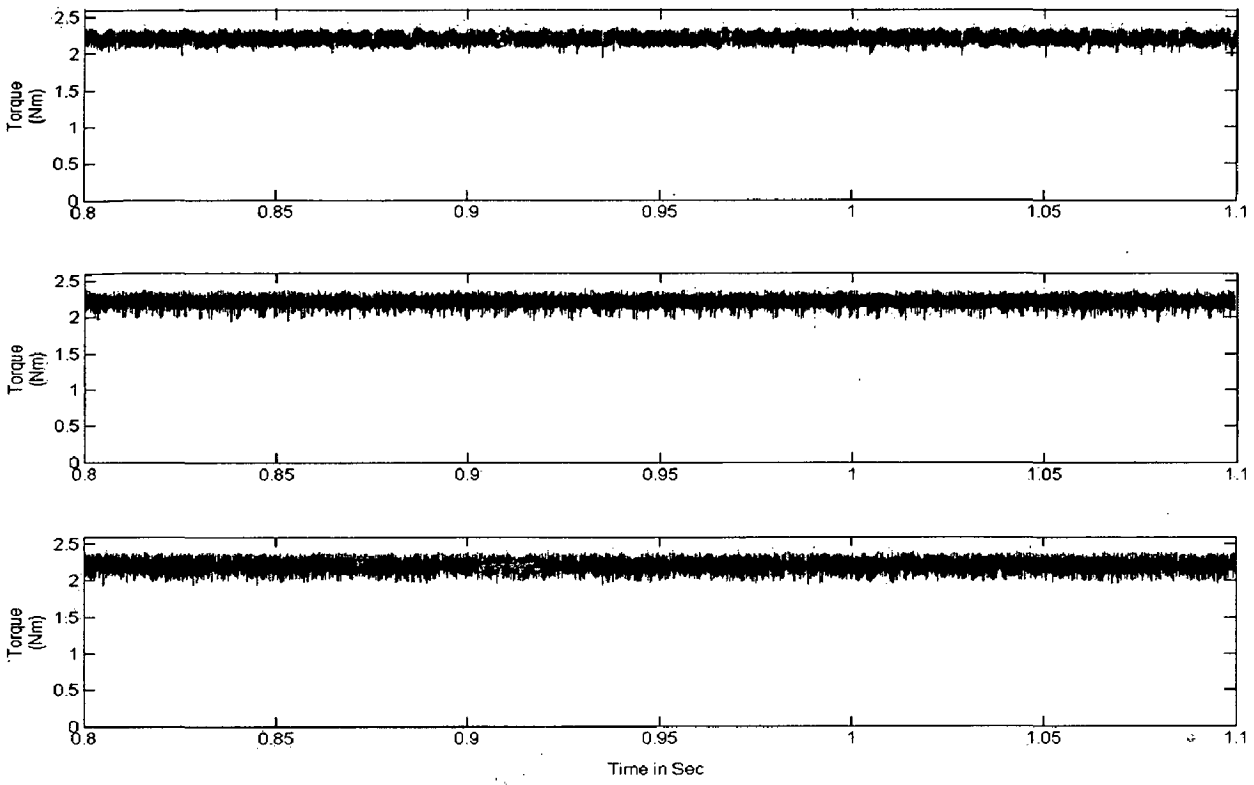

Fig 5.7: Torque (DTC), 2000, 1000, 200 rpm and load torque 2.2 Nm

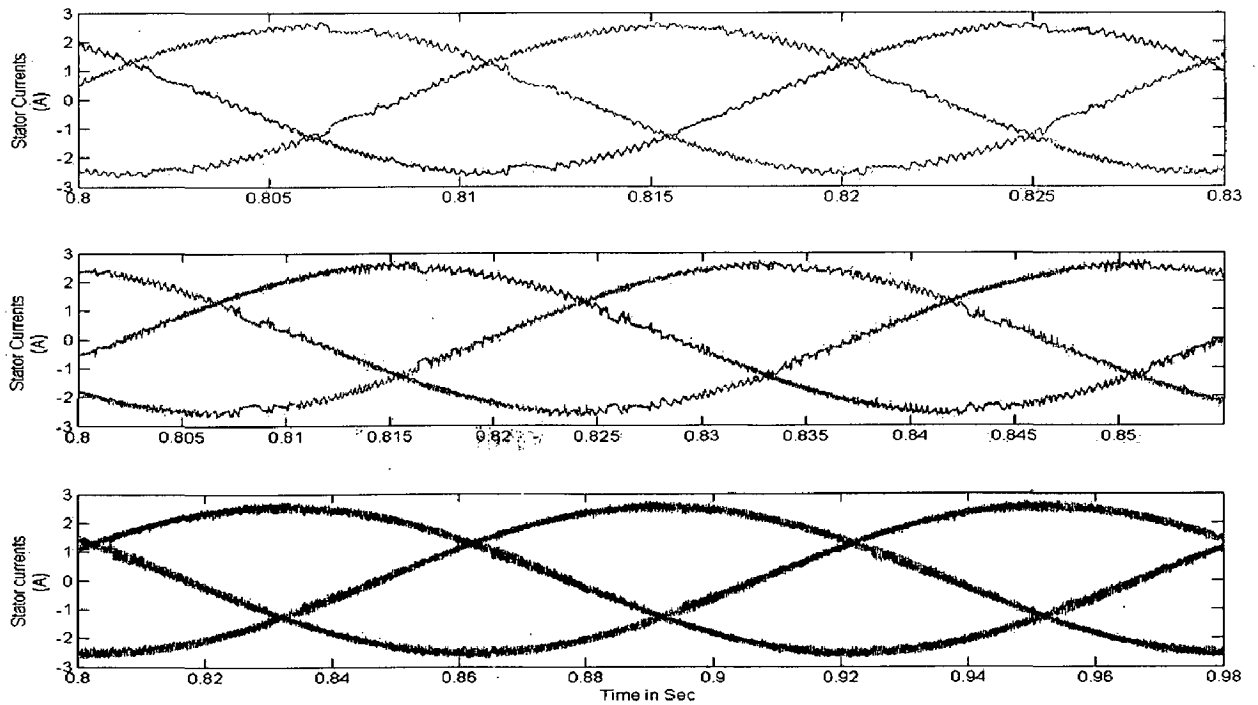

Fig 5.8: Stator Currents (DTC), 2000, 1000, 200 rpm and load torque 2.2 Nm

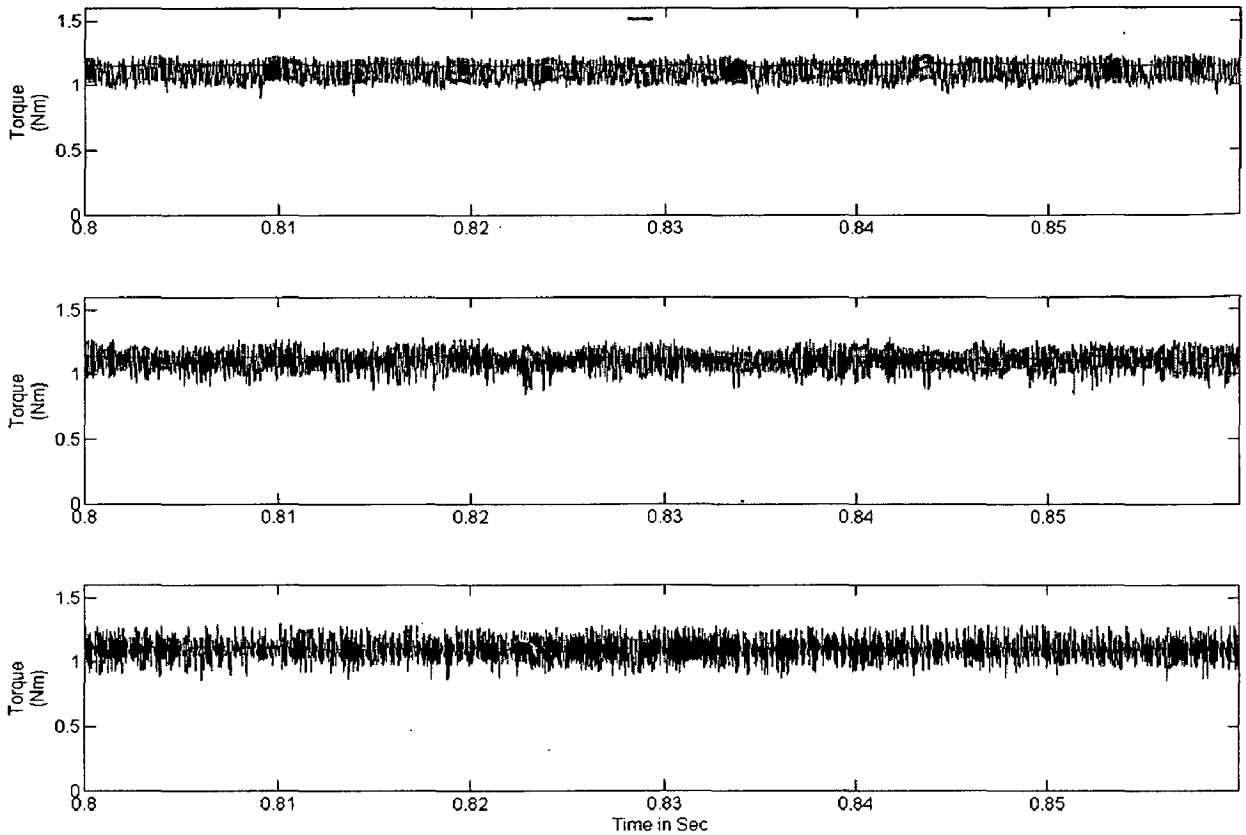

Fig 5.9: Torque (DTC), 2000, 1000, 200 rpm and load torque 1.1 Nm

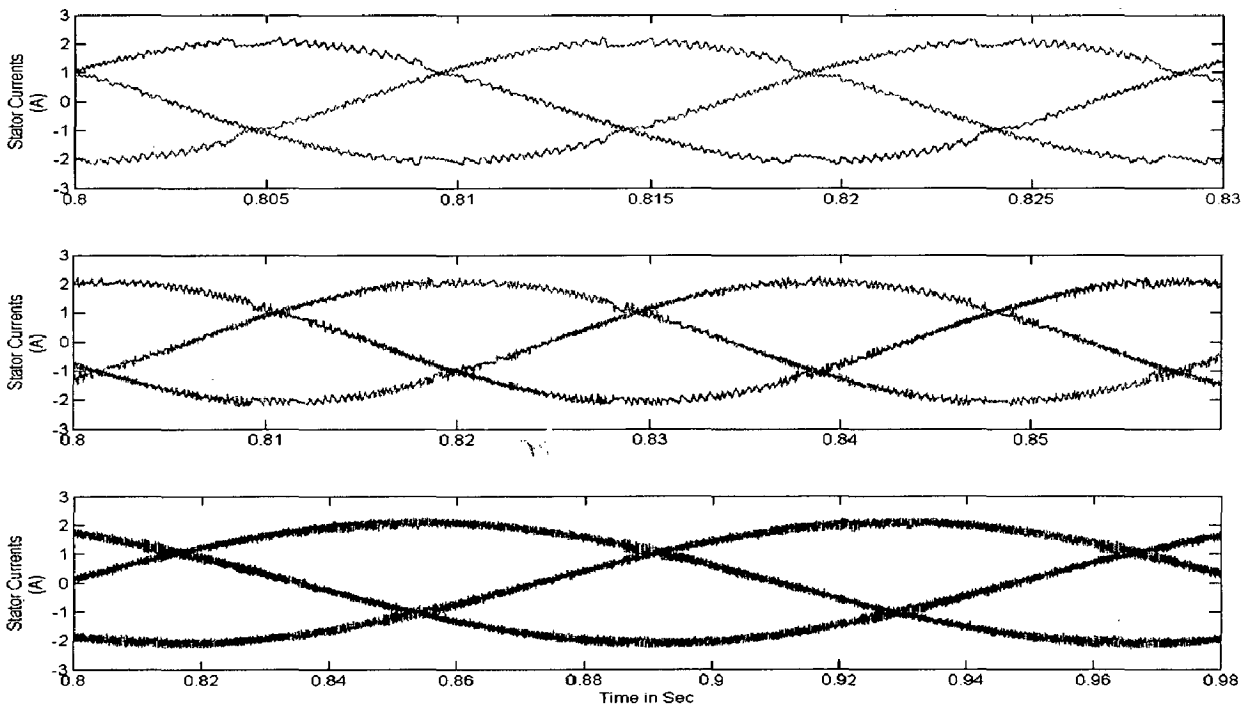

Fig 5.10: Stator Currents (DTC), 2000, 1000, 200 rpm and load torque 1.1 Nm

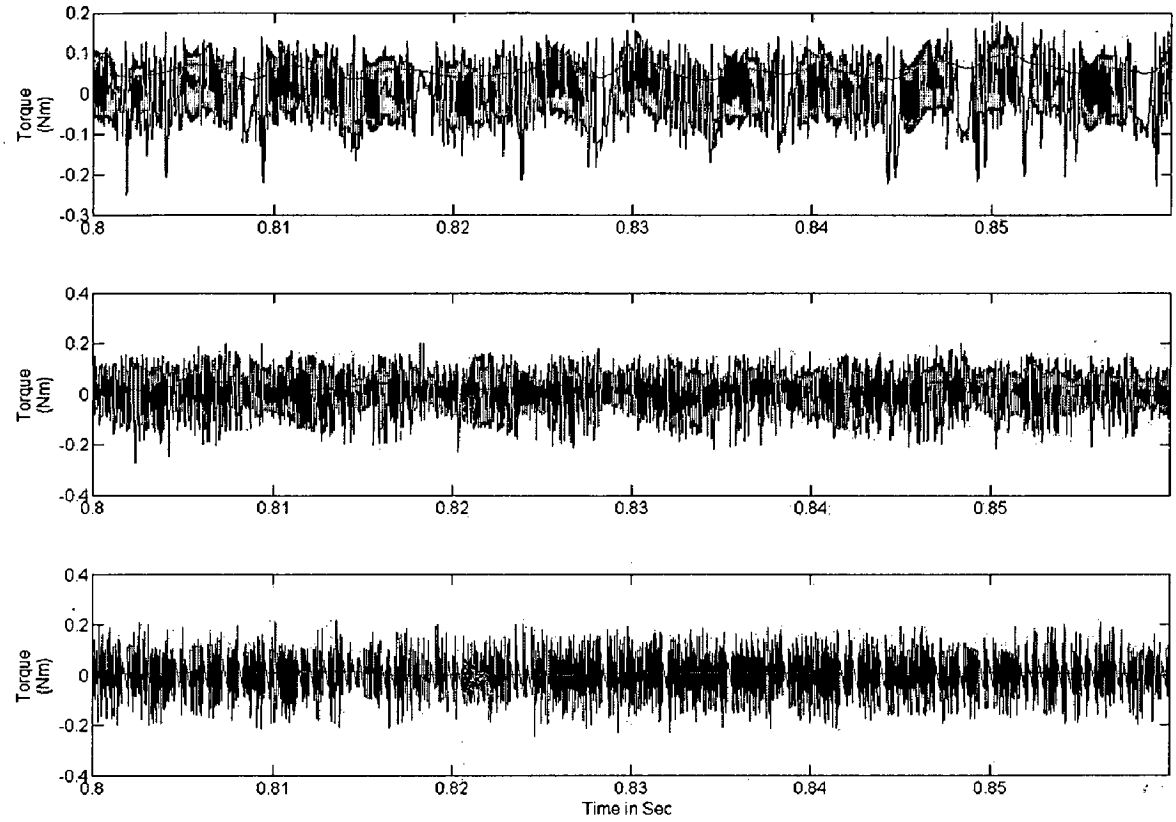

Fig 5.11: Torque (DTC), 2000, 1000, 200 rpm and load torque 0 Nm

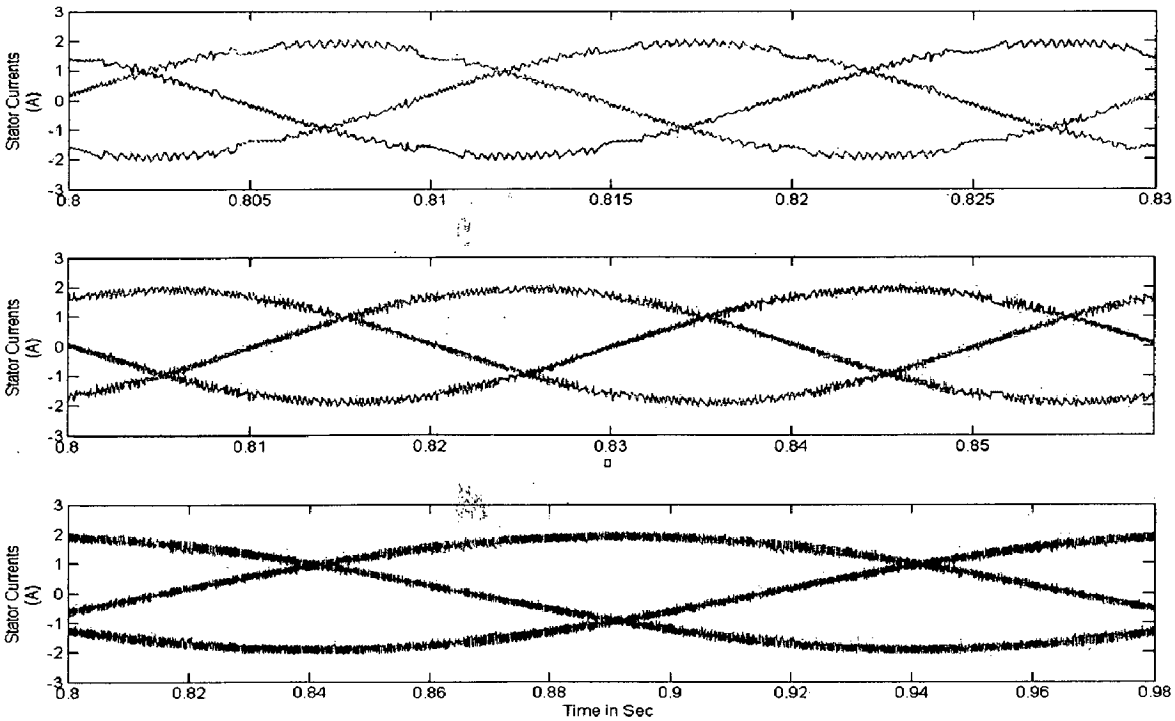

Fig 5.12: Stator Currents (DTC), 2000, 1000, 200 rpm and load torque 0 Nm

5.2.2: Dynamic Response

The transient performance of the proposed two control scheme has been tested with reference to a step torque command from 2.2 to -2.2 Nm, with high inertial load at 2000 RPM, the electromagnetic torque shows a very good response and the current waveform is almost sinusoidal immediately after the step command. Fig 5.13-5.14 shows the torque responses obtained using FOC and DTC at 2000 RPM for step change in torque. These results show that using the DTC scheme a better torque response can be achieved in terms of settling time and maximum overshoot.

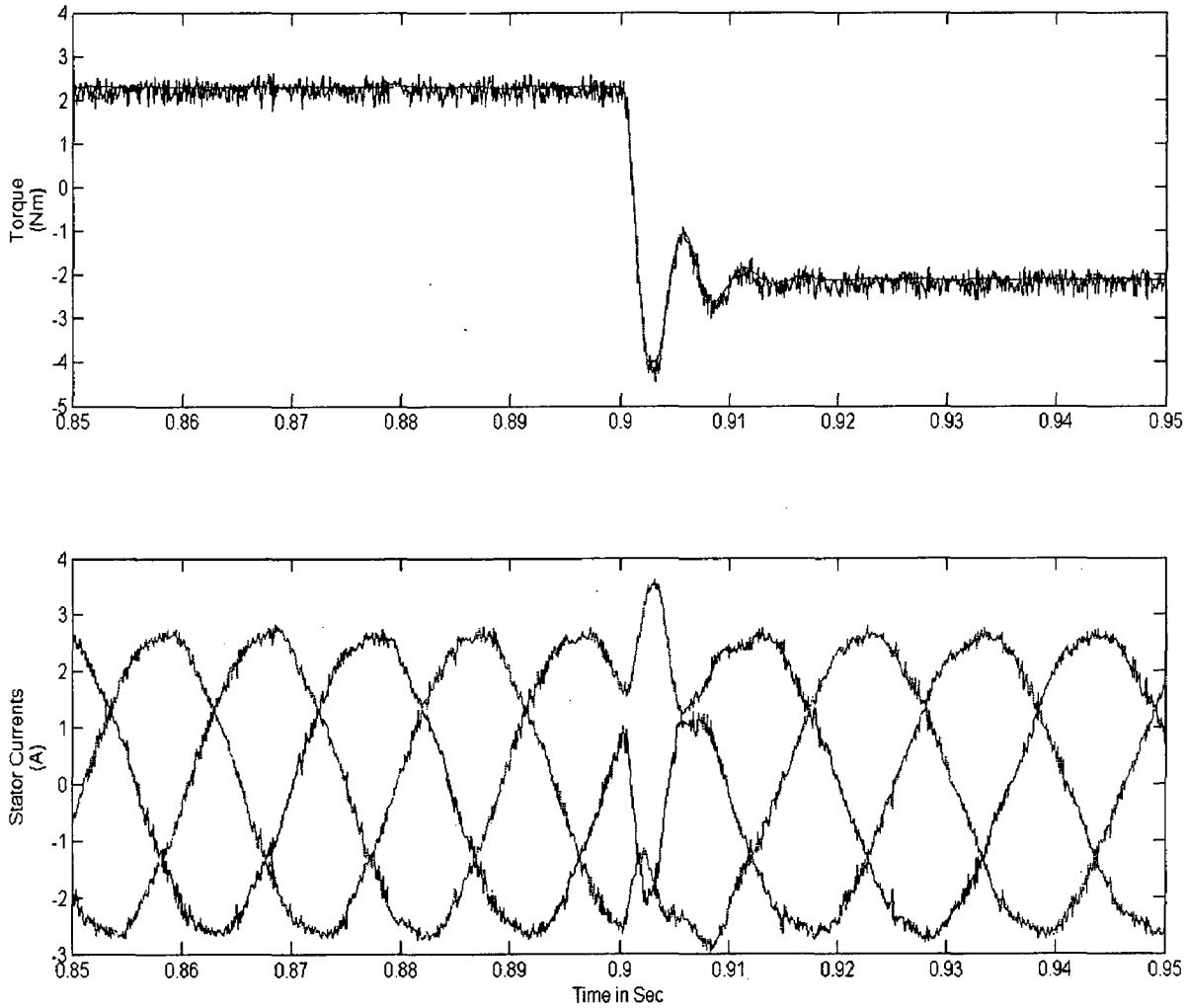

Fig 5.13: Electromagnetic torque (FOC) and stator currents (FOC) during a torque step command from +2.2 to -2.2 Nm, 2000 rpm.

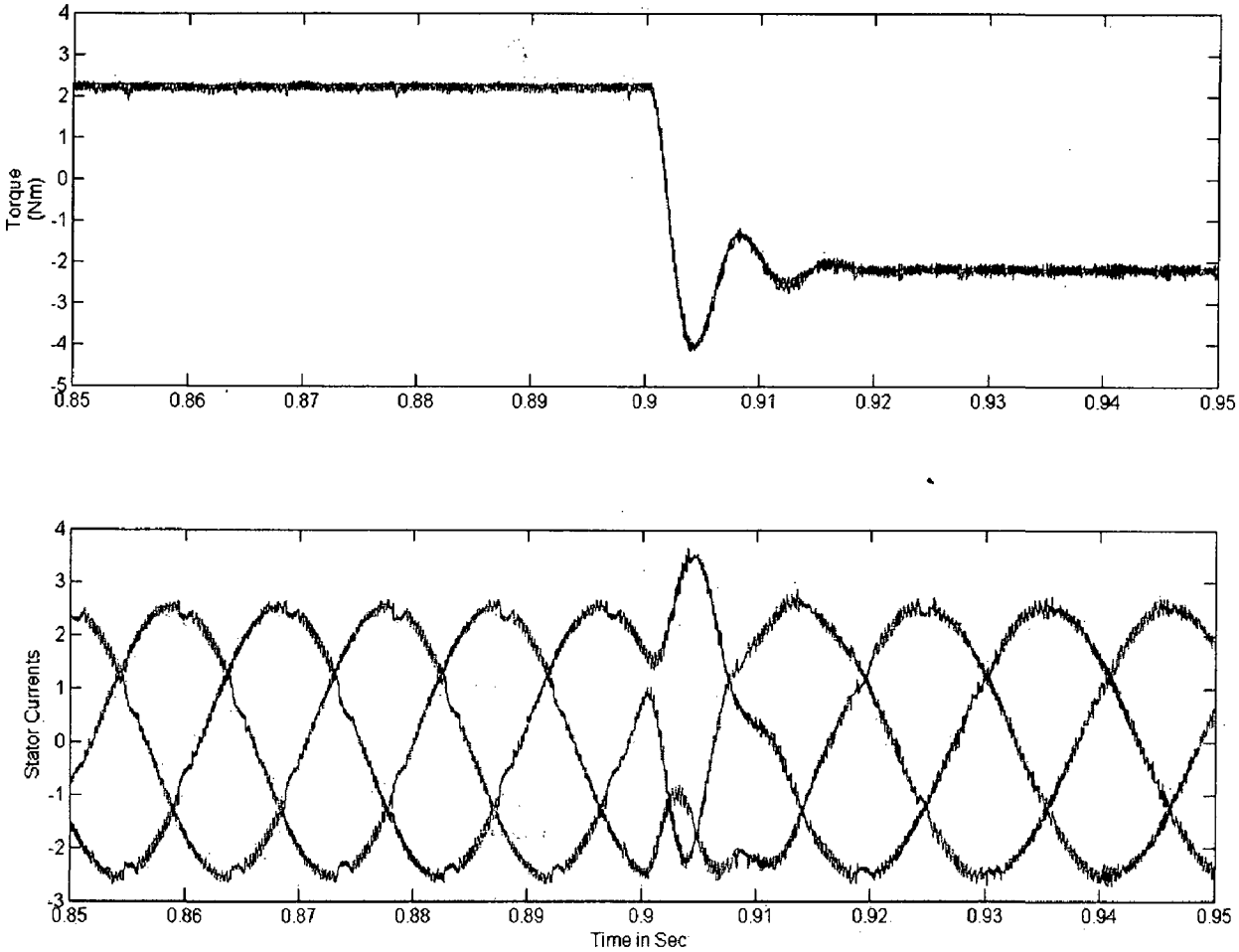

Fig 5.14: Electromagnetic torque (DTC) and stator currents (DTC) during a torque step command from +2.2 to -2.2 Nm, 2000 rpm.

5.2.3: Four Quadrant Operation

Fig 5.15-5.18 shows the four quadrant operation characteristics. The inertial load was accelerated to ±3000 RPM with a speed reference with step function. The waveforms indicate that the speed reversal and change over from motoring to the regenerating mode is achieved smoothly. During regeneration, except for the small MC switching losses, most of the inertial energy is immediately (and directly) returned to the AC line. Thus, in all the four quadrants, high energy-efficiency and very rapid speed response could be achieved. Fig 5.15 and 5.17 shows the no-load characteristics and Fig 5.16 and 5.18 shows the characteristics of load T_L=2.2 at t=0.5s and T_L=-2.2 at t=1s

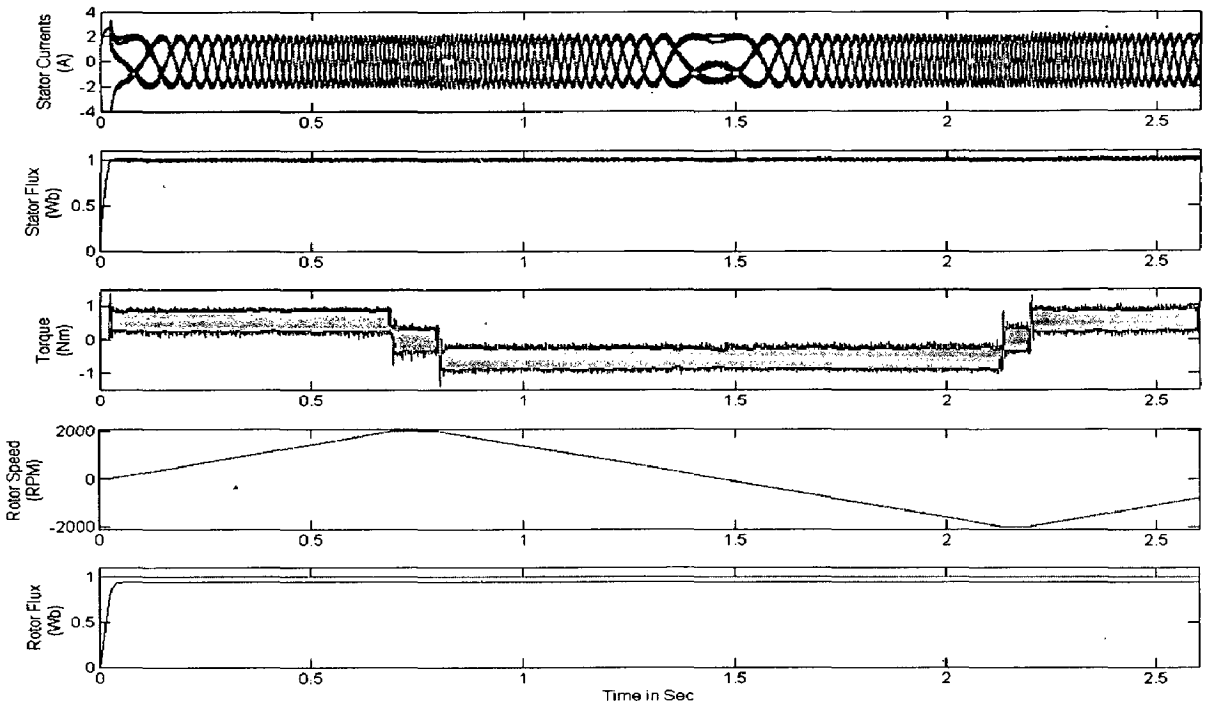

Fig 5.15: Four quadrant operation (DTC) waveforms at T_L=0

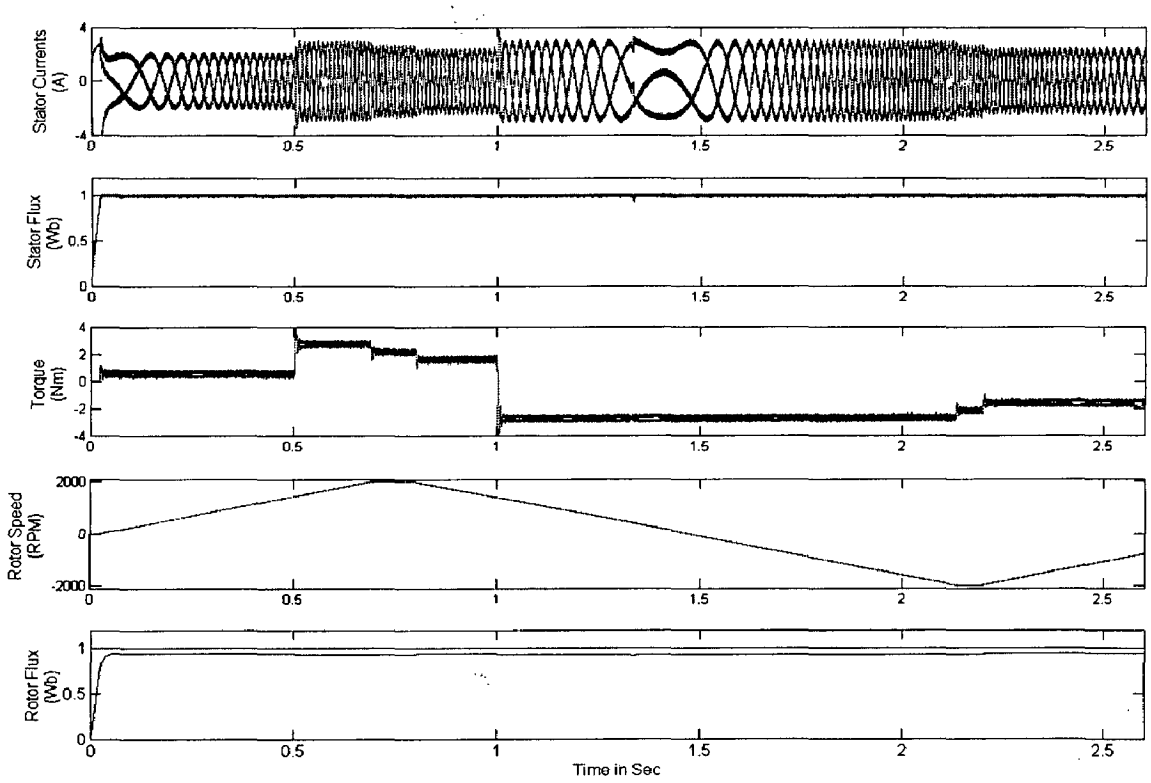

Fig 5.16: Four quadrant operation (DTC) waveforms at T_L=2.2 at t=0.5s and T_L=-2.2 at t=1s

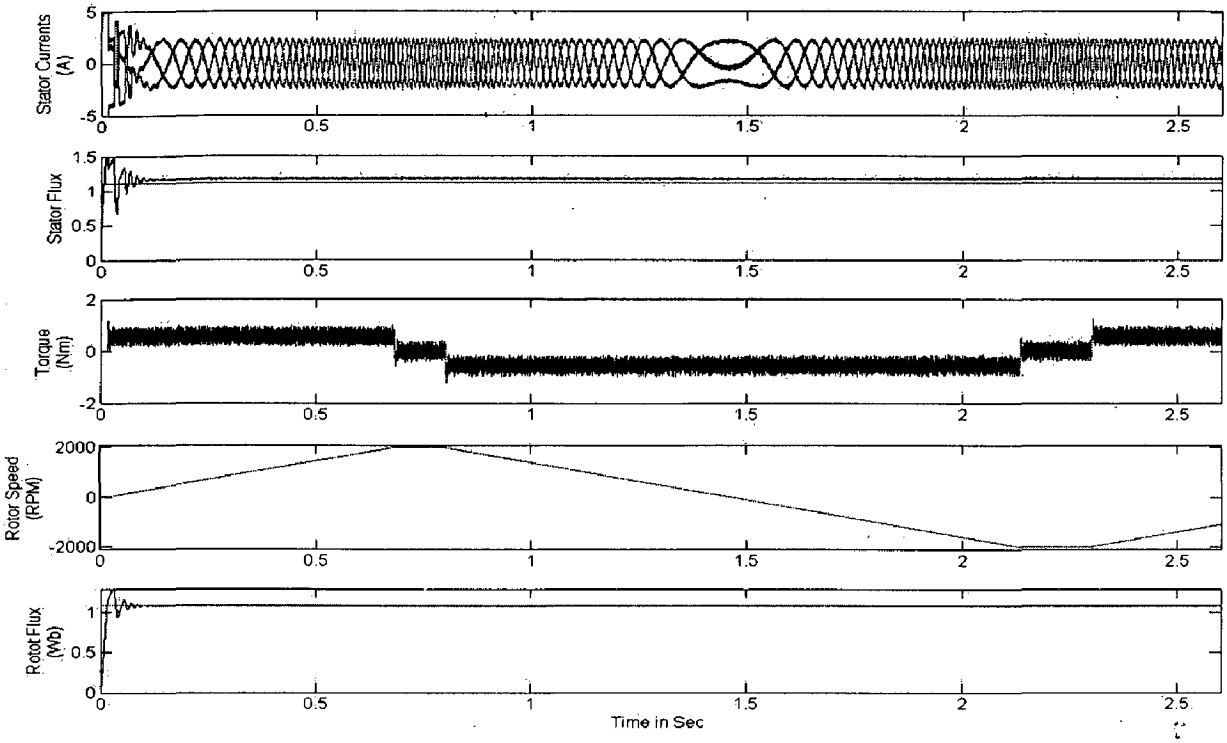

Fig 5.17: Four quadrant operation (FOC) waveforms at T_L=0

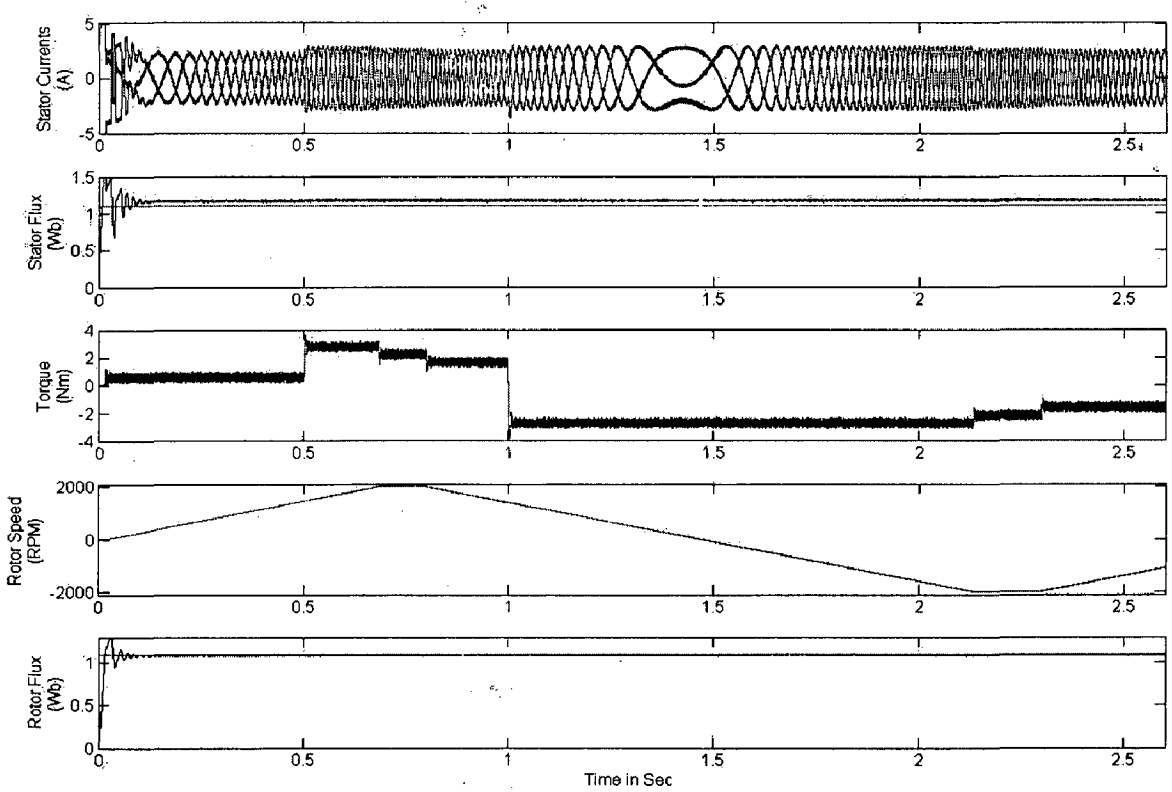

Fig 5.18: Four quadrant operation (FOC) waveforms at T_L=2.2 at t=0.5s and T_L=-2.2 at t=1s

Regeneration Mode:

The power input to induction motor is given by

$$P_{in} = 3VI_s \cos \emptyset_s$$

where $\emptyset_s$ is the phase angle between stator voltage V and stator phase current I_s. For motoring operation $\emptyset_s < 90^0$. This is seen in Fig 5.19 at t=.96s. In regeneration operation $\emptyset_s > 90^0$ so that power flow reverses and fed back to source from load. This ca be seen after t=1s.In regeneration mode frequency decreases so that synchronous speed decreases and rotor speed becomes greater than synchronous speed, relative speed between the rotor conductors and air gap rotating field reverses. This reverses the rotor induced emf, rotor current and component of stator current which balances the rotor ampere turns.

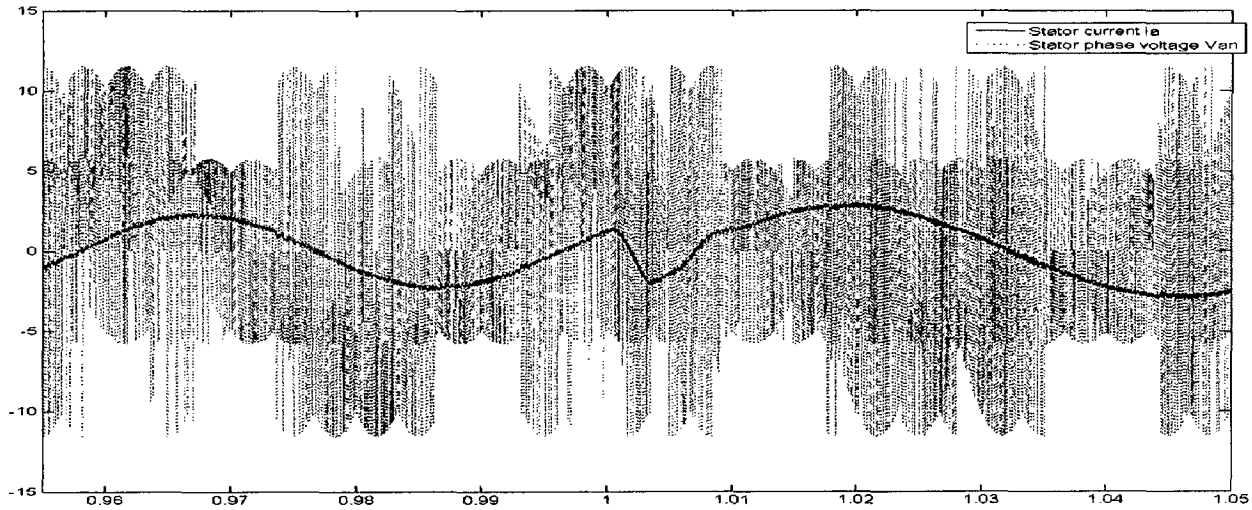

Fig 5.19: Regeneration braking at t=1s

5.2.4: Flux Control Performance:

Flux control is necessary to field weakening operation when the motor is to operate at speeds higher than the nominal value. Flux control dynamic performance of FOC and DTC systems is evaluated by applying a step change (down from nominal value to 75% of nominal value) to flux control input while the torque reference is maintained at its nominal value (2.2 Nm). The motor speed is maintained at 2000 RPM. The obtained responses are shown in Figs. 5.20 and 5.21. We can note that in FOC

system rotor and stator fluxes vary with a time constant equal to the rotor time constant (in this case τ_r=58.3ms). As shown in Fig 3.21, in DTC system the stator flux can vary rapidly because it is directly controlled by the stator voltage vector. The stator flux response time in this test is about 0.5ms. The rotor flux tracks the stator flux with a time constant equal to $\sigma.\tau_r$ (in this case $\sigma.\tau_r$ = 4ms). One can note also a much higher ripple in stator currents because they are indirectly controlled.

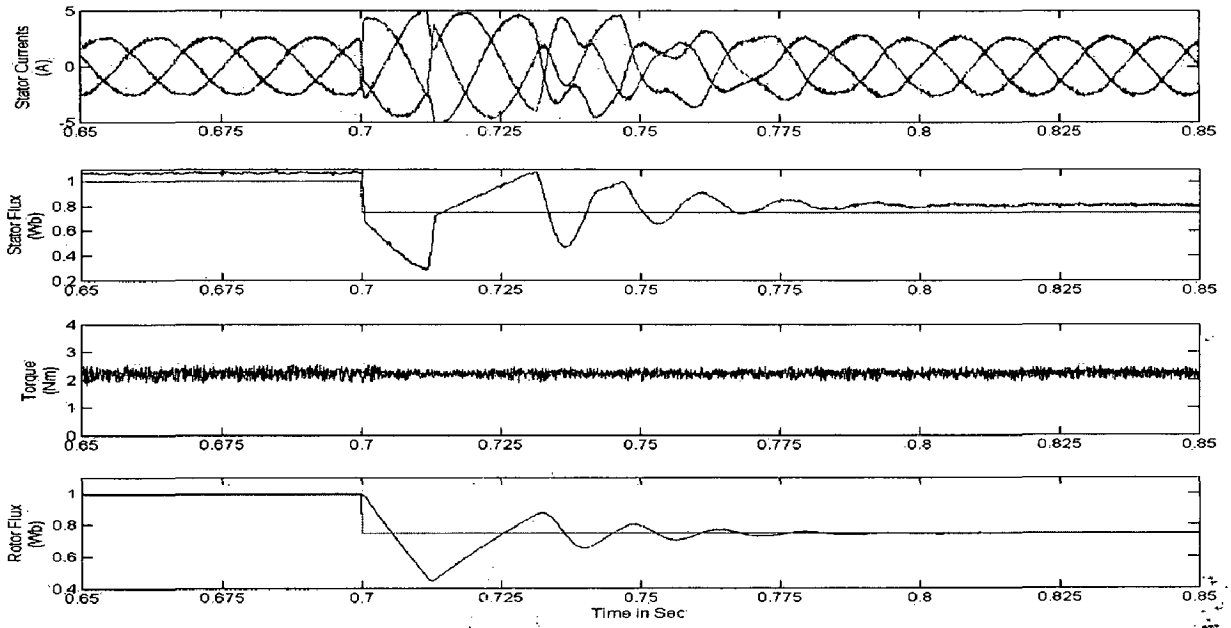

Fig 5.20: Flux control step response of FOC scheme

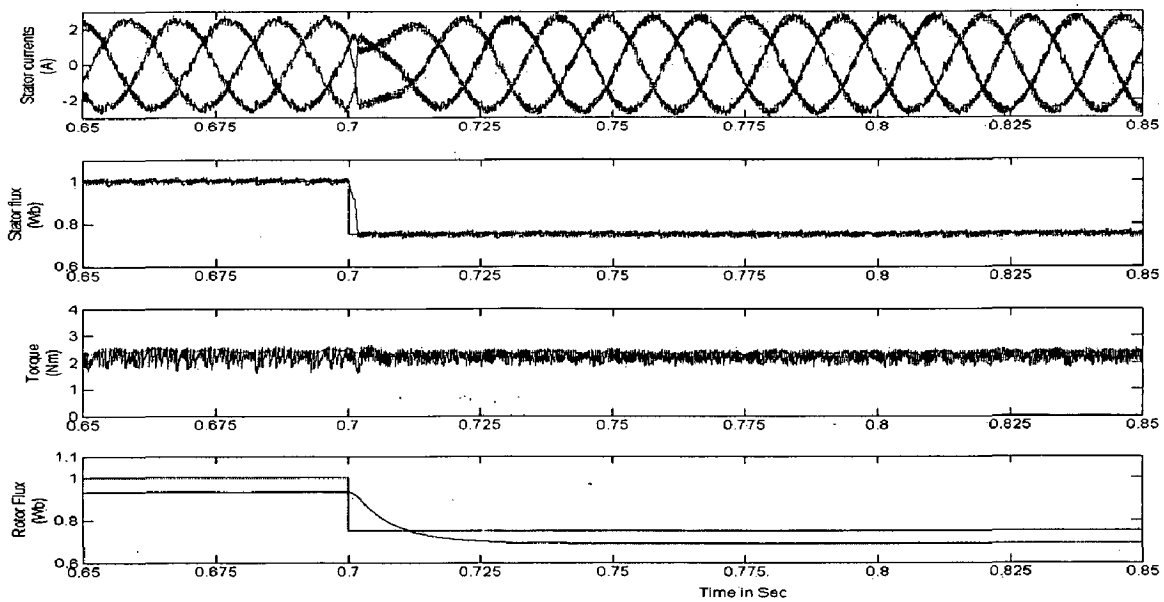

Fig 5.21: Flux control step response of DTC scheme

5.2.5: Parameter Sensitivity:

Since both FOC and DTC schemes are based on estimated variables, the estimation accuracy has a direct influence on the control performance.

Parameter Sensitivity in FOC:

In FOC scheme, the operation is based essentially on the slip frequency estimation which is dependent on the rotor time constant $\tau_r = L_r/R_r$. The rotor resistance varies as a function of the temperature while the rotor inductance changes with flux level. Typical variation of τ_r, can cover a range of $0.75\tau_{r0} < \tau_r < 1.25\tau_{r0}$ where τ_{r0} is the nominal value. An error in the estimation of τ_r, will deteriorate the control performance. The effects of the estimation error of R_r, are studied by applying a step change in the value of R_r, used in the slip frequency estimator while the motor is running in steady-state at 50 RPM with nominal load (2.2 Nm). Fig 5.22 shows the variation of rotor flux and torque for the cases where the estimated value of R_r is suddenly changed to 75% and 125% the actual value. In both case, this variation has resulted in control errors in rotor flux and torque. Transient responses of flux and torque are oscillatory with low damping. This torque oscillation can cause acoustic noise in the motor. Also, one can note a dependence of the torque ripple on the value of R_r used in the estimator.

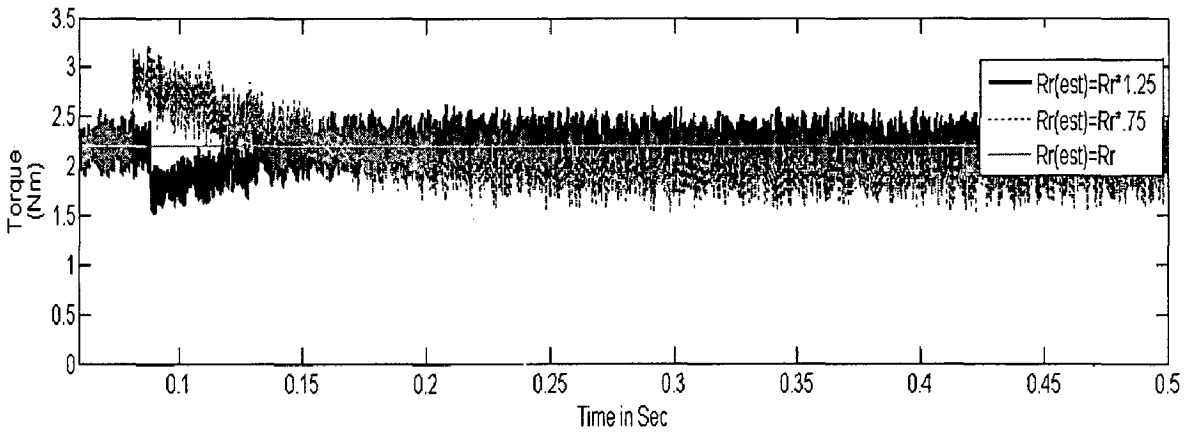

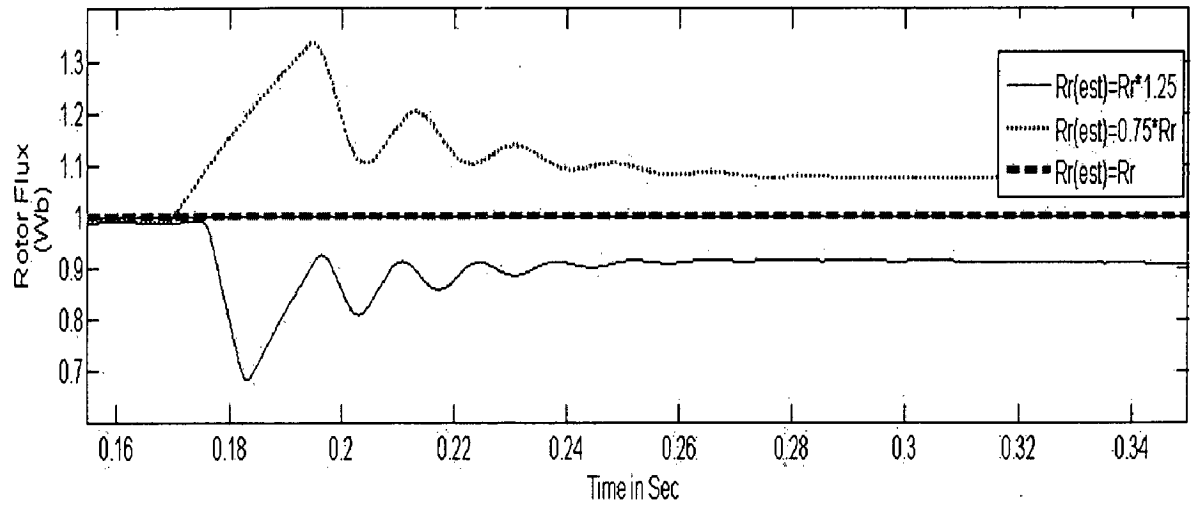

Fig 5.22: Influence of the estimated rotor resistance on FOC performance

Parameter Sensitivity in DTC:

The DTC operation is essentially based on the calculated stator flux which is the integral of the emf ($\overline{V}_s - \overline{I}_s R_s$). The value $\overline{\varphi}_s$, computed by (4.10) is mainly dependent on the value of the stator resistance R_s which varies as a function of temperature. Also, at very low speeds where the difference ($\overline{V}_s - \overline{I}_s R_s$) is very small, a small error in R_s can produce very inaccurate results. This will result in a deterioration of the control performance. The effects of the estimation error of R_s are studied by applying a step change in the value of R_s used in the stator flux estimator while the motor is running in steady-state at 50 RPM with nominal load (2.2 Nm). Fig 5.23 shows the variation of rotor flux and torque for the cases where the estimated value of Rs is suddenly changed to 75% and 125% of the actual value. In the case of underestimation of R_s, a control error is resulted in rotor flux and torque. Transient responses of flux and torque are also oscillatory with low damping. One can note an increase of the torque ripple in spite of the torque regulator. This lost of control is due to torque estimation error. In the case of overestimation of R_s, the deterioration is more severe. The rotor flux and torque oscillate slowly with increasing amplitude: the system becomes instable.

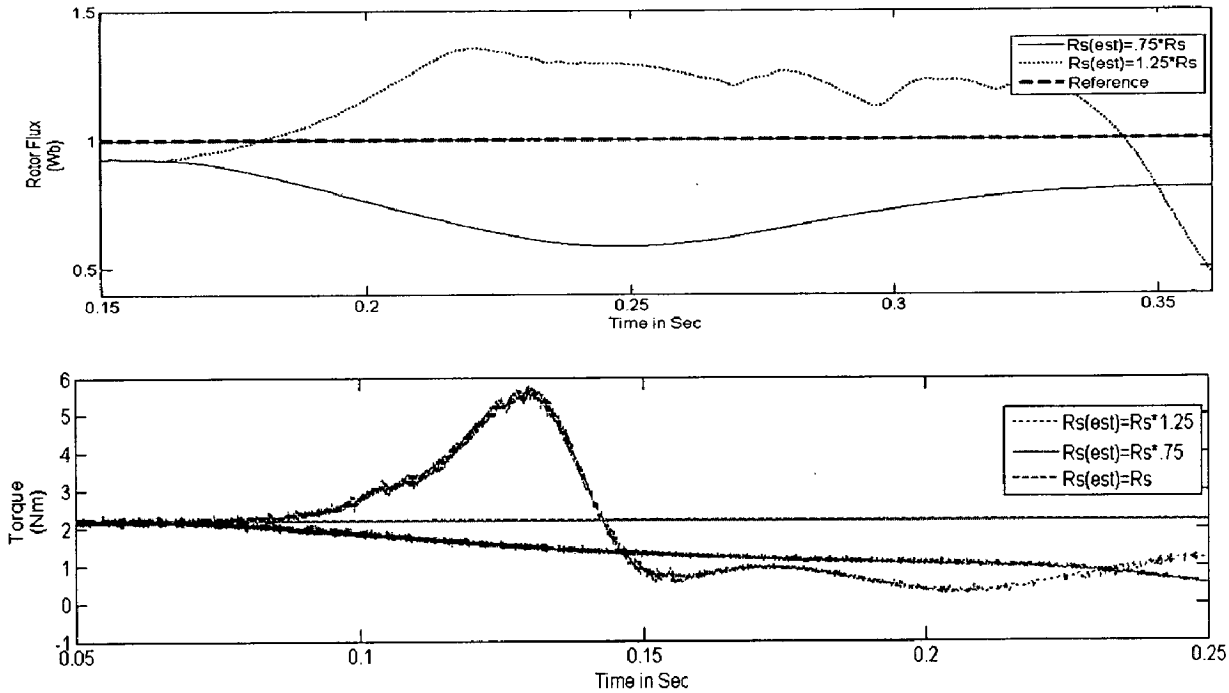

Fig 5.23: Influence of the estimated stator resistance on DTC performance.

5.2.6: DTC Behavior at Low Speed:

It is known that the basic DTC scheme is affected by undesired flux weakening phenomena at low speed. In these operating conditions the control system selects many times zero voltage vectors, determining a reduction of the flux level owing to the effects of the stator resistance voltage drop. Fig 5.24 shows the stator flux variations obtained by numerical simulations at a rotor speed of 10 RPM, and with a torque of 0.5Nm.

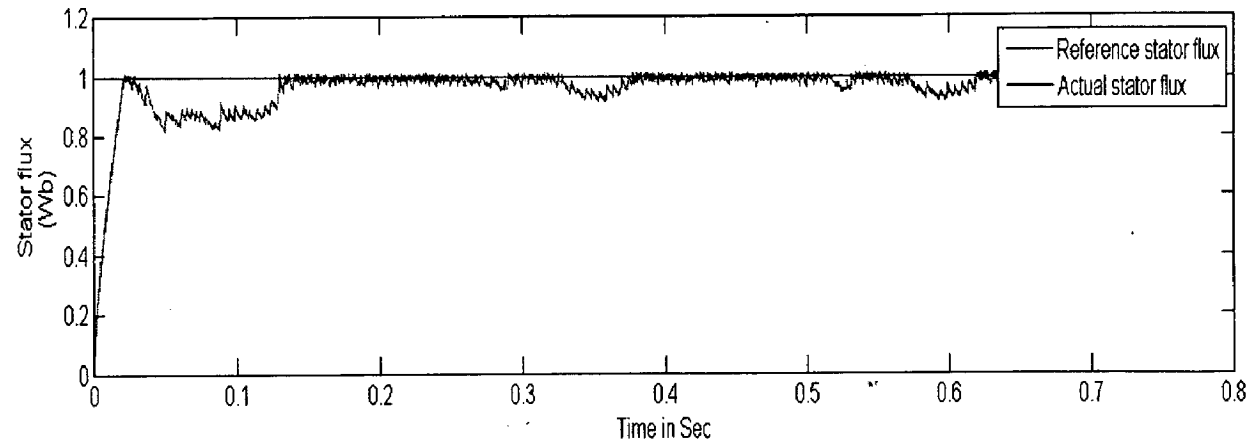

Fig 5.24: Stator flux magnitude in DTC, 10 rpm, 0.5Nm.

5.2.7: Input Current:

Fig 5.25 and 5.26 shows the current without and with input filter. Without filter there are higher order harmonics which is shown in FFT analysis in Fig 5.27, the higher order harmonics can be filtered out using input filter which is confirmed by Fig 5.28.

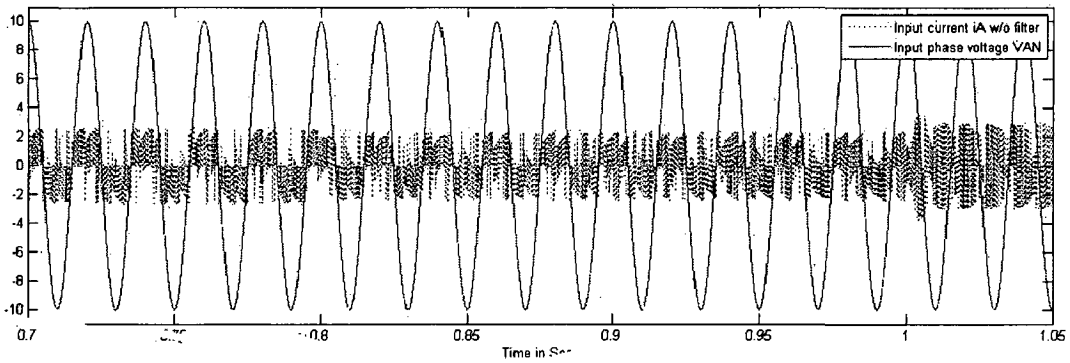

Fig 5.25: Input current i_A without filter

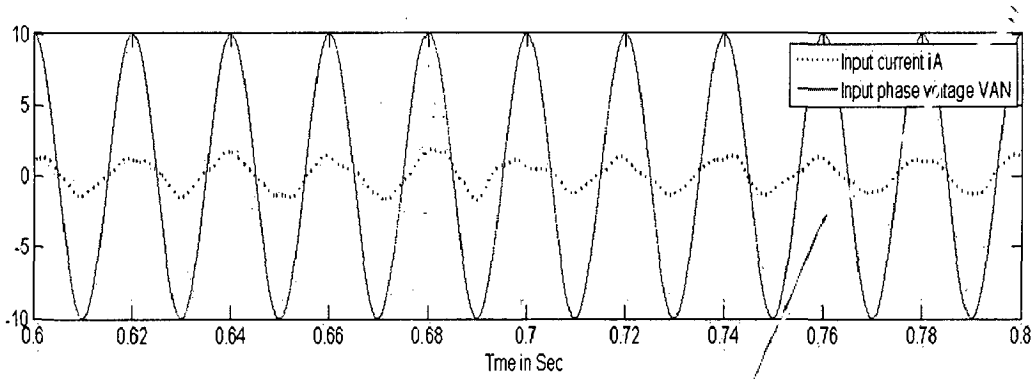

Fig 5.26: Input current i_A with filter

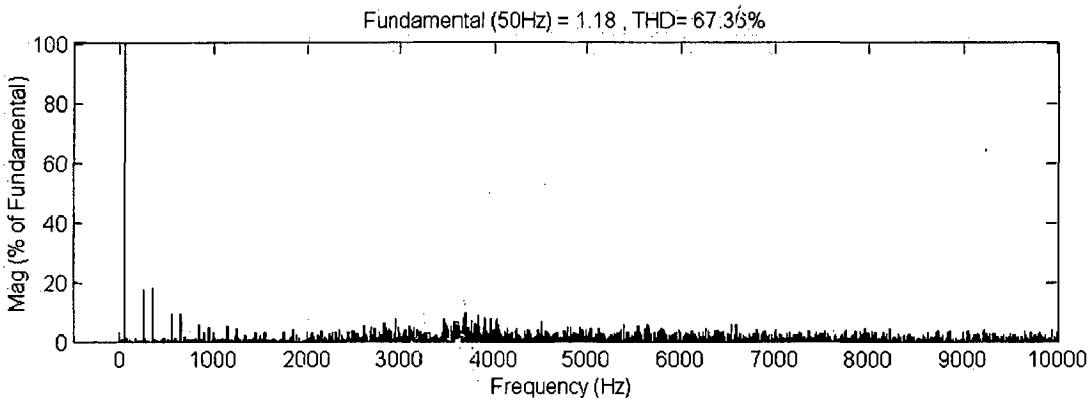

Fig 5.27: FFT of input current i_A without filter

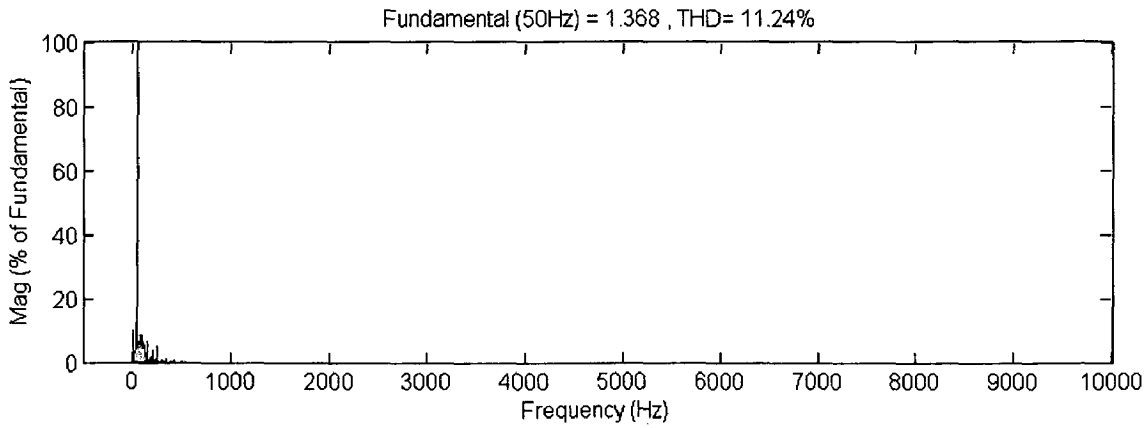

Fig 5.28: FFT of input current i_A with filter

5.3 Conclusions

The control method for FOC is based on Modified Venturini method, which is simple control technique and maintains unity power factor and inherent bidirectional power flow.

The control method for DTC is based on switching tables which allows the direct control of the matrix converter accordingly to the motor and input power factor requirements. By means of this new control method the advantages of matrix converters over traditional VSI-PWM converters, such as unity power factor control, inherent bi-directional power flow and sinusoidal input current capability, have been combined with the control simplicity and robustness of the DTC technique.

It is difficult to clearly state on the superiority of DTC versus FOC because of the balance of the merits of the two schemes. Based on the simulation results, we can nevertheless say that the two control schemes provide, in their basic configuration, comparable performance regarding torque control performance and parameter sensitivity. We can note a slight advance of DTC scheme compared to FOC scheme regarding the dynamic flux control performance and the implementation complexity on the other hand, shows higher current and torque ripple. Then, the choice of one or the other scheme will depend mainly on specific requirements of the application.

Chapter 6

Conclusion and Future Scope

Conclusion

Matrix converter is a modern energy conversion device that has been developed over the last two decades. As the prices of semiconductors continues to fall the matrix converter is also becoming a more attractive to the back-to-back inverter in applications where sinusoidal input currents or true bi-directional power flow are required. Furthermore, matrix converter allows a compact design due to the lack of dc-link capacitors for energy storage.

There are various strategies used for matrix converter, some of these have been discussed. In this thesis Venturini and SVM modulation strategy has been implemented for 3-phase to 3-phase matrix converter and performance was simulation study is carried out on RL load. This thesis presents a comparative study on Field-Oriented Control (FOC) and Direct Torque control (DTC) for Induction Motor Drives using Matrix Converter.

Simulation study is carried out on 3-phase to 3-phase matrix converter using Venturini and SVM modulation techniques. Matrix converter is loaded with R-L load. In Venturini method with switching frequency of 5 KHz, voltage transfer ratio 0.5 and output frequency of 100Hz the THD of output current is 1.52%. With same switching frequency, voltage transfer ratio and output frequency 25Hz the THD of output current is 0.74%. In simulation the output frequency is changed suddenly and results are recorded to know the performance. It is also shown that the THD of source current has reduced to 2.55% from 109% after inception of input filter. It is also shown with simulation results that the modulation algorithm provides a unity input displacement factor even the load has an inductive characteristics. In Venturini method there is a limitation for voltage transfer ratio to be less than 0.5. In SVM method this limitation can be overcome;

with switching frequency of 5 KHz, voltage transfer ratio 0.8 and output frequency of 100Hz the THD of output current is 2.13%. With same switching frequency, voltage transfer ratio 0.8 and output frequency 25Hz the THD of output current is 2.88%. In simulation the output frequency is changed suddenly and results are recorded to know the performance. It is also shown that the THD of source current has reduced to 4.79% from 92.45% after inception of input filter. It is also shown with simulation results that this modulation algorithm provides a input displacement factor control.

The superior overall performance characteristics of an MC drive have been demonstrated via simulation results. Simulation results illustrate that in addition to the full controllability of the MC output voltage; this technique also yields near unity power factor and high waveform quality at the input. Steady state and dynamic transient operating characteristics have been obtained over a wide operating range by detailed simulation study. The following important conclusions can be reached from these results.

1) The steady state attributes such as the speed regulation, torque capability, etc. of the Matrix Converter (MC) drive match those of the PWM inverter drive. In addition, MC drive exhibits significantly better speed step response and impact-load response. The four quadrant operating capability results in significantly wider dynamic performance.

2) Under all the normal speed and voltage operating conditions, a near unity power factor could be achieved. The input current is sinusoidal and has a significantly lower THD than the diode rectifier front-end type PWM inverter drives.

3) Due to the four quadrant operating capability, the energy efficiency of the MC drive is superior to the PWM inverter. During regenerative operation, most of the load energy is returned to the input source. The only losses are the power semiconductor losses and input filter losses (comparable to the PWM inverter semiconductor losses, accounting for the front-end diode rectifier

losses also) that are small compared to the regenerated energy. Thus, very high overall energy efficiency could be obtained.

In this thesis, main characteristics of field-oriented and direct torque control schemes for induction motor drives are studied by simulation with a view to highlighting the advantages and disadvantages of each approach. It is difficult to clearly state on the superiority of DTC versus FOC because of the balance of the merits of the two schemes. Based on the simulation results, we can nevertheless say that the two control schemes provide, in their basic configuration, comparable performance regarding torque control performance and parameter sensitivity. We can note a slight advance of DTC scheme compared to FOC scheme regarding the dynamic flux control performance and the implementation complexity on the other hand, shows higher current and torque ripple. With the additional computation required to improve the basic FOC and DTC schemes, they will attain comparable performance and implementation complexity. Then, the choice of one or the other scheme will depend mainly on specific requirements of the application.

Future Scope

In this thesis, performance of the matrix converter was investigated using Venturini and SVM modulation methods for different output frequencies. Control methods for matrix converters for implementation of DTC and FOC are presented. FOC is based on Modified Venturini method and DTC is based on hysteresis control. Using SVM discussed in Chapter 3 DTC and FOC can be implemented for Matrix Converter.

The simultaneous commutation of controlled bidirectional switches used in matrix converters is very difficult to achieve without generating overcurrents and overvoltage spikes that can destroy the power semiconductors. Burany [20] introduced semi-soft current commutation technique. So using this technique this work can be extended to practical application.

References

[1] L. Gyugyi, B.R. Pelly, "Static Power Frequency Changers. Theory, performance and applications," ISBN 0-471-678000-7, 442 pages, John Wiley & Sons, USA, 1976.

[2] A. Alesina and M. Venturini, "Solid-state power conversion: A Fourier analysis approach to generalized transformer synthesis," *IEEE Trans.Circuits Syst.*, vol. 28, no. CS-4, pp. 319–330, Apr.1981.

[3] A. Alesina and M. Venturini, "Analysis and design of optimum amplitude nine-switch direct AC-AC converters," *IEEE Trans. Power Electron.*, vol. PE-4, no. 1, pp.101–112, Jan. 1989.

[4] J. Rodriguez, "A new control technique for AC-AC converter", in proceedings of IFAC control in Power Electronics and Electrical Drives Conference, Lausanne (Switzerland), 1983, pp. 203-208.

[5] P. Wheeler, J. Rodriguez, J. Clare, L. Empringham and A. Weinstein, "Matrix Converters: A technology review", *IEEE Transactions on industrial Electronics,* 49, pp. 276-288, 2002b.

[6] P. D. Ziogas, S.I. Khan and M. H. Rashid, "Some improved forced commutated Cycloconverter structures", IEEE Trans. Ind. Electron., vol. 1a-21, pp. 1242-1253, Sep./oct. 1985.

[7] P. D. Ziogas, S.I. Khan and M. H. Rashid, "Analysis and Design of Forced commutated cycloconverter structures with improved transfer characteristics", IEEE Trans. Ind. Electron., vol. IE-33, pp.271-280, Aug. 1986.

[8] L. Huber, D. Borojevic and N. Burany, "Voltage Space vector based PWM control of forced commutated cycloconverters", in proc. IEEE IECON'89, 1989, pp. 106-111.

[9] L. Huber and D. Borojevic, "Space vector modulator for forced commutated cycloconverter," in Conf. Rec. IEEE-IAS Annu.Meeting, 1989, pp 871-876.

[10] L. Huber, D. Borojevic and N. Burany, "Analysis design and implementation of the space-vector Modulator for forced commutated cycloconverters", Proc. Inst. Elec. Engg., pt. b, vol.139, no. 2, pp. 103-113, Mar. 1992.

[11] L. Huber, D. Borojevic and N. Burany, "Digital implementation of the space vector modulator for forced commutated cycloconverters", in Proc. IEEE PEVD conf. 1990, pp. 63-65.

[12] L. Huber and D. Borojevic, "Space vector modulated three-phase to three-phase Matrix converter with input power factor correction", IEEE Trans. on Industrial Electronics, 31, pp. 1234-1246, 1995.

[13] Jun Oyama, Xiaorong Xia, Tsuyoshi Higuchi, Koji Kuroki and Eiji Yamada, "Variable Voltage Variable Frequency (VVVF) online control of matrix converter", Scripta technical, Inc. Electr Eng Jpn, Vol-119, No. 2, pp. 81-90, 1997.

[14] Frede Blaabjerg, Domenico Casadei, Christian Klumpner and Marco Matteini, "Comparison of Two Current Modulation Strategies for Matrix Converters Under Unbalanced Input Voltage Conditions" IEEE Transactions on Industrial Electronics, vol. 49, NO. 2, pp. 289-296, April 2002.

[15] P. Mutschler and M. Marcks, "A Direct Control Method for Matrix Converters" IEEE Transactions on Industrial Electronics, vol. 49, no.2, pp. 362-369 April 2002

[16] Domenico Casadei, Giovanni Serra, Angelo Tani, and Luca Zarri, "Matrix Converter Modulation Strategies: A New General Approach Based on Space-Vector Representation of the Switch State", IEEE Transactions on Industrial Electronics, vol. 49, no. 2, pp. 370-381 April 2002.

[17] Lars Helle, Kim B. Larsen, Allan Holm Jorgensen, Stig Munk-Nielsen, and Frede Blaabjerg, "Evaluation of modulation schemes for three-phase to three-phase matrix converters," *IEEE Trans. Ind. Electron.*, vol. 51, no. 1, pp. 158–171, Feb. 2004.

[18] Christian Klumpner, Frede Blaabjerg, Ion Boldea and Peter Nielsen, "New Modulation Method for Matrix Converters" IEEE Transactions on Industry Applications, vol. 42, no. 3, pp. 797-806 May/June 2006.

[19] Matti Jussila and Heikki Tuusa, "Comparison of Simple Control Strategies of Space-Vector Modulated Indirect Matrix Converter Under Distorted Supply Voltage", IEEE Transactions on Power Electronics, vol. 22, no. 1, pp. 139-148, January 2007.

[20] N. Burany, "Safe control of four-quadrant switches," in *Conf. Rec. IEEE-IAS Annu. Meeting*, 1989, pp. 1190–1194.

[21] L. Empringham, P. W. Wheeler, and J. C. Clare, "Intelligent commutation of matrix converter bi-directional switch cells using novel gate drive techniques," in *Proc. IEEE PESC'98*, Fukuoka, Japan, 1998, pp. 707–713.

[22] Patrick W. Wheeler, Jon C. Clare, Lee Empringham, Michael Bland and Maurice Apap, "Gate Drive Level Intelligence and Current Sensing for Matrix Converter Current Commutation" IEEE Transactions on Industrial Electronics, vol. 49, no. 2, pp. 382-389, April 2002.

[23] Patrick W. Wheeler, Jon Clare and Lee Empringham, "Enhancement of Matrix Converter Output Waveform Quality Using Minimized Commutation Times", IEEE Transactions on Industrial Electronics, vol. 51, no. 1, pp. 240-244, February 2004.

[24] Marcus Ziegler, Wilfried Hofmann, "Semi-natural two steps commutation strategy for Matrix Converters" PESC, pp.727-731, Fuknokal, JAPAN 1998.

[25] M. Zeigler and M. Hoffman, "Performance of a two steps commutated matrix converter for AC variable speed drives," in *Proc. IEEE PESC'99*, 1999, pp. 175–180.

[26] Ziegler, M.; Hofmann, W. "New One-Step Commutation Strategies in Matrix Converters", PEDS01 Bali 2001 Proceedings pp. 560-564.

[27] J. Adamek, W. Hofmann, M. Ziegler, "Fast Commutation Process and Demand of Bidirectional Switches in Matrix Converters", IEEE Transactions on Industrial Electronics, 2003.

[28] Lixiang Wei and Thomas. A Lipo, "A Novel Matrix Converter Topology with Simple Commutation", IEEE Transactions on Industrial Electronics, 2001.

[29] A. Dasgupta, S. Mukherjee, M. Sengupta, P. Syam and A. K. Chattopadhyay, "Implementation of a universal logic system of generating commutating pulses in matrix converters using FPGAs", IEEE Transactions on Industrial Electronics, 2006.

[30] P. Nielsen, F. Blaabjerg, J. K. Pedersen, "Novel Solutions for Protection of Matrix Converter to Three Phase Induction Machine", IEEE Industry Applications Society Annual Meeting New Orleans, Louisiana, October 5-9, 1997.

[31] P. Nielsen, F. Blaabjerg, J. K. Pedersen, "New Protection Issues of a Matrix Converter: Design Considerations for Adjustable-Speed Drives", IEEE Transactions on Industry Applications, vol. 35, no.5, September/October 1999.

[32] C. Klumpner and F. Blaabjerg, "Experimental evaluation of ride-Through capabilities for a matrix converter under short power Interruptions," *IEEE Trans. Ind. Electron.*, vol. 49, pp. 315–324, Apr. 2002.

[33] C. Klumpner and F. Blaabjerg, "Short Term Braking Capability during Power Interruptions for Integrated Matrix Converter—Motor Drives",

IEEE Transactions on Power Electronics, vol. 19, no. 2, pp. 303-311, March 2004.

[34] Eduardo P. Wiechmann, Rolando P. Burgos and José Rodriguez, "Continuously Motor-Synchronized Ride-Through Capability for Matrix-Converter Adjustable-Speed Drives", IEEE Transactions on Industrial Electronics, vol. 49, no. 2, pp. 390-400, April 2002.

[35] Han Ju Cha and Prasad N. Enjeti, "A New Ride-through Approach for Matrix Converter Fed Adjustable Speed Drives", IEEE Transactions on Industrial Electronics, 2002.

[36] B. W. Augdahl, H. L. Hess, B. K. Johnson and D.C. Katsis, "Output Protection Strategies for Battlefield Power Supplied by Matrix Converters", IEEE Transactions on Industrial Electronics, 2005.

[37] J. Rodriguez, E. Silva, F. Blaabjerg, P. wheeler, J. Clare and J. Pontt, "Matrix converter controlled with the direct transfer function approach: analysis, modeling and simulation", International Journal of Electronics Vol. 92, No. 2, February 2005,63–85.

[38] Christian Dufour, Lixiang Wei. Thomas A. Lipo, "Real Time simulation of Matrix Converter Drives", EPE 2005 Dresden.

[39] M. Imayavaramban, K. Latha, G. Uma and S. Sunter, "Matlab/Simulink Implementation for reducing the motor derating and torque pulsation of Induction motor using Matrix Converter", IEEE Power Engineering Society, PSCE 2004, No. 0-7803-8178-X/04.

[40] M. Imayavaramban, A.V. Krishna Chaithanya and B.G. Fernandes, "Analysis and Mathematical Modeling of Matrix Converter for Adjustable Speed AC Drives", IEEE Power Engineering Society, PSCE 2006, No. 142440178X/06.

[41] Sedat Stinter and Jon C Clare, "Development of a matrix converter induction motor drives", IEEE Power Engineering Society, PSCE 1994, No. 0-7803-1772-6/94.

[42] D. Casadei, G. Serra and A. Tani, "The use of matrix converters in direct torque control of induction machines", IEEE Trans. Indust. Electron., 48, pp. 1057–1064, 2001.

[43] C. Klumpner, P. Nielsen, I. Boldea and F. Blaabjerg, "A new matrix converter-motor (MCM) for industry applications," IEEE Tran. IE, vol. 9, No. 2, pp. 325-335, April 2002.

[44] Thomas F. Podlesak, Dimosthenis C. Katsis, Patrick. Wheeler, Jon C. Clare, Lee Empringham and Michael Bland, "A 150-kVA Vector-Controlled Matrix Converter Induction Motor Drive", IEEE Transactions on Industry Applications, vol. 41, no. 3, pp. 841-847, May/June 2005.

[45] Hassan Nikkhajoei and M. Reza Iravani, "A Matrix Converter Based Micro-Turbine Distributed Generation System", IEEE Transactions on Power Delivery, vol. 20, no. 3, pp. 2182-2192, July 2005.

[46] S. M. Barakati, M. Kazerani and X. Chen, "A New Wind Turbine Generation System Based on Matrix Converter", IEEE Power Engineering Society, PSCE 2005, No. 0-7803-9156-x/05.

[47] Yang Mei, Kai Sun, Daning Zhou, Lipei Huang and Kouki Matsuse, "Application of Matrix Converter in Auxiliary Drive System for Diesel Locomotives", IAS 2005, No. 0-7803-9208-6/05.

[48] Yang Mei, Kai Sun, Daning Zhou, Lipei Huang and Xuansan Cai, "Novel improvements for matrix converter fed adjustable speed drive system", HAIT Journal of Science and Engineering B, Volume 2, Issues 5-6, 2006.

[49] K. B. Lee, C. H. Bae and F. Blaabjerg, "An improved DTC-SVM method for matrix converter drives using a deadbeat scheme", International Journal of Electronics, Vol. 93, No. 11, November 2006, 737–753.

[50] Kyo-Beum Lee and Frede Blaabjerg, "Improved Sensorless Vector Control for Induction Motor Drives Fed by a Matrix Converter Using

Nonlinear Modeling and Disturbance Observer", IEEE Transactions on Energy Conversion, vol. 21, no. 1, pp. 52-59, March 2006.

[51] Kyo-Beum Lee and Frede Blaabjerg, "Reduced-Order Extended Luenberger Observer Based Sensorless Vector Control Driven by Matrix Converter With Nonlinearity Compensation", IEEE Transactions on Industrial Electronics, vol. 53, no. 1, pp. 66-75, February 2006.

[52] Siyoung Kim, Seung-Ki Sul and Thomas A. Lipo, "AC/AC Power Conversion Based on Matrix Converter Topology with Unidirectional Switches", IEEE Transactions on Industry Applications, vol. 36, no. 1, pp. 139-145 January/February 2000.

[53] Christian Klumpner and Frede Blaabjerg, "A New Cost-Effective Multi-Drive Solution based on a Two-Stage Direct Power Electronic Conversion Topology", IEEE Power Engineering Society, PSCE 2002, No. 0-7803-7420-7/02.

Appendix

Induction Motor Parameters:

Power Rating:	1HP
Stator Voltage:	420V/50Hz
Number of poles:	2
Stator Resistance:	11.124Ω
Stator Leakage Inductance:	33.36mH
Rotor Resistance:	8.9838Ω
Rotor Leakage Inductance:	33.36mH
Mutual Inductance:	490.45mH
Inertia:	0.0018Kg.m^2/s
Friction Coefficient:	0